CRANFIELD UNIVERSITY

Scott Christopher Connors

The effects of gamma radiation on a PBX containing TATB and the fluoropolymer FK-800

Cranfield Defence and Security

PhD
Academic Year: 2013 - 2014

Supervisor:
Prof. Jackie Akhavan
Dr. James Padfield

January 2014

CRANFIELD UNIVERSITY

Cranfield Defence and Security

PhD

Academic Year 2013 - 2014

Scott Christopher Connors

The effects of gamma radiation on a PBX containing TATB and the fluoropolymer FK-800

Supervisor:
Prof. Jackie Akhavan
Dr. James Padfield

January 2014

ABSTRACT

The polymer bonded explosive TCV is analogous to PBX compositions used in some nuclear weapons where the PBX will be exposed to high energy ionising gamma radiation. It is therefore important to study how gamma radiation affects the mechanical and chemical properties of the PBX.

In this study ^{60}Co was used to irradiate samples of the TCV, its FK-800 binder and TATB explosive filler, at 37.5 °C, to total doses up to 200 kGy in air and under vacuum. Post irradiation analysis consisted of mechanical, thermal and chemical analysis of the irradiated materials.

Results from the radiolysis of the FK-800 showed predominant main chain scission taking place, these results in the release of volatile fluorine containing products and an increase in the polymer's crystallinity. The changes to the FK-800's structural properties result in an increase in Young's modulus and yield stress whilst reducing both ultimate tensile strength and elongation at maximum stress. Dynamic mechanical analysis shows the material softening initially upon irradiation, then stiffening as crystallinity increased. TATB was found to turn green and have increased sensitiveness to impact and electric spark discharge with gamma radiation. Analysis by HPLC and LC-MS identified a decomposition product with a mass of 240 g mol^{-1}. No significant changes to the mechanical properties of TCV were identified; however, its sensitiveness to impact and electric spark discharge were found to increase similar to TATB's.

In conclusion, gamma irradiation of TCV has identified significant changes to the mechanical and chemical properties of the FK-800 binder, have little to no effect on mechanical properties of PBX up to 100 kGy. The predominant radiolytic effects on TCV were to its hazard characteristics caused by changes in the TATB. A mono-furazan derivative of TATB has been suggested as the decomposition product identified, and as a possible cause for the increase in sensitiveness of TATB upon gamma irradiation.

Keywords: Mechanical properties, Tensile load testing, DMA, Brazilian disc test, chain scission, mono-furazan, crystallinity

ACKNOWLEDGEMENTS

My thanks must go to my supervisors, Prof Jackie Akhavan and Dr James Padfield, for having the faith in me to undertake this project. This project also owes a debt of gratitude to Dr Paul Deacon of AWE $_{plc}$ for both funding the work, and his unwavering support and friendship.

I must also thank the whole of the Department of engineering and applied science, Cranfield University, Shrivenham; especially the members of the Chemistry tea club for their support and many discussions ranging from academic matters to the ridiculous. Without the support of the many people within the department who contributed assistance and advice, rarely questioning my eccentric ideas, this project would not have been possible. However, there are some people whose assistance deserves special mention here; Dr Nathalie Mai for general support, analytical and as the world's greatest listener, Dr Guillaume Kister for allowing me to experiment with the DMA and general polymer science discussions, Peter Wilkinson for equipment training and technical support and finally Richard Hall glass blower extraordinaire, who made all of the many sample vials used in this study and never complained once.

Recognition must also be paid to the contributions of Dr Annette Glauser and Paul O'nion of AWE plc. Annette's assistance, advice and running of X-ray diffraction samples went far beyond that which could be expected, and to that end I will be indebted for many years to come. Thanks to Paul's running of the LC-MS samples at AWE plc alongside his regular work load, some of the most interesting results contained in this study were found.

Finally I must thank my partner Sarah-Jane Nicholls for her love, support and skills with a highlighter, without which I wouldn't be where I am today.

TABLE OF CONTENTS

LIST OF FIGURES

LIST OF TABLES

GLOSSARY

ATR	Attenuated total reflectance
CTFE	Chlorotrifluoroethylene
$Đ_M$	Molecular mass dispersity
DMA	Dynamic mechanical analysis
DMSO	Dimethyl sulfoxide
DOE	Department of Energy
DSC	Differential scanning calorimetry
DTA	Differential thermal analysis
E	Young's modulus
E'	Storage modulus
E''	Loss modulus
E*	Complex modulus
EMTAP	Energetic Materials Testing and Assessment Policy committee
ESR	Electron spin resonance spectroscopy
F of I	Figure of insensitiveness
FT-IR	Fourier transform infrared spectroscopy
GC	Gas chromatography
GC-MS	Gas chromatography–mass spectrometry
GPC	Gel permeation chromatography
Gy	Gray
HMX	Octahydro-1,3,5,7-tetranitro-1,3,5,7-tetrazocine
HNS	1,3,5-Trinitro-2-[2-(2,4,6-trinitrophenyl)ethenyl]benzene
HPLC	High performance liquid chromatography
HTPB	Hydroxyterminated polybutadiene
kGy	Kilogray
LC-MS	Liquid chromatography - mass spectroscopy
m/z	Mass to charge ratio
MeV	Megaelectronvolt
M_n	Number average molecular mass
MS	Mass spectroscopy
M_w	Mass average molecular mass
NMR	Nuclear magnetic resonance spectroscopy
PBX	Polymer bonded explosive
PETN	Pentaerythritol tetranitrate
PID	Proportional integral derivative
PMMA	Poly(methyl methacrylate)
ppm	Parts per million
RDX	1,3,5-Trinitroperhydro-1,3,5-triazine
TADNB	1,3,5-Ttriamino-4,6-dinitro-2-nitrosobenzene

tan δ	Ratio of E'' / E'
TFE	Tetrafluoroethylene
T_g	Glass transition temperature
TGA	Thermogravimetric analysis
THF	Oxolane
T_m	Melt temperature
TNT	2,4,6-trinitrotoluene
UV	Ultra violet
VDF	Vinylidene fluoride
X_p	Pauling electronegativity
XPS	X-ray photoelectron spectroscopy
ΔH_{fus}	Latent heat of fusion
ε	Strain
θ	Angle
λ	Wavelength
σ	Stress
σ_s	Ultimate tensile strength
σ_y	Stress at yield
χ_c	Percentage crystallinity

1 Introduction

1,3,5-Triamino-2,4,6-trinitrobenzene (TATB) - based polymer bonded explosive (PBX) compositions are used both in nuclear weapons and space applications[1]. Both of these environments subject a PBX to penetrating high energy ionising gamma (γ) radiation which may have an effect on the properties of the PBX and its constituent binder or explosive. It is therefore important to understand the changes caused by γ-radiation to any PBX and it constituents used in an environment where they will be exposed to γ-radiation. This study has been undertaken to investigate the effects of γ-radiation on the mechanical and chemical properties of a PBX with a formulation of 95/5 w/w insensitive high explosive TATB and the fluoropolymer FK-800. For the study, the PBX was given the designation TCV signifying its composition of TATB and a fluoropolymer containing chlorotrifluoroethylene (CTFE) and vinylidene fluoride (VDF).

The thesis has been divided into ten sections, starting with an introduction to the materials of interest and a review of previous literature relating to their irradiation. This is followed by two sections describing the equipment developed for this study and the sample characterisation techniques. The results have been broken down into two sections (Section 6 and 7), separating the work conducted on the FK-800 polymer (Section 6) and the explosives TCV and TATB (Section 7). A discussion of the results can be found in Section 8 before the thesis closes by drawing conclusions and making recommendations for further work to be conducted (Sections 9 and 10).

1.1 Polymer bonded explosives background

A PBX is a composite material of crystalline explosive contained in a polymeric matrix and characterised as having high mechanical strength, good explosive properties, excellent chemical stability, high thermal input insensitivity and relative insensitivity to handling and shock[2]. Within a PBX the explosive crystals are coated in the polymeric material which acts as a binder to hold the explosive crystals in place and fill the gaps between crystals; once formulated

PBXs give a moulding powder - which can be pressed into pellets for use, or billets for further machining into complex shapes - or using cross-linkable binders - such as hydroxyterminated polybutadiene (HTPB) - can be cast as pourable mixtures and then the binder cured to form a cross-linked matrix. A plasticiser can be added to the PBX along with the explosive and polymer to improve its mechanical properties[3].

The first true PBX was developed by Los Alamos Laboratory in 1952 to desensitise 1,3,5-Trinitroperhydro-1,3,5-triazine (RDX) from shock and handling for use in nuclear weapons. The PBX consisted of RDX with plasticised polystyrene[2]. Around the same time the US Naval Surface Warfare Centre (NSWC) was developing a range of PBX's for conventional munitions designated PBXN. This programme led to the use in 1954 of PBXN-2, a composition of 95% octahydro-1,3,5,7-tetranitro-1,3,5,7-tetrazocine (HMX) with 5 % Nylon[4], for the Gimlet air to air rocket[2]. Further developments saw a heat-resistant PBX of 1,3,5-Trinitro-2-[2-(2,4,6-trinitrophenyl)ethenyl]benzene (HNS) and Teflon™ (poly-tetrafluoroethylene) used by NASA during the moon landings of the late 1960s and early 1970s for seismic experiments on the surface of the moon[5]. Further PBX's utilising HNS with silicon rubbers were also produced by the NSWC along with Silicon rubber / tetranitrodibenzo-1,3 a,4,6 a-tetrazapentalene (TACOT) formulations. However, these PBXs were found to be of little use due to low detonation velocities[2].

Several pressed, machineable PBX formulations based on RDX and HMX have been developed by the Los Alamos and Lawrence Livermore National Laboratories for the US Department of Energy (DOE). These formulations have used a range of binders including Estane (PBX-9011), Viton A (LX-11) nitrocellulose / chloroethylphosphate (PBX-9404) and KelF (PBX-9010), to give the correct combination of explosive power, detonation velocity, mechanical properties and safety characteristics required for use in nuclear weapons[2-4].

Along with their present use in nuclear weapon, PBXs are finding uses in conventional munitions as a replacement to melt castable 2-Methyl-1,3,5-trinitrobenzene (TNT) / RDX compositions. The Australian Navy's Penguin anti-

ship missile uses a PBX based on PBXN-109, a castable composition of RDX, Aluminium and HTPB-IPDI binder in a 64 / 20 / 16 ratio[6]. Castable PBXs have also been developed for use in artillery shells; a British formulation for this purpose is ROWANEX 1100 a 88 % RDX 5 % HTPB binder 7 % plasticiser[7]. The development of castable PBXs has been driven by the desire to improve the safety of munitions without the need to redesign the delivery system. The castable formulation can be poured into the munitions casing in a similar process to the use of melt-castable explosives, then the binder cured to form a solid PBX.

Modern developments in PBXs for nuclear weapons often use the insensitive crystalline high explosive TATB. This is due to TATB's low vulnerability to accidental ignition, heat resistance and insensitivity to accidental shock initiation. These insensitive TATB based PBXs are ideal for use in nuclear weapons, where the risk of nuclear explosion and pollution from aerosolised-plutonium in an accident has to be considered and mitigated against[1]

1.2 PBX Compositions and materials of Interest

1.2.1 PBX composition

The PBX composition TCV is of interest to the defence industry and has been chosen for use in this project; TCV uses the crystalline explosive TATB as its explosive filler in a 95% to 5% by mass mixture with a fluorinated polymer. The formulation of the TCV is shown in Table 1.2.1, and Table 1.2.2 shows the composition of two PBXs closely related to TCV.

Table 1.2.1 Formulation by mass for the PBX of interest

PBX formulation	Explosive	%	Binder	%
TCV	TATB	95	3M FK-800	5

Table 1.2.2 Two PBX formulations closely related to TCV

PBX formulation	Explosive	%	Binder	%
EDC35	TATB	95	3M Kel F-800	5
PBX 9502	TATB	95	3M Kel F-800	5

The two TCV - related PBX formulations in Table 1.2.2 use the 3M fluoropolymer Kel-F 800 which has been replaced with FK-800. This change was made due to the phasing out of perfluorooctanoyl derivatives, used as an emulsifier in the manufacturing process for environmental reasons. DePiero and Hoffman quoted work by Manzara of 3M which described FK-800 as indistinguishable from Kel-F 800[8]. EDC35[9] is a UK formulation containing Kel-F 800 whilst PBX 9502[10] is an analogous US (DOE) formulation.

TCV is produced by dissolving the FK-800 binder in excess solvent; either methyl ethyl ketone or ethyl acetate can be used. The insoluble crystalline TATB is added and the mixture continuously mixed at high shear rates whilst a vacuum is applied to draw off the solvent. This method of PBX production forms a moulding powder (Figure 1.2.1) of TATB crystals coated with a layer of polymer which can then undergo pressing and machining to form the explosive component required (Figure 1.2.1) of billets for further machining.

Figure 1.2.1 Picture of sample of TCV moulding powder and a pressed pellet.

When the moulding powder is pressed the TCV forms a consolidated highly filled polymer composite. In this composite the TATB particles are held within a polymer matrix shown, a micrograph showing an example of this structure is shown in Figure 1.2.2.

Figure 1.2.2 shows a micrograph of the polished and stained surface of a pellet of PBX 9501, a PBX formulation of 95 % HMX, polyurethane binder 2.5 % and

2.5 plasticiser[11]. The HMX filler particles of mixed sizes are clearly visible held within the stained polymer matrix.

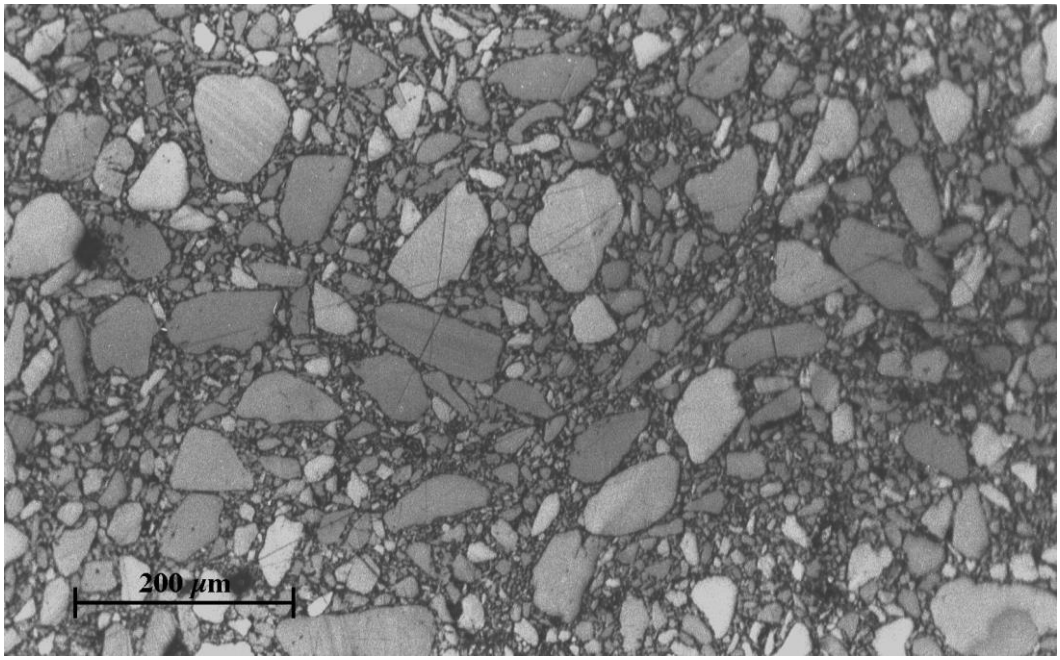

Figure 1.2.2 A micrograph of the stained surface of a pellet of PBX9501 from [11]

1.2.2 TATB (1,3,5-Triamino-2,4,6-trinitrobenzene)

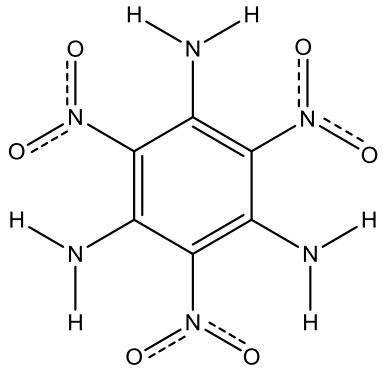

Figure 1.2.3 Structure of TATB

TATB (Figure1.2.3) is a crystalline high explosive described as an insensitive high explosive (IHE) due to its insensitivity to heat, friction and impact (some properties of TATB are shown in Table 1.2.3). TATB is mainly produced by the nitration of trichlorobenzene and amination of the resulting trinitrotrichlorobenzene to TATB. The explosive performance of TATB is better than that of TNT (2,4,6-trinitrotoluene) but not as great as HMX and production

costs are also high with non-US DOE customers paying approximately US$ 200 per kg in 2009[12]. Even with its high cost TATB has found uses in applications where safety is paramount such as nuclear weapons, and it is likely that use will become more widespread as production costs decrease[12; 13].

Table 1.2.3 Properties of TATB adapted from "Explosives" by Meyer [13]

Form	Yellow crystals
Density	1.93 g cm^{-3}
Decomposition temperature	350 °C
Heat of Explosion	3062 kJ kg^{-1}
Detonation velocity confined	7350 m s^{-1}
BAM Impact sensitivity	5 Nm
BAM Friction sensitivity	No reaction at 353 N pistil load

1.2.3 Fluoropolymer binder

Fluoropolymers are characterised by their thermal stability and resistance to acids and bases[14]. A good example of this is poly-tetrafluoroethylene (poly-TFE) (Figure 1.2.4), known by its trade name Teflon™ which is used as a non-stick coating for cookware. Due to their stability and high densities fluoropolymers have been widely used in the formulation of PBXs.

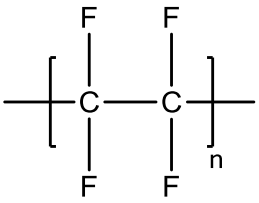

Figure 1.2.4 Structure of poly-TFE

1.2.4 FK-800

FK-800 is a copolymer of three parts CTFE and one part VDF (Figure 1.2.5) produced commercially by 3M. FK-800 is produced by emulsion polymerisation creating a random semi-crystalline polymer with a linear backbone; it can be dissolved in conventional solvents but is still resistant to acids and most bases. FK-800 and its predecessor Kel-F 800 have been used in PBX compositions

with TATB by the US DOE since at least 1979[15]. Some properties of FK-800 are given in Table 1.2.4.

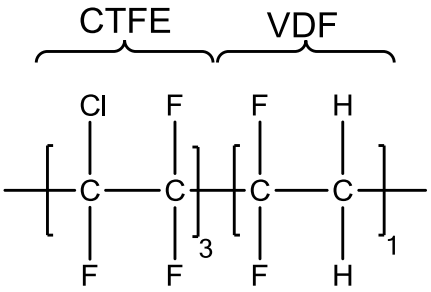

Figure 1.2.5 Structure of FK-800

Table 1.2.4 Some properties of FK-800[16]

Density	2.00 g cm^{-3}
Glass transition temperature (T_g)	30 °C
Crystalline melt temperature (T_m)	105 °C

1.3 Introduction to gamma radiation

During this study the materials of interest were irradiated using gamma radiation before being tested for mechanical and chemical changes. The gamma radiation source used in this study was a ^{60}Co source; further details of the radiation facility are in Section 4.2. The amount of radiation received by a sample (dose) is measured using the SI unit gray (Gy), where one Gy is equal to the absorption of 1 J kg^{-1} of material. The rate of the sample's exposure to the radiation is recorded in Gy hr^{-1} or more commonly kGy hr^{-1}.

^{60}Co produces two gamma photons (γ-photons) by beta decay to ^{60}Ni and has a half-life of 5.25 years. The decay scheme of ^{60}Co is shown in Figure 1.3.1; one gamma photon of 1.173 MeV is given off during the beta decay of ^{60}Co to excited ^{60}Ni with the production of an electron and antineutrino. The second of 1.332 MeV is given off as a result of the relaxation of the daughter ^{60}Ni from its excited state. ^{60}Co can decay via a rare secondary pathway directly to ^{60}Ni without the production of excited ^{60}Ni. During this decay only a single 1.332 MeV γ-photon and a beta particle of 1.491 MeV are released.

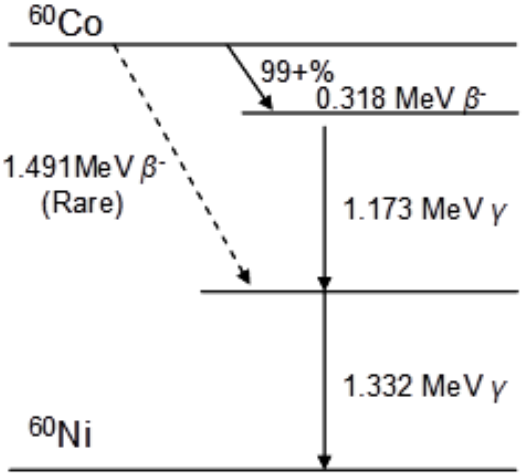

Figure 1.3.1 A diagrammatic representation of the beta decay of ^{60}Co to ^{60}Ni with the release of two gamma photons at 1.173 and 1.332 MeV. Adapted from Atoms, Radiation, and Radiation Protection[17]

1.3.1 Interaction of gamma radiation

Gamma radiation is a form of very short wavelength electromagnetic radiation generated during radioactive decay. The electromagnetic photons interact with matter by one of three different means dependent on the energy of the photon and the mass of the incident atom. The three methods by which γ-photons interact with matter are the photoelectric effect, Compton scattering and pair production.

The photoelectric effect is the principal effect when light, X-rays and low energy γ-photons interact with atoms. Incident photons which have energy greater than the binding energy of atomic electrons can be completely absorbed by an atom's electron cloud resulting in the ejection of an electron known as a photoelectron. The photon energy required to generate photoelectrons increases with atomic mass from a few electron volts up to 1 MeV.

When photon energies exceed the electron rest mass energy of 0.511 MeV then Compton scattering can take place. In this reaction a photon are absorbed by one of the outermost electrons in an atom. The excited electron is ejected from its atomic orbital and a new photon with a longer wavelength and lower energy is emitted. A diagrammatic representation of Compton scattering is

shown in Figure 1.3.2; a photon with wavelength λ is absorbed by an electron and is scattered by angle θ to emitting a photon with the new longer wavelength λ´ and a free electron. The emitted photon λ´ can continue on to interact with further atoms giving up some of its energy with each interaction.

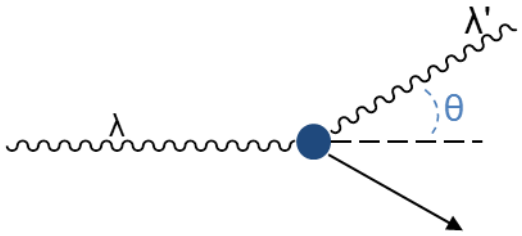

Figure 1.3.2 Compton scattering; photon with wavelength λ is absorbed by an outer orbital electron ejecting the electron. A new photon with the longer wavelength photon λ´ is emitted and scattered by angle θ.

Pair production can result when a photon with at least twice the electron rest mass energy (1.022 MeV) interacts with the field of an atomic nucleus. All of the photon's energy is converted into an electron-positron pair. The likelihood of pair production increases with increasing photon energy and with increasing atomic number of the incident nucleus.

The two γ-photons released during decay of ^{60}Co have energies of 1.17 and 1.33 MeV which, although having enough energy to cause pair production, will be considered to interact only via Compton scattering because of the low atomic number of the elements which make up the materials of interest to this project. The positive ions and free electrons produced during Compton scattering quickly recombine due to columbic attraction giving rise to excited atoms which can undergo homolytic bond cleavage producing free radicals.

Before experimental work began a comprehensive literature review was conducted (Section 2) to ensure this study covered new research and to gain an understanding of how the materials might behave under radiation conditions. The literature review covered not only the materials of interest to this study but also, some other closely related materials.

2 Literature review

2.1 Gamma radiation effects on explosives

Historically, a range of γ-ray sources have been used for the irradiation of explosives; uranium was used in early work along with ^{198}Au and even nuclear power reactors before ^{60}Co became the predominant gamma source. Each different source of γ-rays emits photons at different energies as they decay, often making work to the same total doses difficult to compare. A comprehensive review of the irradiation of energetic materials was carried out in 1980 by Louis Avrami for the Picatinny Arsenal's "Encyclopaedia of Explosives and Related Items"[18]. In his review Avrami covered work on all major primary and secondary high explosives dating back to the early work at Los Alamos and Oak Ridge National Laboratories in 1948. This early study by Noyes and Goodman used a nest of uranium slugs to irradiate RDX, 2,4,6-Trinitrophenylmethylnitramine (Tetryl), TNT and Comp B (60/40 mix of RDX/TNT) to a dose of 86 kGy over 10 days at an unspecified dose rate. Although not comprehensive this study found no visible changes, gas evolution was slight and there was negligible change to the explosive's melting point.

Most of the studies reviewed by Avrami[18] used high total doses in excess of 100 kGy at high dose rates. This level of radiation is equivalent to many tens of years of service life and combined with high dose rates in excess of 5 kGy hr^{-1} may not give relevant information on stockpile behaviour. One study carried out by Avrami and Jackson in 1976[19] used ^{60}Co at a low dose rate of 2.2 Gy hr^{-1} over periods of up to 150 days to irradiate RDX and HMX up to doses of 8.06 kGy. Avrami and Jackson looked at the changes in sensitivity to impact and extremes of temperature concluding "Long term low-level gamma irradiation had no significant effect on the thermal stability or thermal and impact sensitivities".

The overall conclusion which Avrami drew in his review [18] was "Steady-state γ-irradiation of any explosive has not been known to initiate a detonation. The effect of such irradiation appears to result in slow decomposition with a

deterioration in the functional properties of the explosive, or more generally, energetic material." Although this is the conclusion which can be drawn for the majority of the energetic materials, there have been two studies which have shown spontaneous explosion can be caused by γ-irradiation. Piantandia and Piazzi[20] published an article in 1961 in which they irradiated PETN using ^{60}Co; the PETN was found to rapidly decompose during the irradiation at a dose of 26.3 kGy with a dose rate of 263 Gy hr^{-1}. A second study which was published after the Avrami review looked at the impact sensitivity of gamma-irradiated HMX[21]. During the study Miles et al. tried to collect radicals formed during irradiation by irradiating samples at liquid nitrogen temperatures sealed under vacuum. "Frequent accidents" occurred in samples irradiated to 100 kGy at an un-stated dose rate with some exploding spontaneously and others only requiring gentle shock or changes in temperature to explode. The authors also noted that many samples were irradiated to 75 kGy without incident. The accidents were attributed to unstable radicals increasing the sensitivity of the HMX; the exact radical responsible for the increase in sensitivity could not be identified with only a large number of NO_2 radicals found. Miles et al. proposed that the NO_2 radicals were secondary radicals that were less reactive than the species causing the sensitivity issues. Irradiation atmosphere dependence was also shown with the accidents only occurring in vacuum-irradiated samples. The authors proposed that in oxygen-rich environments the oxygen could react with the radicals possibly forming more stable peroxy radicals.

2.1.1 Gamma radiation effects on TATB

In 1995 Dobratz published a report on the history of TATB covering its development and characterization between 1888 and 1994[1]. In the report Dobratz described the work of Loughran and Wewerka at Los Alamos Scientific Laboratories in 1973 looking at the effects of ^{60}Co irradiation on TATB. Loughran and Wewerka irradiated samples of TATB to total doses of 2.6, 5.2, 21, 100 and 210 kGy; the samples were then aged at 175 °C in air at a pressure of 266 mbar for 4, 8 and 16 weeks. The results of this study showed a lowering

of the temperature at which thermal decomposition started, with the rate of decomposition increasing with increasing radiation dose.

In their 1973 report “Radiation-induced changes in explosive materials”[22] Avrami, Jackson and Kirshenbaum conducted an investigation into the effects of ^{60}Co γ-radiation on a range of explosives. TATB samples were irradiated as powders and 12.5 mm diameter pellets in air to total doses of between 87.7 and 24,500 kGy at a dose rate between 5.6 and 8.1 kGy hr^{-1}; tests were carried out to look at the irradiated samples’ thermal stability, purity, sensitivity and explosive performance.

Table 2.1.1 Thermal stability results for samples irradiated between 5.6 and 8.1 kGy hr^{-1}. Adapted from Avrami et al.[22]

Total Dose (kGy)	Vacuum Stability at 200°C Gas evolved in 1 hour (cm^3)	DTA Exotherm Onset at 20°C min^{-1} (°C)	DTA Exotherm Peak at 20°C min^{-1} (°C)	TGA Start of Decomposition at 20°C min^{-1} (°C)	TGA 10% Mass Loss	TGA Total mass loss (%)
0	0.41	325	387	285	353	83% @ 420°C
87.7	0.46	340	377	280	341	20% @ 400°C
789.5	0.57	320	372	250	327	80% @ 385°C
6,491.2	0.96	305	369	250	329	77% @ 405°C
24,561.4	4.65	300	363	125	303	52% @ 345°C
61,403.5				125	299	52% @ 342°C

Thermal stability tests consisted of vacuum stability, mass loss, differential thermal analysis (DTA) and thermogravimetric analysis (TGA) (Table 2.1.1). Avrami et al. described the vacuum stability results for the sample irradiated to 24,561.4 kGy as “very acceptable”; there was however a significant change in both the DTA and TGA data. The exotherm onset and peak both show a 25 °C drop at 24,561.4 kGy; TGA data show that the highest exposure of 61,403.5 kGy causes the start of decomposition to drop from 285 to 125 °C and the 10% mass loss to drop from 353 to 299 °C. The samples irradiated to 24,561.4 and 61,403.5 kGy “detonated” during the TGA tests at 345 and 342 °C respectively. Exposure to the lowest dose of 87.7 kGy showed a drop in the

DTA exotherm peak of 10 °C although there was an increase in the onset temperature of 15 °C for which no explanation is given in the study.

Tables 2.1.2 and 2.1.3 show the colour change, impact sensitivity, detonation performance and mass loss data collected by Avrami et al. TATB was shown to change from yellow to green to blackish-green with increasing dose, although no attempt was made to explain this in the study. Impact sensitivity tests were carried out using the Picatinny Arsenal impact machine; this involved dropping a 2 kg weight on to an unspecified number of samples, to measure the fall height at which 50% of samples would explode. A 12.86 cm lowering of the drop height mean 50% value was seen between the un-irradiated samples and the samples irradiated to a dose of 6,491.2 kGy; there is however a standard deviation of 8.1 cm in the un-irradiated results which could be an indication that this result could vary with further repeat testing. The samples for the impact study which were irradiated to 87.7, 789.5 and 6,491.2 kGy showed little change in the impact sensitivity. The irradiated samples have mean 50% drop heights within 1.3 cm of each other. Some of the impact test results in the Avrami et al. study show large standard deviations; there is also no reference to a standard material or any variation in the equipment. This lack of a reference value makes these results difficult to compare with a test such as the Rotter impact test in which all results are given against a RDX standard.

Mass loss results (Table 2.1.3) show a 0.7% loss in mass at 9,649.1 kGy with a 0.03% loss recorded at the lower dose of 96.5 kGy. All samples showed a small change in mass increasing with total dose. The velocity of detonation results presented in Table 2.1.3 show no significant change until 9,649.1 kGy at which point there is a 75 m s^{-1} lowering of the rate of detonation; this is mirrored in the detonation pressure results which show no change at 96.5 and 1,140.4 kGy from the un-irradiated sample. The detonation rate and pressure results show very little change up to 9,649.1 kGy and combined with the other results from their study led Avrami et al. to conclude “TATB is another aromatic compound that seems to withstand gamma radiation”

Table 2.1.2 Colour change and impact sensitivity results for samples irradiated at dose rates between 5.6 and 8.1 kGy hr^{-1}. Adapted from Avrami et al.[22]

Total Dose (kGy)	Colour Change	50% Fire Impact sensitivity mean (cm)	50% Fire Impact sensitivity std. dev (cm)
0	Yellow	56.29	8.10
87.7	Yellow green	44.70	3.25
789.5	Green	46.71	2.36
6,491.2	Dark green	43.43	7.92
24,561.4	Blackish green		

Table 2.1.3 Detonation and mass loss results for samples irradiated at dose rates between 5.6 and 8.1 kGy hr^{-1}. Adapted from Avrami et al.[22]

Total Dose (kGy)	Velocity Detonation (m sec^{-1})	Detonation pressure (kbar)	Mass loss %
0	7,510	260	
96.5	7,520	260	0.03
1,140.4	7,525	261	0.2
9,649.1	7,435	250	0.7

Skidmore et al. presented a paper to the 1998 conference Life Cycles of Energetic Materials[15], in which they discuss their experiments with gamma radiation and TATB. TATB was irradiated to 90 and 700 kGy at 0.61 kGy hr^{-1} using an enriched uranium fuel rod source; all samples used in the study were irradiated as powders before being pressed into test samples if required. Skidmore et al. noted that the total doses used “are comparable to thousands of years of [nuclear weapon] stockpile life”.

The paper reports the use of many chemical analysis techniques but does not supply results for most and those that are given will be summarised here. A colour change was noted from yellow to lime-green at 90 kGy and dark green at 700 kGy. In the 700 kGy irradiated samples, mono- and difurazan decomposition products (Figure 2.1.1) were detected by thin layer chromatography, although no change was found in the scanning electron

microscopy or infrared and mass spectrometry. Vacuum stability results (Table 2.1.4) show a decrease in thermal stability with increasing total dose which was accelerated by increasing the test temperature. DTA showed a 3.5 °C decrease in the exotherm onset temperature at 700 kGy consistent with the results of Avrami et al.[22] who noted a 5 °C change with a dose of 789.5 kGy. It was found that by recrystallising the sample the change in onset temperature could be partially reversed; if the sample was recrystallised a second time, the effect on the exotherm onset could be completely reversed. Although not discussed by Skidmore et al., it is likely that dissolving the samples for recrystallisation resulted in the separation of any radiation induced decomposition products from the TATB. Differential scanning calorimetry (DSC) showed a reduction in exotherm onset from 325 °C to 310 °C at 700 kGy. Accelerated rate calorimetry tests measured the induction time to run away for a 200 mg sample held at 240 °C; for the sample irradiated to 700 kGy the induction time was reduced from 54 to 28 hours.

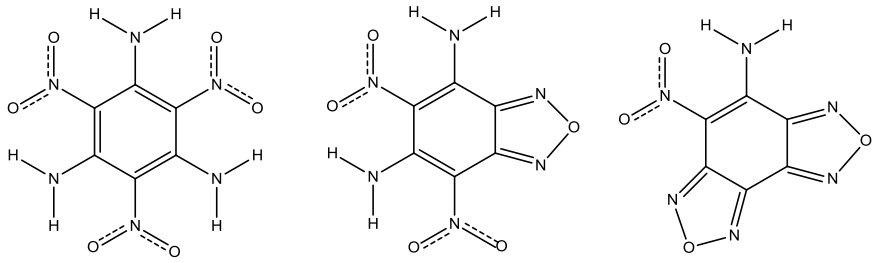

Figure 2.1.1 . Structures for TATB and its mono- and difurazan decomposition products

Table 2.1.4 Vacuum stability results adapted from Skidmore et al, samples irradiated at 0.61 kGy hr^{-1}.[15]

Total Dose (kGy)	Gas evolved at 250°C after 2 hours (cm^3 g^{-1})	Gas evolved at 270°C after 2 hours (cm^3 g^{-1})	Gas evolved at 300°C after 2 hours (cm^3 g^{-1})
0	0.2	1.2	12.0
90	0.4	2.0	22.8
700	0.7	4.3	>23.0

A second set of tests was conducted investigating the macroscopic behaviour of irradiated TATB; the tests included drop weight impact, ballistic chamber and

mushroom tests. In the drop weight impact test, none of the 40 mg samples reacted to the 2.5 kg weight although no indication of the drop height is given in the paper. Ballistic impact chamber tests* carried out on the 90 kGy sample showed a reduced energy release from 50 to 6 J g^{-1} and a reduced pressure release rate from 310.3 to 0.83 kPa μs^{-1}. Skidmore et al. hypothesised that this reduction in sensitivity is caused by water being released during the breakdown of TATB to form the furazans. Mushroom test† analysis investigating changes in initiability and corner turning performance of 2.54 cm hemisphere of TATB showed no change between the control and irradiated samples.

The TATB study reported by Skidmore et al. was a comprehensive chemical analysis and partial sensitivity study which allowed the authors to draw the conclusion "Irradiation of TATB with penetrating radiation….had little to no effect on the macroscopic behaviour". Although this study included an extensive set of chemical analysis techniques, the use of only two total doses means that meaningful trends for the radiation behaviour of TATB cannot be drawn from this paper.

Padfield carried out a feasibility study in 2008[24] looking at the effects of ^{60}Co gamma radiation on polymer bonded explosives. During the study Padfield carried out irradiations of TATB and two PBXs - EDC35 a 95/5 mass percentage mix of TATB and Kel-F 800 and EDC37 91/1/8 mass percentage mix of HMX/nitrocellulose/K10 plasticiser - to 10 and 100 kGy both in air and under vacuum at a constant rate of 0.3 kGy hr^{-1}. The results (Table 2.1.5) show a reduction in both the onset and exotherm temperatures as measured by DSC.

---

*Ballistic Impact chamber test - a drop weight test in which a 10kg weight is dropped 1.5m onto a sample in a closed cup which has a high speed pressure gauge and a 30cm, 0.177 caliber gun barrel attached. The test measures the pressure time profile of the resulting explosion gases and calculates the energy of the pellet as it exits the gun barrel[23].

†Mushroom test - measures initiability and corner turning ability of a pressed explosive. Streak cameras are used to monitor the detonation wave breakout as the wave passes through a 2.54cm hemisphere of explosive initiated by a thin cylindrical booster stem[15].

The TATB decomposition exotherm was seen to develop into two joined peaks at 100 kGy (Figure 2.1.3) along with a reduction in exotherm onset. It was also noted that the TATB samples changed colour from yellow to green as previously reported. The Rotter Figure of Insensitiveness (F of I) (Section 5.14.1) results showed no change in the impact sensitiveness. There was also no variation noted in the results of samples irradiated in air and under vacuum and it was suggested by Padfield that the Chromacol vials with rubber septa had not held a vacuum for the duration of the irradiation. It would therefore be reasonable to assume that all the vacuum results may have been contaminated with oxygen.

Table 2.1.5 Adapted from Padfield Samples irradiated at 0.3 kGy hr^{-1} [24]

	F of I			Density ($g\ cm^{-3}$)			DSC Exotherm onset at 5°C min^{-1} (°C)			DCS Exotherm peak at 5°C min^{-1} (°C)		
dose (kGy)	**0**	**10**	**100**	**0**	**10**	**100**	**0**	**10**	**100**	**0**	**10**	**100**
In Air	121	129	124	1.93	1.93	1.94	365.8	362.5	355.6	378.6	369.8	363.5
											375.3	370.2
Under Vacuum	121	123	124	1.93	1.93	1.93	365.8	362.5	355.6	378.6	370.1	363.9
											375.6	370.2

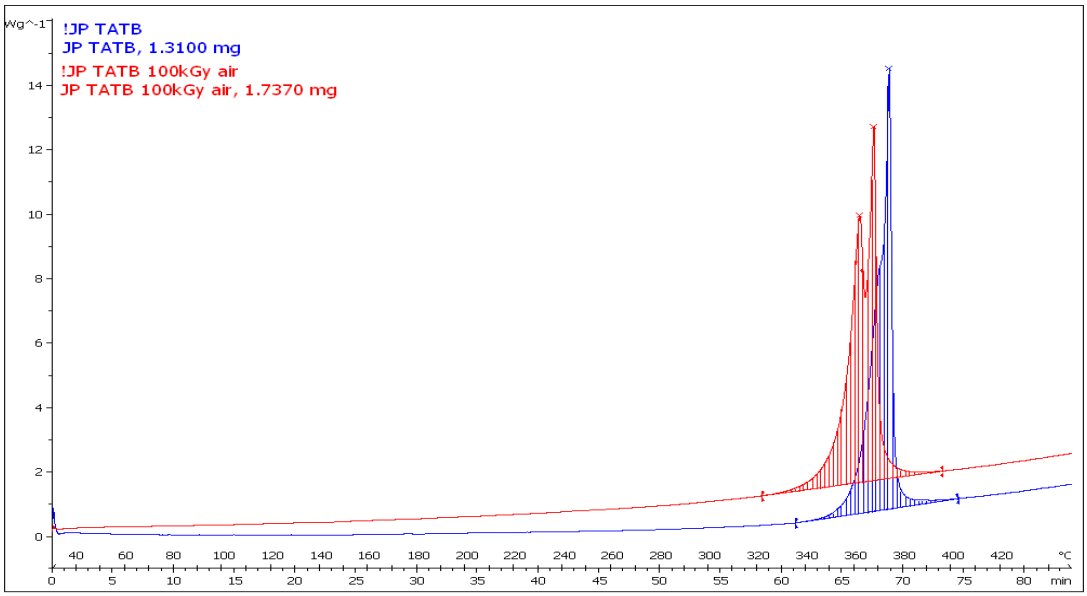

Figure 2.1.2 DSC thermograms for pristine and 100 kGy irradiated TATB from Padfield[24]

All of the studies where irradiated TATB was tested by DTA or DSC found reductions in the onset and peak temperatures exotherms. The other change noted consistently was the colour change from yellow through green to dark green/black. Even with the molecular changes and or furazan decomposition products noted by Skidmore et al.[15], overall, no significant changes in the safety or performance of irradiated TATB have been reported at this time.

The colour change seen in gamma-irradiated TATB is also known to occur when TATB is exposed to other forms of radiation including X-ray and ultra violet (UV)[24-27]. As part of a 1991 PhD study looking at “Inter-phase Modification in TATB-filled Polymer-Bonded Explosives”[26], Kinloch performed a study looking at surface-decomposed TATB. The study was both a comprehensive literature review of the previous work - which is summarised and discussed here - and new experiments attempting to identify the green TATB species. The first work discussed by Kinloch is that of Sharma and Owens in 1979 who studied the decomposition of TATB by ultra violet (UV) radiation and physical shock. X-ray photoelectron spectroscopy (XPS) was used to analyse the samples in a process which uses X–rays to excite a molecule and then counts and energy-analyses the released electrons. The 1s electrons released from the nitrogen in the TATB were analysed and plotted, a lowering of the peak related to nitrogen from nitro groups was noted when compared to the amine-associated nitrogen peak for both UV lamp irradiation and physical shock. The result was attributed to the severing of a carbon nitrogen bond of a nitro group and the release of NO_2, similar to that seen in RDX[28]. Kinloch then went on to review work by Britt et al. in 1980 who discussed the formation of a long-lived radical species formed using X-ray and UV radiation[25]. Electron spin resonance was used to detect the radicals which remained present even after two years at ambient temperatures in air. A tentative structure showed the addition of hydrogen to one of the nitro groups forming a $–NO_2H$ group.

Neither Sharma and Owens or Britt et al[25]. were able to confirm the proposed decomposition products suggested in their initial papers. Both theories

continued in parallel with Kinloch discussing further published papers reporting to support both species. These theories were however discounted in 1984 in papers by Miles et al. and Firsich and Guse, were discussed by Kinloch. Miles et al. noted that mechanical work, UV and gamma radiation all produced the same radical but were unable to find any evidence of this radical being NO_2 as proposed by Sharma and Owens. In the same year Firsich and Guse published a paper in which they used quantum mechanical calculations to form a predicted electron spin resonance spectrum for the Britt et al. proposed radical. The experimental and theoretical spectrum showed a large discrepancy and it was proposed that the H-adduct radical proposed by Britt et al. was incorrect, although an alternative was not offered.

The next significant development in the identification of the green TATB species discussed by Kinloch was a collection of work by Sharma et al. published between 1987 and 1991. In their papers Sharma et al. discussed XPS spectra from the products of mechanical hot-spot initiation centres; these spectra suggested the presence of furoxan and furazan derivatives of TATB. Sharma later noted that these furoxan and furazan products could not be the green TATB species found after irradiation of the explosive due their solubility in acetone compared to the insoluble green species.

Kinloch concluded the literature review by commenting that if the surface substrate was to be employed in the formation of PBX composites then “clarification of its identity and the effects of its presence upon the sensitivity of the bulk explosive would be desirable”.

Kinloch went on to irradiate TATB to doses of 125 and 290 kGy using ^{60}Co with the intention of identifying the green species. The 290 kGy irradiated TATB was compared with pristine TATB using electron spin resonance spectroscopy (ESR), Fourier transform infrared spectroscopy (FT-IR) and Raman spectroscopy; the ESR spectra was described as consistent with previous studies by Britt and Miles. The FT-IR and Fourier transform raman spectrum taken by transmission, specular reflectance and photoacoustic methods proved to be identical to that of the pristine TATB. The spectroscopic analysis

suggested that decomposition products were only present in small quantities and so Kinloch attempted to refine the green species.

Thermal gradient sublimation was used to attempt to isolate the green species; a glass tube containing the sample of the irradiated TATB at its base was continuously evacuated whilst the sample-containing end was introduced into a heating oven and a temperature gradient formed along the glass tube. Sublimation of the sample occurred between 160 and 200 °C forming two distinct bands on the tube walls. After sectioning the more volatile product, (assumed by Kinloch to be the decomposition product), it was found to be partially soluble in dichloromethane; Kinloch's next step was to employ Wiley extraction into dichloromethane refluxing for seven days and after evaporation of the solvent a green solid was present although the solubility of this product was found to be low. Proton nuclear magnetic resonance spectroscopy (NMR) spectra of the extracted product were compared with pristine TATB and Kinloch was able to confirm that the extract was a single product and not a mixture of compounds from the appearance of a doublet at 5.75 ppm.

Kinloch was unable to confirm the identify the TATB radiation decomposition product although, a method for the extraction was tested and proven to be a viable way of extracting samples for further analysis. Although most of the major spectroscopic techniques were utilised on the bulk-irradiated material only NMR was carried out on the Wiley extracted material. This study could have been expanded to include the FT-IR and FT Raman spectra of the extract; this combined with a technique such as mass spectrometry may have indicated as to the identity of the green decomposition product.

Manaa et al. offered a third alternative for the identity of the green decomposition product in their paper "Towards Unravelling the Photochemistry of TATB"[27]. A mixture of computational chemistry and mass spectrometry was used to show that 1,3,5-triamino-4,6-dinitro-2-nitrosobenzene (TADNB) (Figure2.1.3), a nitroso derivative of TATB was the most likely candidate for the green TATB decomposition species.

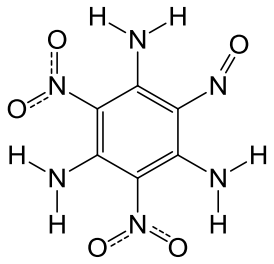

Figure 2.1.3 Structure of TADNB

Semi-empirical calculations were used to produce UV spectra for the previously suggested H-adduct, furazan and difurazan species and the suggested TADNB. Only the calculated TADNB spectrum showed an absorbance peak at 600 nm which is close to the ~550 nm at which green appears in the electromagnetic spectrum.

Mass spectrometry was conducted on samples of TATB, UV-irradiated and synthesised TADNB that had been generated as a by-product from the direct synthesis of TATB from aminotrinitrobenzene. Pristine TATB gave peaks at 258 and 228 atomic mass units due to the loss of NO and it was found that both the UV-irradiated TATB and synthesised TADNB exhibit additional peaks at 242 - corresponding to the mass of TADNB - and 225 atomic mass units. The peak at 225 was attributed to the loss of O and not an amine group by comparison of the high resolution mass spectra for both compounds. Further weight was added in favour of the green detected species being TADNB from *ab initio* quantum mechanical calculations of the energy required to break the C-NH_2 bond (435 kJ mol^{-1}) being significantly more than that required to break the N-O bond (318 kJ mol^{-1}). Finally Manaa et al. noted that TADNB had “been detected as a major product in early shock-induced decomposition TATB”.

As part of their study Manaa et al. also calculated changes in sensitivity and performance which might be caused by TADNB contamination of TATB. The Lawrence Livermore National Laboratory thermochemical code CHEETAH was used and performance calculations were based on TADNB having the same density as TATB. The heat of formation calculated for TADNB was -79 kJ mol^{-1} compared to -146 kJ mol^{-1} for TATB and the energy released was calculated to be 6% less than that of TATB. The reduction in the energy released was

attributed to the poorer oxygen balance of the TADNB. Drop weight impact hazard calculations based on the weakest bond in the molecule were performed. The results revealed that TADNB would be classified as an insensitive explosive, although, the drop hammer height of 100 cm calculated for TADNB was much less than the drop hammer height of >300 cm for pure TATB.

The work by Manaa et al. has offered substantial evidence for TADNB being the molecule responsible for the green species formed from the UV-irradiation of TATB. It can also be concluded based on the comparative work of Miles et al. that the green product of gamma irradiation is also TADNB. Further work still needs to be carried out to assess the hazard implications of the formation of TADNB in irradiated TATB.

2.2 Gamma radiation effects on polymers

The effect of γ-radiation on polymers is almost as vast a subject as that of polymers themselves and will be summarised only before an in-depth look at the polymers of interest to this study is conducted. There are two main types of reaction which are common to all polymers exposed to high energy radiation – cross-linking and chain scission - and the rate at which they occur gives the polymer its radiation characteristics.

Cross-linking is the process in which the absorption of energy from a gamma photon into the molecule causes a covalent bond to break and the formation of a radical. The radical is then able to react with a radical on a neighbouring polymer chain forming a bond between the two chains; H-type cross-linking is the formation of a bond between two adjacent polymer chains whilst Y-type cross-linking is the branching effect where a cross-link forms between the middle of one chain and the chain end of the other. Figure 2.2.1 shows the Y-type and H-type cross-linking of poly-TFE as described by Oshima et al. in 1995[29]. Cross-linking increases the molecular mass of the polymer unit and can result in the formation of a 3D polymer matrix whilst generally causing an increase in Young's modulus, increased hardness, reduced viscous flow and reduced elongation at break[30] .

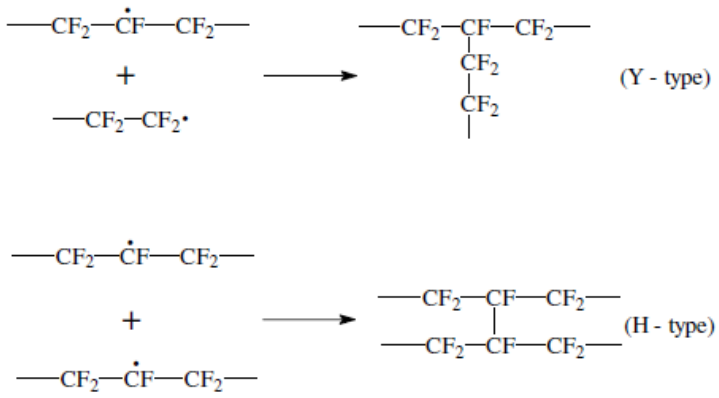

Figure 2.2.1 Possible cross-linking of poly-TFE as described by Oshima et al.[29]

Chain scissions, a break in the polymer chain backbone, result when a bond in the backbone is broken forming a radical. The radical formed is either long lived or reacts with a small molecule to form a new chain end. Chain scissions cause the breakup of polymers into smaller chains resulting in a reduction in molecular mass, decreasing Young's modulus, yield load and elasticity whilst increasing elongation at break[30] .

Both chain scission and cross-linking reactions occur during the γ-irradiation of polymers but the rate at which each reaction happens determines the overall effect on the polymer. Total dose, dose rate and the presence of oxygen can each have an effect on the properties of an irradiated polymer; the total dose given to a polymer will directly relate to the damage inflicted on the polymer. However, dose rate can affect the way a polymer reacts to irradiation when oxygen is present. In an oxygen environment, oxygen is able to react with radicals stopping any further reactions from taking place; therefore, in an oxygen-rich environment chain scission type properties should dominate due to oxidation of radicals before cross-linking can occur. At a higher dose rate radical formation can occur at such accelerated rates, oxygen is unable to react with all the radicals formed and so other radical reactions can occur. Sample thickness can also influence the radiation effects in an oxygen atmosphere. The ability of oxygen to oxidise radicals formed in the centre of a sample is affected by the oxygen diffusion rate through the sample; whilst the outside of the sample shows complete oxidation, the centre may show properties of a sample irradiated without oxygen present. Therefore, if a polymer is irradiated at low dose rates oxygen may be able to diffuse across the sample to oxidise the

radicals resulting in a predominance of chain scission, whilst at a higher dose rate cross-linking is the prominent reaction due to the radical formation rate being faster than the oxygen diffusion rate[14; 30; 31].

It has been well reported that although fluoropolymers are able to withstand degradation by thermal or chemical means, they are susceptible to radiolysis[14; 31; 32]. In their comprehensive 2000 review of "The radiation chemistry of fluoropolymers" Forsythe and Hill[14] discuss the differences between hydrocarbon and fluorocarbon polymers to γ-radiation. Differences are attributed to the characteristics of the carbon-fluorine bond; this bond has the strongest bond energy of any carbon bond at 530.5 kJ mol^{-1}; this compares to the 429.7 kJ mol^{-1} of the carbon-hydrogen bond. Because of this high bond energy and Pauling electronegativity (χ_p) of 3.98, fluorine atom transfer is unlikely. In contrast to hydrocarbons where H_2 is formed, when fluorine radicals are released by scission of a C-F bond, F_2 is not formed because the fluorine radical is not able to abstract other fluorine atoms from the backbone. However it can easily abstract hydrogen atoms to form hydrogen fluoride and cause further chain scissions or chain branching. It was also noted in this review that the fluorine radical formed has been seen to further react with glass to form the compound silicon tetrafluoride. An unusual effect of γ-radiation on fluoropolymers is preferential breaking of the C-F bond and not the weaker (386 kJ mol^{-1} [33]) C-C bond; discussion by Forsyth and Hill of work carried out in the 1960s by Florin and Wall concludes that cage effects and relative diffusion rates and not energetics control the radiation chemistry of fluoropolymer.

2.2.1 Gamma irradiation of FK-800

There is little available work on the effects of γ-radiation on FK-800 or its predecessor Kel F-800; because of this, work on both poly-CTFE and poly-VDF will be considered. Poly-chloritrifluoroethylene (poly-CTFE) as the major component of FK-800 (75%) will be considered in depth while the main radiation effects on poly-VDF will be summarised. Burgess et al.[34] commented in their aging of PBXs report that "Little data exist for the degradation of Kel-F or

Estane by γ-irradiation but it is expected the greatest effect would be caused by exposure at low doses in an oxygen atmosphere". It was true that at the time of writing no reports were available on the γ-radiation effects on Kel F-800 but no attempt was made by Burgess et al. to review the work available on poly-CTFE.

2.2.2 Gamma irradiation of poly-chlorotrifluoroethylene

In their review Forsythe and Hill[14] discussed the irradiation of poly-CTFE and noted the existence of long lived radicals of up to 5 years. Work by Florin and Wall[32] and Lovejoy et al. (cited by Forsythe and Hill[14]) was discussed; in their studies it was found that poly-CTFE only underwent scission reactions, with Lovejoy et al. reporting main chain scission. Florin and Wall found, in mechanical Zero Strength Time tests, little difference between samples irradiated in air and under vacuum and it was also reported by Florin and Wall, but not commented on by Forsythe and Hill, that when irradiated in air poly-CTFE produced high yields of ionic products which were not present when irradiation took place under vacuum. Florin and Wall noted a "curious" absence of SiF_4 when poly-CTFE was irradiated which they attributed to breaking of the C-Cl bond over the C-F bond[32]. It has since been reported that the gaseous products of poly-CTFE when irradiated in glass are carbon dioxide, silicon tetrafluoride and less than 1% halides[35].The case for the preferential loss of fluorine over chlorine was further supported by Hill et al.[36] who found preferential loss of fluorine by infra-red spectroscopy of poly-CTFE irradiated to 1500 kGy at 150 °C.

In a NASA report from 1970 titled "Nuclear and Space Radiation Effects on Materials"[30] , poly-CTFE branded as Kel-F was rated based on physical properties after γ-irradiation as "nearly always usable" up to 100 kGy, "often satisfactory" up to 1020 kGy, before becoming "of limited use" at higher doses. Nigrey and Dickens[37] irradiated several storage container polymer liners to 1.4, 2.9, 5.7 and 36.7 kGy before filling them with a simulated solvent waste for periods of time up to 180 days at 18, 50 and 60 °C. The aim of the work was to test which of the polymer liners would be best suited to handling US DOE process waste. It was concluded that the liner made from 3M Kel-F branded

poly-CTFE had the greatest durability in the tests and outperformed high density polyethylene, cross-linked polyethylene, polypropylene and Teflon™. Neither of these studies included dose rates and so it cannot be determined if dose rate dependence would have affected the results seen.

NMR, FT-IR and DSC studies on vacuum ^{60}Co irradiated poly-CTFE were carried out by Hill et al. in 2002[36]. Poly-CTFE was irradiated at 27, 150 and 220°C to a range of doses up to 1500 kGy at an unreported dose rate. FT-IR analysis of the 150 °C 1500 kGy sample showed new peak formations which were assigned to the formation of double bonds and new CF_3 end groups caused by chain scission. It was also noted that the relative intensity of the C-F peak compared to that of the C-Cl peak decreased with increasing dose, suggesting preferential loss of fluorine over chlorine. It was suggested by Hill et al. that the preferential loss of fluorine could be attributed to the smaller size of the fluorine atom allowing it to diffuse from the polymer cage more readily than chlorine. ^{19}F NMR studies below the melt point of the poly-CTFE confirmed the results of the FT-IR study, with an increasing peak assigned to the formation of new CF_3 chain ends and the relative change in the peaks for CF_2 and CFCl groups confirming the preferential loss of fluorine. A new small broad peak indicating the formation of new double bonds was also seen at approximately -155 ppm. Above the melt point peak, intensities were seen to increase suggesting that the radiolytic reactions took place at a higher rate due to the increased molecular mobility of the polymer. A new peak was also seen at -185 ppm which Hill et al. assigned to the formation of branching points on the polymer chain. However, main chain C-C scission was still the predominant reaction seen in this study.

DSC analysis at a heating rate of 20 °C a minute showed that in the first scan the melting onset of the irradiated polymers started well below the main melt endotherm. Figure 2.2.2 reproduced from Hill et al.[36] shows the first and second DSC scans of poly-CTFE irradiated to 748 kGy at 30 °C. The shoulder in the first scan was attributed to the formation of imperfect crystals formed by polymer chain alignment at ambient temperature following chain scission. The

chain scissions relieve main-chain orientational stress of lamella tie molecules and stresses caused by chain entanglements allowing chains to rotate and align above T_g. The endotherms for the second scans were measured and the degree of crystallinity calculated; Table 2.2.1 presents the DSC crystallinity data from Hill et al. It can be seen from the data that the percentage crystallinity increases whilst the melting temperature decreases with increasing dose. These results were found to be consistent with overall chain scission.

Table 2.2.1 Melting point and percentage crystallinity results from the study of vacuum γ-irradiated poly-CTFE after thermal cycling. Adapted from Hill et al.[36]

Dose (kGy)	Melting temp (°C)	Crystallinity (%)
0	211	30
48	209	35
144	208	44
323	205	50
748	190	55

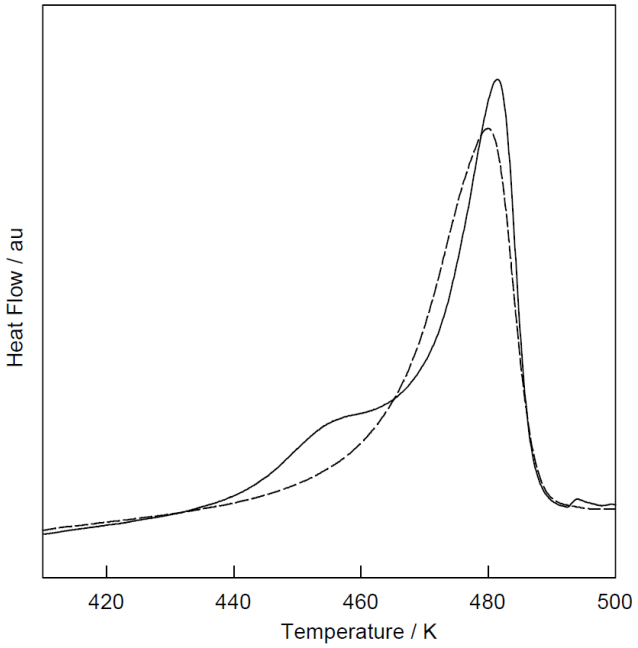

Figure 2.2.2 DSC traces for poly-CTFE, vacuum γ-irradiated at 30 °C to a dose of 748 kGy; first trace (___) and second trace (---). From Hill et al.[36]

It has been concluded by all of the reviewed studies that poly-CTFE predominantly undergoes chain scission when γ-irradiated. It was initially

suggested by Florin and Wall that chlorine was lost in preference to fluorine as would be expected from their relative bond energies. This was later contradicted by Hill et al., who using newer and more sensitive analysis methods, showed that it was in fact fluorine which was preferentially lost. It has also been shown that γ-irradiation under vacuum affects the percentage crystallinity and melt point of the polymer when measured by DSC; no results have yet been published for samples irradiated in air.

2.2.3 Gamma irradiation of poly-vinylidenefluoride

Poly-VDF is known to polymerise by head-to-head and tail-to-tail addition which creates a dipole within the polymer allowing it to dissolve in polar solvents. This ability to dissolve is why a percentage of VDF is often added to fluoroplastics co-polymers. Forsythe and Hill reviewed[14] the radiation chemistry of poly-VDF; they noted that poly-VDF was found to readily cross-link in the presence of ionising radiation. Work by Yoshida et al. was commented on by Forsythe and Hill and gave a chain scission to cross-linking ratio of 0.15 chain scissions per crosslink. Mechanical properties testing reviewed showed a 40% increase in tensile strength at 100 kGy but this dropped to 80% of the start value after further irradiation and the percent elongation was seen to drop to half that of a pristine sample after 10,000 kGy. The reduction in tensile strength and elongation at higher doses was attributed to limited movement of the polymer chain segments in the cross-linked network.

The radiation chemistry of poly-VDF was discussed by Forsythe and Hill and it was noted that the predominant reaction was the elimination of HF, resulting in unsaturation of the polymer chain which could result in the formation of conjugated double bonds. The formation of peroxy radicals when poly-VDF is irradiated in an oxygen atmosphere was also noted. Zhang et al.'s XPS study of the fluorine/carbon (F/C) ratios in poly-VDF before and after irradiation was discussed. It was found that pristine poly-VDF had a F/C ratio of 0.62; after irradiation to 1,200 kGy the ratio had dropped to 0.08 demonstrating a significant loss of fluorine during the irradiation.

2.2.4 Gamma irradiation of Kel F-800

Padfield γ-irradiated granules of Kel F-800 to total doses of 10 and 100 kGy at 300 Gy hr^{-1} as part of his feasibility study[24]. Gas chromatography–mass spectrometry (GC-MS) headspace gas, DSC, He gas pycnometry density, mass change and gel permeation chromatography (GPC) analysis were carried out on the samples; the main results are presented in Table 2.2.2. The results of irradiation in air and vacuum are almost identical and Padfield noted in his report that the seals of the vials showed signs of degradation and so it can be assumed that oxygen was present during all irradiations. DSC results showed no change in glass transition temperature (T_g) at 10 kGy but a four degree change was noted at 100 kGy. The change in T_g along with the highly significant changes in mass average molecular mass measured by GPC (up to 59% lowering) clearly suggest chain scission as the predominant effect on radiolysis. GC-MS headspace found no evidence of the previously reported HF or HCl although when damp indicator paper was placed above the samples an acidic environment was indicated. The sample irradiated to 100 kGy in air showed a small peak at 8.31 minutes which was assigned by Padfield to formyl fluoride. The presence of formyl fluoride has been confirmed as a product when fluorocarbons are UV irradiated and by the ozonolysis of vinyl fluoride. It should also be taken into account that polymer septa were used to seal the vials for Padfield's experiments. Therefore, the presence of formyl fluoride could result from the irradiation of the septa and not the Kel F-800. The lack of other headspace gases detected by GC-MS was attributed to leaking of the vial seals during irradiation and storage. It was concluded by Padfield that further study was necessary to look at the mechanical effects γ-radiation has on Kel F-800.

Table 2.2.2 Results of Padfield's radiation study of Kel F-800 adapted from Padfield[24]

	T_g (°C)			Mass change (%)			Density (g cm^{-3})			GPC M_w change %		
dose (kGy)	0	10	100	0	10	100	0	10	100	0	10	100
Air	24.2	24	20.4	-	-0.2	0.0	2.04	2.05	2.03	-	-18	-54
Vacuum	24.2	24.2	20.2	-	0.0	0.1	2.04	2.03	2.00	-	-15	-59

A recent study by Mayer et al.[38] at Lawrence Livermore National Laboratory used historical ^{60}Co irradiated Kel F-800 samples. The samples had been irradiated to doses of 50, 250, 410 and 700 kGy at a dose rate of 24 kGy hr^{-1} before being stored for an undisclosed period of time. In the study principal component multivariate statistics was used to interpret the results from ^{19}F NMR and these results were then compared to results from GPC. The NMR study showed cross-linking was taking place in the samples and was the prominent reaction in all but the 700 kGy sample which showed evidence of chain scission. The NMR results generally reflect those of the GPC number average molecular mass (M_n) results shown in Table 2.2.3. GPC results shows the M_n and molecular mass dispersity ($Đ_M$) increasing with doses to 250 kGy and then decreasing at 410 kGy with the sample at 700 kGy having a M_n less than that of the un-irradiated sample.

Table 2.2.3 GPC results of irradiated Kel F-800 adapted from Mayer et al.[38]

Radiation Dose (kGy)	M_n (kg mol^{-1})	M_w (kg mol^{-1})	$Đ_M$
0	45.7	178.2	3.9
20	47.7	252.8	5.3
250	88.2	476.3	5.4
410	51	188.7	3.7
700	32.1	240.8	7.5

Mayer et al.'s results contradict those seen by Padfield and do not correlate with the theory that because Kel F-800 is 75% CTFE, chain scission reactions would dominate the γ-radiation chemistry of Kel F-800. It is difficult to draw conclusive comparative results from Mayer et al.'s study due to the lack of sample

information. The conditions the samples were irradiated under, how they were stored after irradiation or the length of time between irradiation and testing were not given. Forsythe and Hill noted in their review that radicals had been seen in poly-CTFE five years after irradiation; this combined with Mayer et al.'s result suggest that initially chain scission is the prominent reaction but slow post-irradiation radical reactions could result in cross-linking of the polymer.

2.3 Gamma radiation effects on polymer bonded explosives

Available research into the effects of gamma radiation on PBXs is very limited and this led Burgess et al. in their 1998 literature review on the aging of PBXs for the US DOE[34] to conclude "At this time no publications relating to the γ-irradiation of PBXs have been noted".

Since Burgess made this statement two studies relevant to this project have been carried out. The first was the 1998 conference paper "Aging and PBX 9502" by Skidmore et al.[15]. PBX 9502 is a Los Alamos National Laboratory formulation containing 95% TATB and 5% Kel F-800 binder which has been in use in the US nuclear stockpile since 1979[15]. Skidmore et al. used samples of PBX 9502 which had been returned from the stockpile for this study; the service life of the material was given for each sample as the time from weapon assembly to disassembly only. The service life did not include time between production of the PBX and assembly or time between disassembly and testing. The three samples used were 7 year aged, 7 year aged then heated to 68 °C for 31 hours and 10 year aged PBX 9502 containing 50% recycled PBX. Unfortunately no information is given for the total radiation dose or dose rates which the three samples received from their service life. Samples were subjected to small scale sensitivity, compressive strength at temperatures below the T_g of the Kel F-800 binder, and thermal ignition tests conducted using either a butane flame or CO_2 laser. The results for the aged PBX were compared with reported results for un-irradiated PBX 9502.

Small scale sensitivity tests consisted of electrostatic discharge, friction and drop weight impact. In "human [equivalent] electrostatic discharge" test 30 mg of PBX was subjected to a total energy discharge of 0.36 J. Friction tests used

30 mg samples placed between a ceramic plate and dowel with a 36 kg load applied; the ceramic plate moved 1 cm relative to the dowel causing friction across the sample. The drop weight impact test used was the Los Alamos National Laboratory type 12a test where a 2.5 kg mass impacts a steel striker which is in direct contact with a 40 mg PBX sample centred on sandpaper. All of the drop weight tests were carried out at the maximum 320 cm for the machine used. In all of the 234 small scale tests conducted, no indication of a reaction was reported for any of the aged PBX samples.

Compressive strength tests used machined 2.54 by 2.54 cm cylinders which were compressed at a constant cross head speed of 0.0127 cm min^{-1}. Average values for the compressive strength were 23.8 MPa for the 7 year aged samples, 23.9 MPa for the 7 year aged then heated samples and 27.6 MPa for the 10 year old 50% recycled samples. The result for both the 7 year aged samples was described by Skidmore et al. to “compare well” with the previously reported value of 23.2 MPa for pristine PBX 9502. The 14% higher compressive strength for the 10 year aged 50% recycled samples was deemed to be consistent with the increase in compressive strength found in un-irradiated recycled PBX 9502. It was suggested by Skidmore et al. that the machining processes used to recycle the PBX are likely to result in smaller TATB particles increasing the compressive strength of the sample.

Thermal ignition tests involved the use of a butane flame and a CO_2 laser. The stockpile aged PBX was found to exhibit no significant differences to the nominal un-irradiated samples.

The study conducted by Skidmore et al. showed no “significant” differences between stockpile aged and nominal PBX 9502 aged to 7 and 10 years. This study does not cover a wide enough range of stockpile ages and with no indication to the total dose or dose rate received by the sample – the dose received by samples could vary due to location within the warhead - conclusions on how PBX 9502 will behave in stockpile munitions over time cannot be drawn from this study.

In his feasibility study of 2008 Padfield[24] conducted a small study on the effects of gamma irradiation on the PBX EDC35 containing 95% TATB 5% Kel F-800 binder. Irradiations were carried out to total doses of 10 and 100 kGy at 300 Gy hr^{-1} in air and under “vacuum”; it was noted in the study that the septum used to seal the vacuum vials had degraded during irradiation and air may have entered the vial. The main results from Padfield’s study are shown in Table 2.3.1. The Figure of Insensitiveness (F of I) was calculated from the Rotter-Langlie 10 shot drop test; samples irradiated in air showed an increasing trend with dose suggesting that the sample became less sensitive to impact, although this cannot be confirmed due to the variability of a 10 shot test. The samples irradiated in the contaminated vacuum vials showed an increase in F of I at 10 kGy but then showed a large drop in F of I to 80 suggesting the sample had become significantly more sensitive to impact. Although the drop in F of I for the 100 kGy contaminated vacuum sample is significant, Padfield noted that this result was based on a 10 sample test and not the full 50 shot Rotter test. The smaller 10 shot sample size could allow larger margins of error than the 50 shot test affecting the final F of I reported. If the reduction in F of I for the contaminated vacuum sample is a genuine result, it was suggested that an incompatibility between decomposition products of the binder and the TATB or changes in the mechanical properties of the binder could be responsible.

The 100 kGy sample irradiated in the contaminated vacuum vial showed a 5.5% reduction in mass which if not an error would suggest significant off-gassing was taking place. DSC results were consistent with those of pure TATB including the formation of a double exotherm peak for the irradiated samples.

Table 2.3.1 Padfield's results for the irradiation of EDC35, adapted from Padfield[24]

	F of I			Mass change (%)			DSC Exotherm onset at 5°C min^{-1} (°C)			DSC Exotherm peak at 5°C min^{-1} (°C)		
dose (kGy)	0	10	100	0	10	100	0	10	100	0	10	100
In Air	102	101	124	-	-2.4	-1.6	366.4	361.2	354.3	379.5	369.3	364.1
											374.7	370.4
Under Vacuum	102	120	80	-	-0.3	-5.5	366.4	361.6	356.7	379.5	369.7	364.5
											375.0	370.6

The results of Padfield's feasibility study suggest that gamma radiation could have a significant effect on the hazard properties of EDC35 as an explosive for use in a radiation environment. Further work is required to confirm or refute the results which were based on a single sample of 0.25 g at each irradiation dose.

The gamma irradiation of PBXs is an under-investigated field. Although only present in small percentages, the potential effect of changes in the binder's mechanical properties and the production of reactive decomposition products from the polymers during irradiation require further investigation. There has been very little research published on the effects of radiation on the mechanical properties of either the polymer binders or PBX of interest. Due to the importance of understanding how a PBX and its components change with exposure to gamma radiation to the nuclear weapons industry, an experimental study was conducted. The first part of the study required the design of equipment to irradiate the samples in a safe manner both in an air atmosphere and under vacuum.

3 Equipment

3.1 Introduction

The irradiation experiments required the design of both an explosive containment unit and bespoke glassware. The containment unit, described in Section 3.2, was designed and tested to protect the ^{60}Co source in the event of a sample explosion as well as control the sample temperature.

Sample vials had to be designed specifically for this project to allow the sealing of polymer and explosive samples in air and under vacuum, whilst allowing the headspace gases to be sampled. Several design iterations were required to achieve the correct specifications and are described in Section 3.3.

3.2 Containment unit for irradiation

The containment unit used for this project was adapted from that used previously at Cranfield University by Padfield[24]. The containment unit consisted of a H83 steel ammunition box placed in the centre of a large steel ammunition box surrounded by vermiculite (Figure 3.2.1). The inner H83 ammunition tin contained the samples and heating unit surrounded by polystyrene and vermiculite as shown in Figure 3.2.2. Vermiculite was used in both the inner and outer ammunition boxes to mitigate blast effects, suppress fire, and act as a thermal insulator. 10 watt heaters with added thermal cut-off switches were included to warm the samples to 36.5 °C. The temperature was raised to represent possible in-service temperatures the TCV PBX may encounter, and to ensure that the FK-800 samples were above their T_g (32 - 34 °C) during irradiation. The sample vials were arranged in an arc so that each vial was equidistant from the circular ^{60}Co source. At the start of this project the containment was only rated to 0.75 g of high explosive, which would not allow the irradiation of enough energetic material for this study, and had to be tested and up-rated for this project.

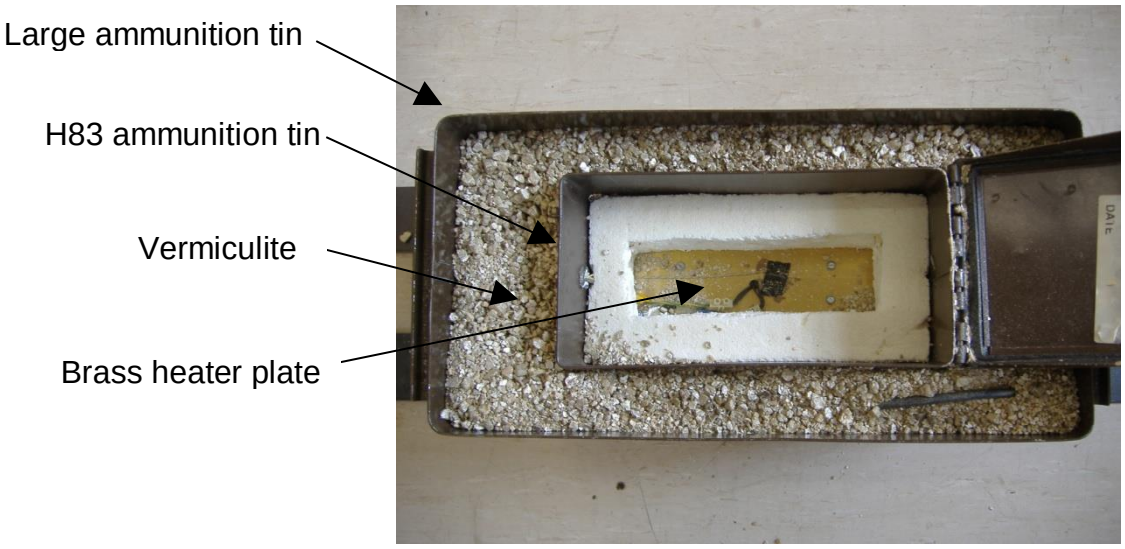

Figure 3.2.1 Photo showing the H83 ammunition tin centred in the large tin and surrounded by vermiculite. The sample holder has been removed to show the heating plate

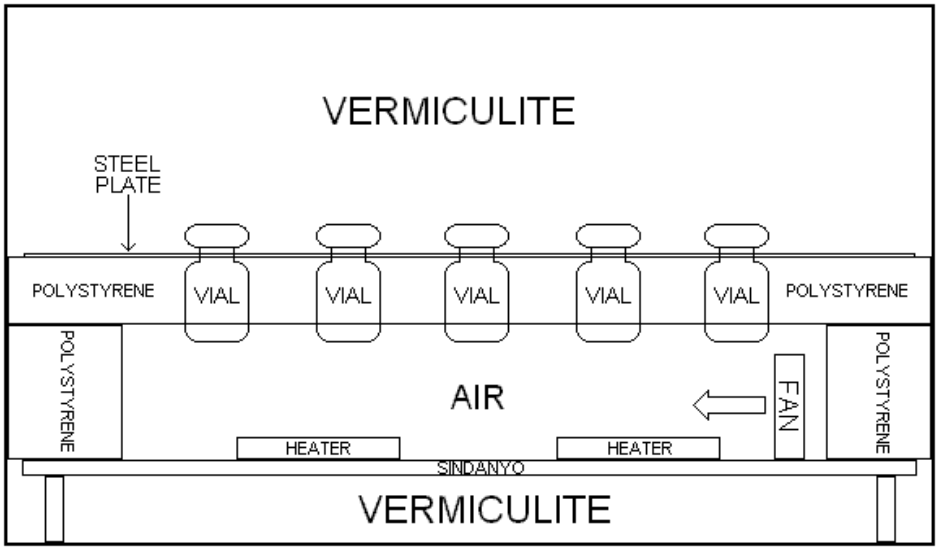

Figure 3.2.2 Diagram showing configuration of H83 ammunition tin as used by Padfield in his study (not to scale)

3.2.1 Up-rating of the containment unit

Fire and explosion containment tests were conducted at the Defence Academy's ERDA range to up-rate the unit for use with quantities of high explosive powder up to 4 g. For the tests, the Sindanyo ceramic plates with heaters attached originally in the containment unit were replaced with blank

Sindanyo plates. This change was made so as not to damage the heater units and wiring during containment testing.

3.2.2 Fire test

The fire test was conducted using 4 g of HMX split evenly between three sample vials, and then placed into the sample holder with an electric match and a small length of ignition cord. HMX - which is a more sensitive and powerful explosive than TATB - was used so that the unit could be rated for use with HMX for future use. The vials containing the HMX were separated by a blank vial, and the H83 unit placed into the large ammunition tin and surrounded with vermiculite as it would be for irradiation experiments. The three HMX samples were then ignited simultaneously and the results recorded on a video camera. An audible click and crackle were heard after ignition with white smoke seen coming from the unit. When the H83 inner ammunition tin was removed, no evidence of an event was noticeable from the outside of the tin (Figure 3.2.3). No evidence of an explosion was evident from any of the sample vials, although the vials shown in Figure 3.2.4 were cracked and blackened from the burning HMX.

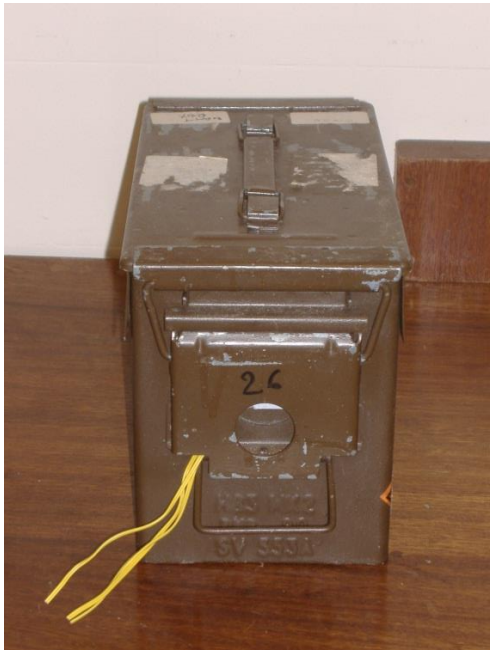

Figure 3.2.3 H83 ammunition tin after burn test; no damage can be observed from the outside.

Figure 3.2.4 Picture of the three glass vials after the burn test. The vials have cracked and been blackened by the burning HMX but no evidence of an explosion can be seen

3.2.3 Explosion test

To prove the containment unit could withstand the force of an explosion, five Daveydet No.8 detonators with 1 g of high explosive each (800 mg PETN plus 200 mg lead azide) were used. One detonator was placed in each of five sample vials and held in place with tape. The H83 was then filled with vermiculite, closed and placed in the large ammunition tin which was clamped to a metal frame as shown in Figure 3.2.5. The detonators were fired simultaneously from a safe distance with the results again being a video record. When the detonators were fired, a loud crack was heard and a puff of smoke seen; the outer ammunition tin was seen to expand and contract and it was estimated from a frame-by-frame analysis of the video that the outer tin expanded no more than 1 cm before returning to its original dimensions. When the H83 inner ammunition tin was removed it could be easily seen that the tin had been damaged under the pressure of the detonation. Figures 3.2.6 and 3.2.7 show front and rear views of the H83 inner unit after the detonation. Extensive distortion can be seen to the H83; however, on closer examination it was found that although the tin had bent and distorted no evidence of splitting or projectile penetration could be found. When the H83 inner unit was opened, the level of the vermiculite had dropped and no evidence of the glass vials was

found (Figure 3.2.8). The cardboard used to form the centre air gap and the Sindanyo plate had been damaged (Figure 3.2.9); however, the steel plate sample holder was intact.

Figure 3.2.5 Picture of the explosion test set-up on the ERDA range

Figure 3.2.6 Picture of the front of the H83 inner containment unit after the explosion test

Figure 3.2.7 Picture of the rear of the H83 inner containment unit after the explosion test

Figure 3.2.8 Picture showing the inside of the H83 inner containment unit after the explosion test

Figure 3.2.9 Picture showing damage to the blank Sindanyo ceramic plate of the H83 inner containment unit after the explosion test

The explosion test conducted was an over-test of the worst case scenario that could take place during an irradiation experiment. The inner H83 ammunition tin was able to contain the explosion without rupturing, and although the outer large ammunition tin was seen to expand and relax by an estimated 1 cm there was no other movement or sign of damage. Based on the results of these tests the containment unit was rated for the irradiation of up to 4 g of explosive as either three powder samples of 1.25 g or six pressed cylinders of 0.6 g.

3.2.4 Design changes to the H83 inner containment unit

Testing was undertaken of the inner containment unit's heating system using the new sample vials designed for this project (vials described in Section 3.3). Empty sample vials with thermocouples attached at the base were placed in the H83 unit and the unit was allowed to heat as normal. As the temperature of the vials was recorded, it was noted that there was uneven heating of the vials, with outer vials being cooler than the centre vial. It was found that the temperature of the centre vial was cyclically exceeding the required temperature as the heaters switched on and off. Measuring of the temperature of the heaters by thermocouple found they were reaching a temperature of 50 °C during their heating cycles; this combined with the positioning of the heaters was causing the uneven heating and cyclic overheating of the sample vials.

A design change was made to resolve the sample heating issue; this involved changing the ceramic plate for a sheet of 0.5 mm thick brass and attaching the two 10 watt heaters to the underside of the brass sheet. By attaching the two heaters to the bottom of the brass sheet the entire sheet was heated, therefore heating the sample vials evenly; overheating was overcome by attaching the proportional integral derivative (PID) controller thermocouple to the brass sheet and regulating the temperature of the sheet at a set temperature. A diagram of the modified H83 inner containment unit is shown in Figure 3.2.10 and a top down picture of the H83 unit situated within the large containment unit is shown in 3.2.11.

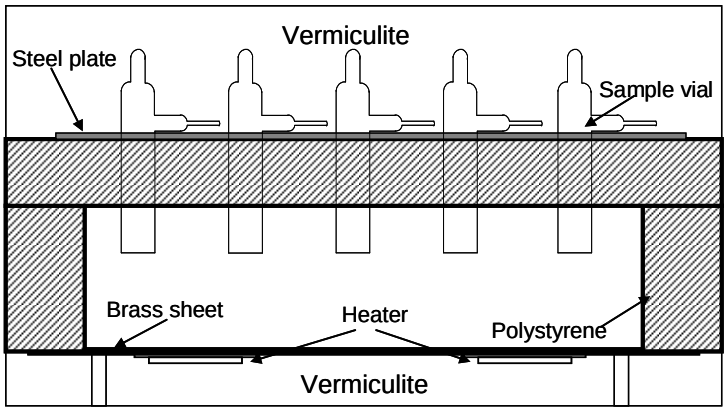

Figure 3.2.10 Diagram of the layout of the H83 inner containment unit used in this study (not to scale)

Figure 3.2.11 Picture of H83 containment unit situated within the large containment unit. The curve in the sample holder can be seen

Due to the changes in the design of the inner containment unit, advice was sought from the explosive experts at Cranfield University on whether further containment testing was required. It was decided that further explosion containment tests were not necessary; the decision was based on the fact that the brass sheet was only 0.5 mm thick and never in contact with explosive samples. Containment of an explosion would be unaffected by an explosion due to the soft metal and there would be no increase in the risk of fragmentation caused by the brisance effect with the explosive never in contact with the brass sheet.

3.2.5 Polymer heater units

In addition to the two containment units built to contain and heat explosive samples during irradiation, two polymer-only heating units were built to enable additional samples to be irradiated at controlled temperatures.

The two polymer heater units were identical in design to the H83 inner containment unit described above but were not contained within a larger ammunition box. The use of four heater units, two within the explosive containment units and two in the polymer heater units, required the construction of a power control unit to power the heaters and regulate the temperature within the units.

3.2.6 Power control unit

The power control unit shown in Figure 3.2.12 consists of four PID controllers, which are used to control solid state relays supplying power to the heaters in each of the individual sample containment units. The temperature within the heater units is monitored using a thermocouple attached to the PID controller; the PID then switches power on and off to the heaters. A wiring diagram is shown in in Figure 3.2.13 and shows the wiring configuration for the control unit and the four containment units. The power control unit was situated outside of the radiation chamber to protect the electronics from radiation effects and connected to the heater and containment units by 15 m cables.

Figure 3.2.12 Picture of power control unit showing PID controllers and containment unit thermocouple and power cables attached

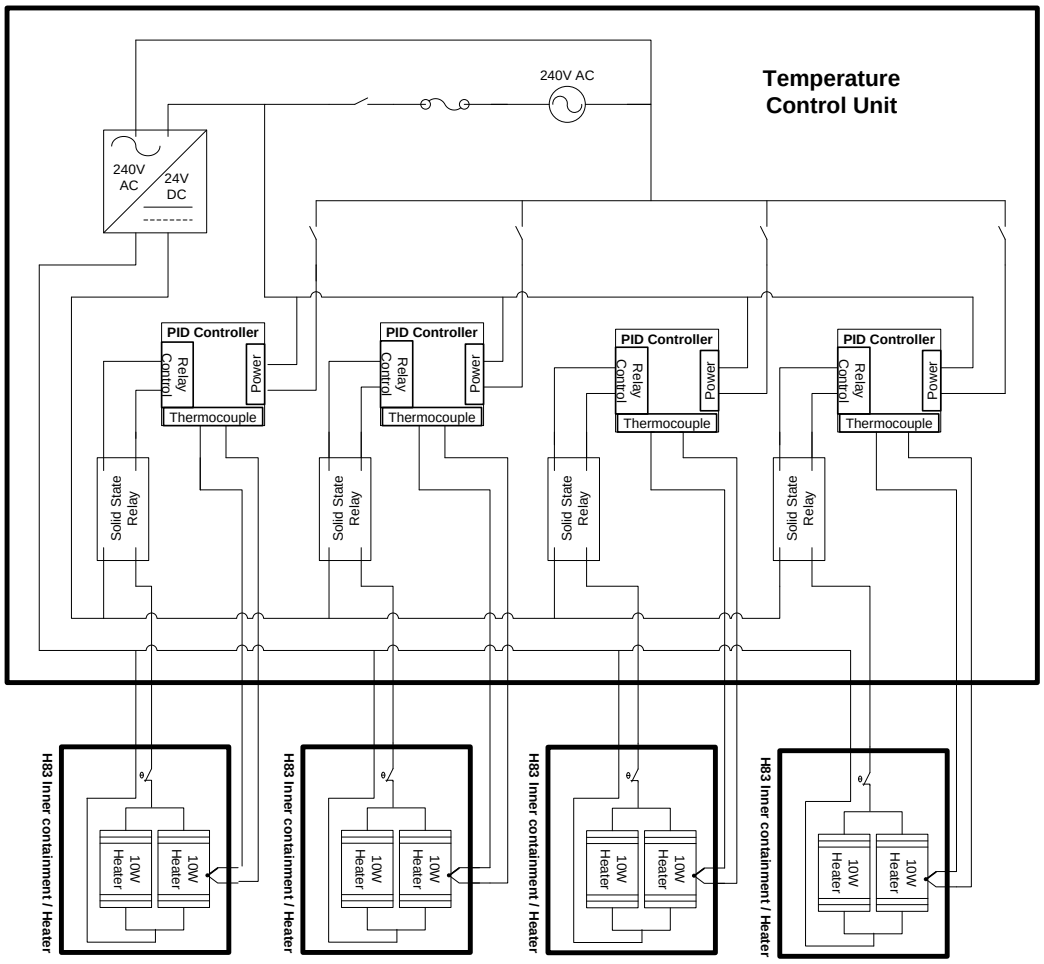

Figure 3.2.13 Wiring diagram of the power control unit and H83 heater units

3.3 Sample vials

In two previous studies at Cranfield University[24; 39]10 ml Chromacol glass vials with rubber septa were used as sample vials for the irradiation of polymers. Padfield[24] found during his study that the rubber septum showed signs of gamma radiation degradation leading to the conclusion that a vacuum could not be guaranteed. Padfield also noted that any gasses given off by the Chromacol septa could mask those given off by the polymer being studied. It was therefore decided that, for this study, an alternative sample vial which could contain a vacuum without the need for polymer seals should be sought. The design of a vial which met these requirements took several design iterations and these are described below.

3.3.1 First glass design

An all-glass vial and tap configuration was produced (Figure3.3.1 and 3.3.2) and tested using a radiation-resistant Apiezon M vacuum grease to seal the ground glass joints and all-glass tap. Vacuum tests were conducted using an electronic pressure transducer to monitor the pressure inside the assembly over a period of time. During bench tests it was found that this design of assembly could only hold a stable vacuum for approximately 48 hours before leaking; this period of time was not sufficient to complete the intended irradiations and so the design was rejected.

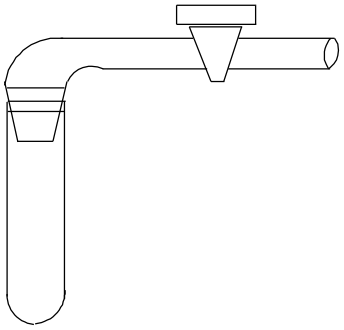

Figure 3.3.1 First glassware design without pressure transducer side arm

Figure 3.3.2 Picture showing first glassware design

3.3.2 Second glass design

After the first design was rejected, a silicone rubber septum with one face coated with aluminium was sourced to fit the Chromocol headspace vials. The aluminium would allow a Chromacol vial to be used as a sample vial without any degradation products produced during irradiation entering the vial. This meant that as long as the seal could hold a vacuum consistently it would be suitable for this project.

Again a pressure transducer was used to monitor the pressure inside the vial whilst the vacuum tests were taking place. The Chromacol vial is shown in Figure 3.3.3 and 3.3.4 with a ground glass tap attached via a side arm. The side arm allowed evacuation of the Chromacol vial without the need to pierce and damage the aluminised septum. It was found that in three tests, two did not form a vacuum seal, and the one vial which initially sealed leaked after only 24 hours.

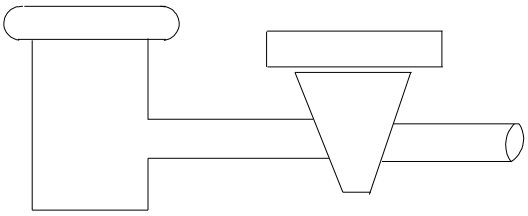

Figure 3.3.3 Chromacol vial with side arm and gas tap

Figure 3.3.4 Picture showing prototype of second glass design consisting of a Chromacol vial and side arm with gas tap attached

3.3.3 Third glass design

The third design of glass vial using a ground glass tap is shown in Figures 3.3.5 and 3.3.6, this design used a ground glass stopper to close the vial and had a tap attached via side arm to allow evacuation. This differed from the first design in not having the mass of the tap affecting the fit of the glass stopper. This design also allowed the stopper to be clamped to the vial by means of a rubber band or clamp.

As with the first design it was found that a stable vacuum could not be sustained for any period of time during tests. It could also not be determined which of the ground glass connections were leaking.

It was at this point that the decision was made to move away from the use of grease-sealed ground glass joints and look for an alternative.

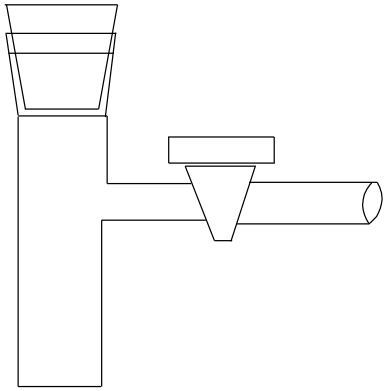

Figure 3.3.5 Third glassware design

Figure 3.3.6 Picture showing a prototype of the third glass design. A rubberband has been used to clamp the glass stopper and the port to the left was used to attach the pressure transducer

3.3.4 Conflat-type all-metal design

Conflat (CF)-type all-metal seals were investigated as an alternative to glass joints. In CF joints a copper gasket is used with an all-metal design; the two CF flanges both have knife edges and when bolted together with a copper gasket, cut into the copper forming a vacuum-tight seal. This type of vacuum joint is widely used in very high vacuum systems and has been proven to hold a secure vacuum without the need for polymer seals. After some investigation it was found that with a height of 120 mm and mass of 0.5 kg[40] the most suitable all-metal valves and sample containers would require a complete redesign of the sample containment unit. It was at this point that with the high costs both financially (£524[40] per valve and £93 per vial[41]) and in time, to

redesign and test the containment unit, it was decided another option was required for this project.

3.3.5 Final sample vial design

After the failure of the glass joints and the decision not to use the all-metal CF type joints, flame-sealing was investigated as a way of sealing glass vials. If it could be proven that during the sealing process any energetic samples would not be heated to such an extent as to cause an accidental ignition then this process could be used safely.

Figures 3.3.7 and 3.3.8 show the design of the glass vial designed to be flame-sealed. The vial has an outer diameter of 22 mm and a length to the loading tube of 75 mm. A narrower glass loading tube is extended out from the top of the vial through which the samples are loaded and the vial flame sealed. The extended length of the loading tube also allows the vial to be evacuated whilst being sealed, thus sealing the samples under vacuum conditions. A side tube which has been narrowed to a fine glass point is also used in this design. The side arm allows a flexible vacuum pipe to be attached for headspace gas extraction. By bending the attached vacuum pipe the fine glass break tube can be broken allowing extraction of headspace gasses from the sample vial.

Once the vial design had been finalised, testing was conducted to prove that the flame-sealing process could be carried out without overheating the samples.

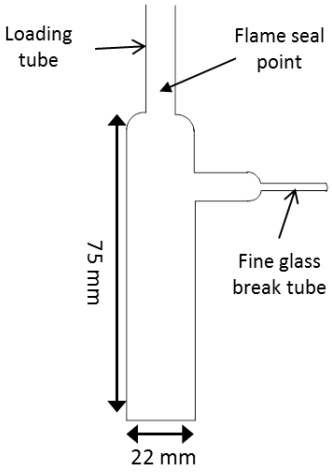

Figure 3.3.7 Final sample vial design

Figure 3.3.8 Picture of the final glass vial design.

3.3.6 Sample vial thermal testing

To show that energetic materials could be safely flame-sealed in the sample vials, experiments were conducted to show that sample heating could be controlled. The first test used 1.3 g of cyanuric acid (acting as an energetic substitute) loaded into the sample vial and the temperature was measured using three type K thermocouples. Two thermocouples were pressed up against the glass, one near the top and the other about halfway down; the third was inserted into the powder at the bottom to measure the temperature in the sample. A picture of the experimental set up is shown in Figure 3.3.9. The vial was clamped during the test to stop the thermocouple detaching from the glass. A natural gas and oxygen torch was used to seal the vial whilst a Grant 1200 series Squirrel data logger recorded the temperature at two second intervals. It can be seen from Figure 3.3.10 that the maximum temperature reached during this test was 54 °C at the top of the vial. Within the powder sample the maximum temperature rise was 2 °C from 23 to 25 °C, well below the 60 °C which was set as a maximum sample temperature to avoid melting of the polymer binders or the risk of thermal decomposition in the explosive / PBX formulation.

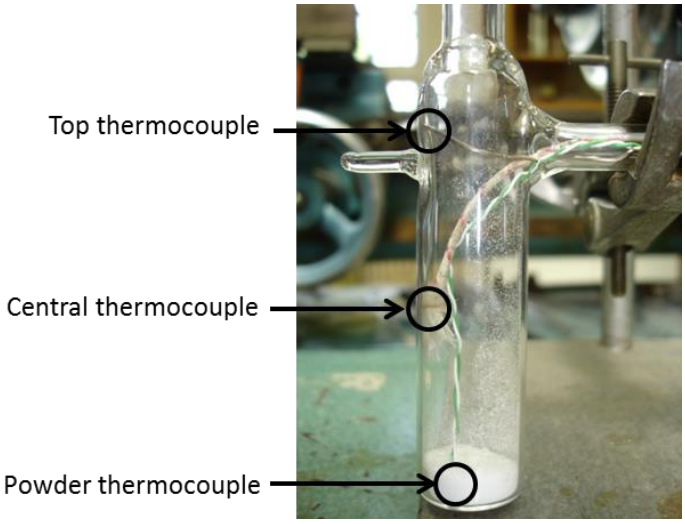

Figure 3.3.9 Picture showing vial ready to be sealed for thermal test 1. The position of the three thermocouples used are indicated

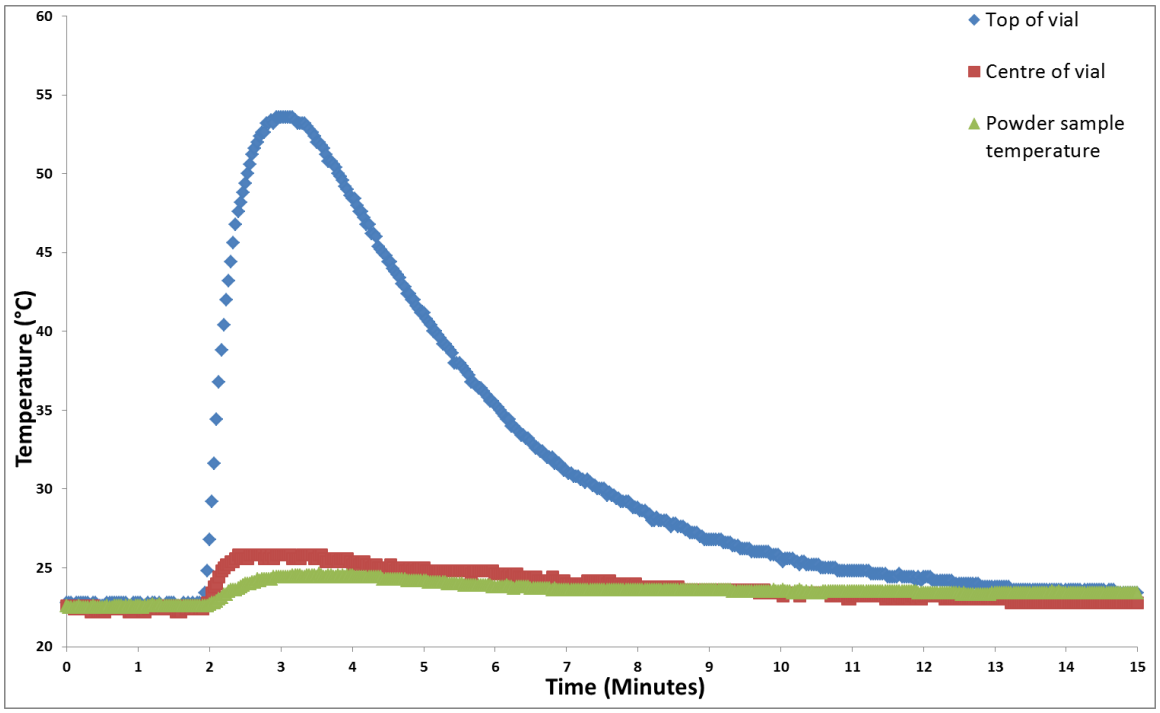

Figure 3.3.10 Plot of the thermocouple data from glass vial (heating test 1)

A second thermal test was carried out to ensure that if a vial was heated for an excessive time during sealing, the sample temperature would still remain below the 60 °C limit, and also that molten glass would not drop into the vial.

The experimental set up for the second test was identical to that of the first test. The sample vial was sealed and continuously heated at the seal point using a

flame of higher intensity to generate more heat than would normally be used for 2 minutes 5 seconds. This was four times longer than the thirty seconds required to seal a vial under normal conditions. Figure 3.3.11 shows a maximum temperature of 194 °C at the top of the vial during this test with a much lower rise being shown by the lower thermocouples. The cyanuric acid powder showed a rise of 12 °C from 23 to 36 °C, which is still lower than the proposed maximum temperature of 60 °C.

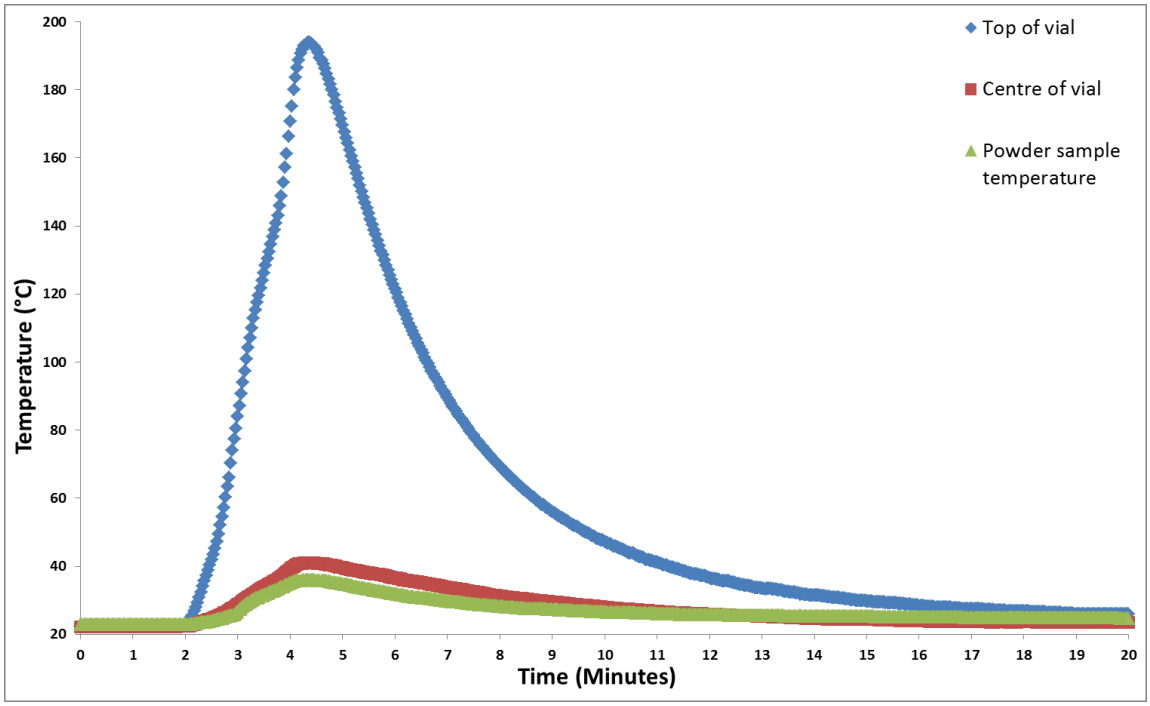

Figure 3.3.11 Plot of the thermocouple data from glass vial (heating test 2)

A final test was required with the vial under vacuum using all of the safety precautions that would be in place for sealing energetic materials. For the final test, the sample vial was clamped with the vacuum line attached to the loading tube, a blast screen was set up in front of the vial (Figure 3.3.12) and the person sealing the vial also wore a full face shield. As an added precaution the vial was stood in a plastic container of ice water. The ice water acted to cool the vial, and also to wet any energetic material in the event of the glass vial cracking, thus rendering the energetic material safe.

Figure 3.3.12 Picture showing the experimental set up for heating test 3. The vial can be seen standing in the container of ice water with a vacuum pipe attached

The results of the third test are shown in Figure 3.3.13. With the addition of the ice water, the maximum temperature reached by the cyanuric acid powder is 9 °C; this is a rise of only 1 °C from the start temperature of 8 °C. The maximum temperature at the top of the vial was 40 °C which was the lowest of all three tests and below the maximum 60 °C originally suggested for the powder sample.

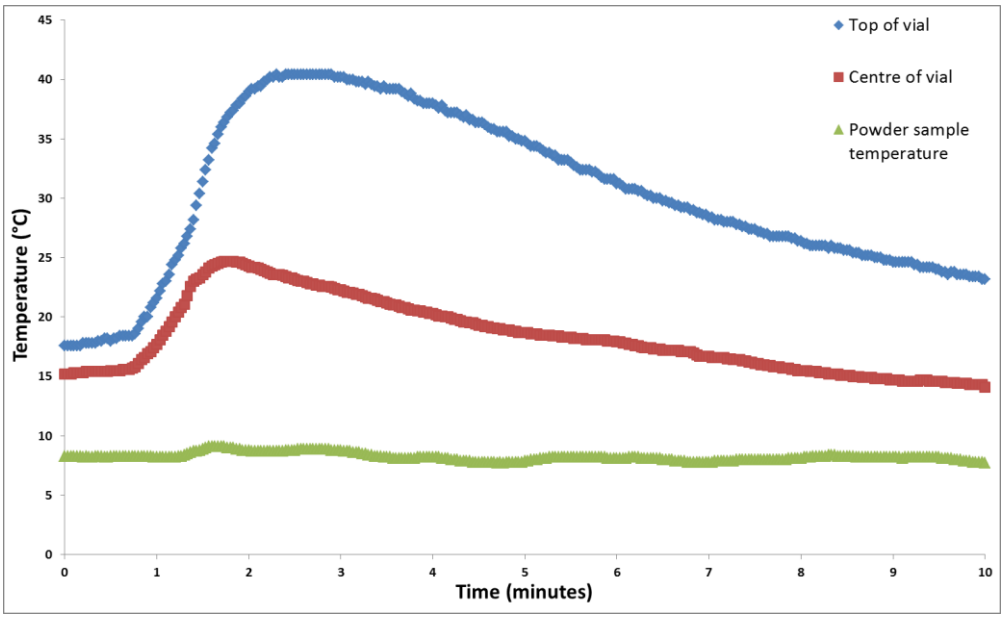

Figure 3.3.13 Plot of the thermocouple data from glass vial (heating test 3)

3.3.7 Conclusion

The results of the three thermal tests showed the final glass sample vial design could be safely flame sealed without risk of an energetic event from sample heating. This design was adopted as the sample vial for use during this project.

Once the initial equipment design phase had been completed, the materials being studied had to be prepared and irradiated before analysis. The materials used and their preparation and irradiation are described in Section 4.

4 Sample preparation and irradiation

Before samples could be analysed, they first had to be prepared and irradiated. The polymers were supplied in either powder or pellet form and explosives were supplied as powders. This section will describe the methods used to prepare the samples before irradiation and the ^{60}Co gamma irradiation of the prepared samples.

4.1 Materials

Below is a list of materials which were irradiated for this project.

4.1.1 Polymer

- **3M FK-800** lot no. 2, commercial copolymer of CTFE (75%) and VDF (25%). Supplied as a powder by AWE plc.

4.1.2 Explosives

- **TATB** Type B batch no. AD/5/101. Supplied as a powder by AWE plc.
- **TCV** (TATB Type B/FK-800 (95/5 w/w)) batch no. BD/49/8. Formulated at Cranfield University.

4.2 Sample irradiation

4.2.1 The JJ Thompson irradiation facility

The JJ Thompson irradiation facility at Cranfield University, Shrivenham is a metal-shielded retractable ^{60}Co type with an activity of 510 TBq at the start of this project. The radioactive material can be raised and lowered mechanically from a shielded position inside the large irradiation cell to expose samples. Dose rates are controlled by adjusting the distance of the sample from the aluminium can (Figure 4.2.1) into which the source is raised. Exposure times can be accurately controlled by the use of an automated timer to lower the radioactive material, allowing for samples to be irradiated to accurate total doses.

Figure 4.2.1 A picture of the irradiation cell showing the aluminium can into which the ^{60}Co is raised from its shielded position in the centre of the metal block

The ^{60}Co source is made up of 12 individual ^{60}Co rods in argon welded steel cans, contained in small steel tubes within a jig to form an open cylinder (Figure 4.2.2). To expose samples, a shutter above the jig opens and the jig containing the ^{60}Co is raised into an aluminium can which protrudes from a work surface in the centre of the 4 m x 3 m x 3 m high irradiation cell[42]. The central dose rate inside the aluminium can at the start of the project was calculated to be 35.6 kGy hr^{-1}.

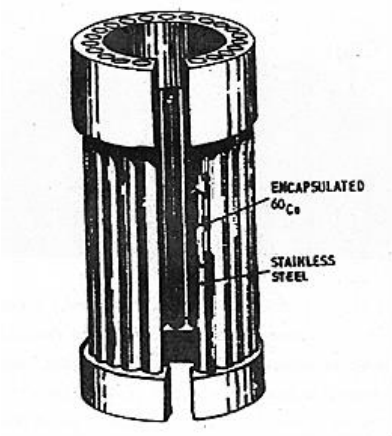

Figure 4.2.2 Diagram of the jig which holds the ^{60}Co within the Cranfield University radiation facility, reproduced from [42]

The JJT source's radiation field behaves as if the ^{60}Co source were a point source. The horizontal maximum intensity, when the jig is raised, is at a height of 11 cm from the bench surface and drops away to 80 % field strength 2 cm either side of the maximum before dropping off rapidly.

4.2.2 Absorbed dose and dose rates dosimitry

As noted in Section 1 absorbed dose is measured in gray (Gy) with one gray being equal to the absorption of 1 J kg^{-1} of material. For all irradiation experiments in this project the absorbed dose is quoted as gray absorbed by water ±5% error.

Dosimetry was carried prior to sample irradiation using a PTW Unidos dosimeter with a 0.6 cm^3 ion chamber with a quoted error of ±5 %. The ion chamber was placed within the containment unit at a height equivalent to 11 cm from the bench surface. Five measurements of dose rate were recorded at various distances from the centre of the source; the recorded dose rates were used to form a calibration curve allowing the distance from the source for any dose rate to be calculated. Equation 4.2.1, was used to compensate for the decay of the ^{60}Co source over time, where A is the present source activity, A_0 is the source activity at time 0, λ is natural log of 2/half-life and t is the time since $A_{0.}$

$$A = A_0 e^{-\lambda t} \quad \textbf{(4.2.1)}$$

The projected maximum dose rate over the 3 year duration of this study, whilst maintaining the required 5 cm safety gap between the containment unit and the source, was calculated to be 1.8 kGy hr^{-1}, this rate was adopted as the higher dose rate for sample irradiation.

4.3 Preparation of polymer samples

The FK-800 was supplied as a powder and before irradiation, the polymer had to be formed into bars and dogbones ready for post-irradiation mechanical analysis. Cut samples were then inserted into sample vials and sealed in air or under vacuum.

Post-irradiation, the polymer samples were stored in their unopened sample vials at -20 °C. Low temperature storage was used to limit the speed of post-irradiation reactions[39] within the samples until the samples were required for characterisation.

4.3.1 Polymer sheets

To enable the production of samples for mechanical properties testing, sheets of polymer were needed from which samples could be cut. An initial trial was made using solvent to dissolve the two polymers and then cast them into a mould. After casting, the sheets were stored open in a fume cabinet to allow the solvent to evaporate. Solvent casting was found to give inconsistent thickness of sheet, and sheets also showed signs of residual trapped solvent. It was decided that a solvent-free method of sample preparation would be required.

Thermal pressing was selected as a method of producing sheets of FK-800. A Moore of Birmingham press with active PID-controlled heating and cooling was used to press the polymers into a mould.

The mould used was made from 2 mm thick sheet steel which had four 85 mm by 85 mm squares cut out of it. Before pressing, the polymers were first heated under vacuum for 2 hours to bind the powder together into a single block. The temperature of the oven was set at 100 °C.

The agglomerated polymer was placed into the mould with a sheet of non-stick heat-resistant poly-VDF film above and below. The press was set to 100 °C and gentle pressure was applied to ensure contact with the heated surfaces was maintained. Once the press had reached the desired temperature, the pressure was raised to 1.17 MPa acting on the mould for 5 minutes at the set temperature. Pressure was maintained whilst the polymer sheets were cooled to ambient temperatures using the active water-cooling of the press before removal from the press.

4.3.2 Polymer bars and dogbones

Both bars and dogbone samples (Figure 4.3.1) were cut from the pressed polymer sheets before being loaded into sample vials for irradiation. Bars were cut from the 2 mm thick sheets using a craft guillotine to dimensions of 25 mm x 5 mm. Dogbone samples with a gauge of 20 mm x 5 mm for tensile load testing were stamped from polymer sheets. To ensure uniformity of shape, the sheets were cooled using ice to ensure the sheets were below their T_g before stamping.

Figure 4.3.1 Picture of a polymer dogbone and bar sample before irradiation.

Sample sets for FK-800 were made up of four vials with three dogbones in each, and four vials with three bars in each. Two vials of dogbones along with two vials of bars were sealed with an atmosphere of air and the remainder were sealed under vacuum. Vacuum vials were degassed for 2 hours to 10 mbar before being evacuated to less than 3 mbar and sealed under continuous vacuum.

One sample set of polymers was irradiated to each total dose of 10, 20, 50, and 100 kGy at 1.0 kGy hr^{-1}, and 10, 20, 50, 100 and 200 kGy at 1.8 kGy hr^{-1}.

4.4 Preparation of explosive samples

Explosive samples were irradiated as both powder and pressed cylinders of 10 mm diameter x 4 mm high for this study. The samples were irradiated in

flame-sealed sample vials and then stored post-irradiation in their unopened vials within a closed metal box at ambient temperatures.

4.4.1 TCV PBX pressed cylinders

Cylinders of TCV were single-end die-pressed using a remotely-operated 10 tonne hydraulic press

PBX moulding powder was weighed to a mass of 0.608 g then loaded into a cylindrical press tool. The press tool was heated using a heater jacket to 100 °C and once the desired temperature was reached a 5 minute equilibrium period was allowed before pressure was applied. Once the temperature had equalised, a pressure of 220.75 MPa was applied to the press tool for 1 minute. After pressing, the samples were allowed to cool before removal from the press tool. The samples were allowed to relax for a minimum of 12 hours before mass, dimension and density measurements (see Section 5 for method) were taken. Tolerances of 4.00 ±0.05 mm were set for the cylinder height and 1.890 ±0.005 g cm^3 for the cylinders' densities were set.

Five cylinders of PBX were irradiated to total doses of 10, 20, 50 and 100 kGy at 1.8 kGy hr^{-1} under vacuum. Each cylinder was placed in a separate sample vial and evacuated for 5 minutes before being sealed as described in Section 3 to a pressure less than 3 mbar.

4.4.2 TCV powder samples

1 g of PBX powder was carefully added to a sample vial and evacuated for 5 minutes before sealing under vacuum as described in Section 3 to a pressure less than 3 mbar. The powder samples were irradiated to doses of 10, 20, 50 and 100 kGy at 1.8 kGy hr^{-1}.

4.4.3 TATB Type B powder samples

Three 1.25 g samples of TATB were placed in 20 mm x 70 mm screw cap vials with caps and irradiated to total doses of 10, 50 and 100 kGy at 1.8 kGy hr^{-1}.

5 Characterisation techniques

Post-irradiation characterisation of samples was intended to study changes in the bulk mechanical properties of the materials, and to identify chemical changes which would explain these changes in bulk properties. A range of characterisation techniques were used, and this section gives a description of the methods used to analyse the samples and the principle behind the technique.

5.1 Tensile load testing

Tensile load testing is the most common mechanical properties technique, often described as stress-strain analysis. The test involves the uniaxial stretching of a material sample across a known gauge length. The technique can be used for the analysis of many different materials including metals, ceramics and polymers. The theory of stress-strain analysis is well described in the literature including references [43-46] and so only the main aspects will be covered here.

When a sample is tested, the sample is clamped in place and pulled at one end at a constant displacement rate (strain rate) set by the operator. The force exerted on the sample is recorded with the use of a load cell attached to the sample; the load in newtons is normalised by dividing the load by the sample cross-sectional area of the sample to give a stress (σ) in Pascals. The displacement of the sample across a known gauge length can be measured and normalised to a strain (ε) by dividing the change in gauge length by the original gauge length.

The sample's tensile or Young's modulus (E) defined as the slope of the linear elastic region of the stress-strain curve, stress at yield (σ_y), ultimate tensile strength (σ_s), elongation at break and permanent elongation are the most important measurements taken. Figure 5.1.1 shows a diagrammatic representation of a stress-strain curve for a typical semi-crystalline polymer, indicating where each of the measurements is taken.

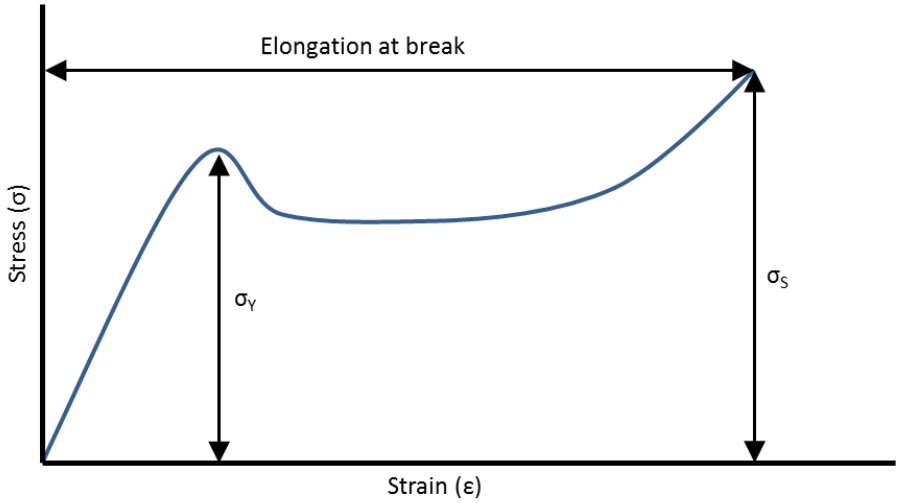

Figure 5.1.1 Diagrammatic representation of the stress-strain curve of a semi-crystalline polymer. The diagram also shows the points at which the main measurements are taken.

Tensile load test results can be affected by both strain rate and sample temperature, often making reported results difficult to compare unless all experimental conditions are known. The sample's temperature when tested can affect whether the material is above or below transitions such as $T_{g,}$ changing the tensile behaviour. For polymers, an increase in the mean molecular mass, or formation of inter-chain crosslinks, will cause a polymer to stiffen and become brittle. This will be indicated in the stress-strain curve by an increase in E and a reduction in elongation at break. Yield behaviour of a polymer is affected by the polymer's crystallinity, while tensile strength can be affected by a combination of factors including, polymer chain molecular weight, crosslink density and monomer composition[44-46].

5.1.1 Tensile load testing of irradiated FK-800

Irradiated and pristine dogbone samples of FK-800 with a gauge length of 20 mm were tested using an Instron 4206 material testing machine. The FK-800 samples were heated in situ to 40 °C to ensure they were above the FK-800's T_g thus representing the possible service temperature. The samples were clamped into the Instron and heated over a period of 5 minutes using a clam shell oven until a temperature of 40 °C was recorded by a thermocouple attaced

to the sample surface. The thermocouple was removed and the sample tested with at a strain rate of 200 mm min^{-1}. A high strain rate was used to ensure the samples failed during the test; when tested at lower train rates sample material was able to draw from the ends of the dogbone holding the sample in place therefore affecting the recorded results Due to the high strain rate, no discrete measurement of strain was used and so sample displacement recorded by the testing machine was used.

5.2 Dynamic mechanical analysis (DMA)

Dynamic mechanical analysis (DMA)[47; 48] is a materials properties technique which allows us to study changes in mechanical properties as a function of temperature, strain rate or both. DMA is a very powerful technique and allows the study of how a sample's modulus changes with temperature and/or strain rate, something which would take a large number of samples to achieve with tensile load testing alone. In this study DMA was used to identify mechanical changes to the polymer samples after irradiation.

DMA applies a sinusoidal stress to a sample at a set frequency and records the sample's response; a diagrammatic representation of this is shown in Figure 5.2.1. From the material's response to a known force, stiffness (storage modulus, E') can be calculated, from the sample recovery, and viscosity (loss modulus, E'') and from the phase lag giving rise to a complex modulus (E*).

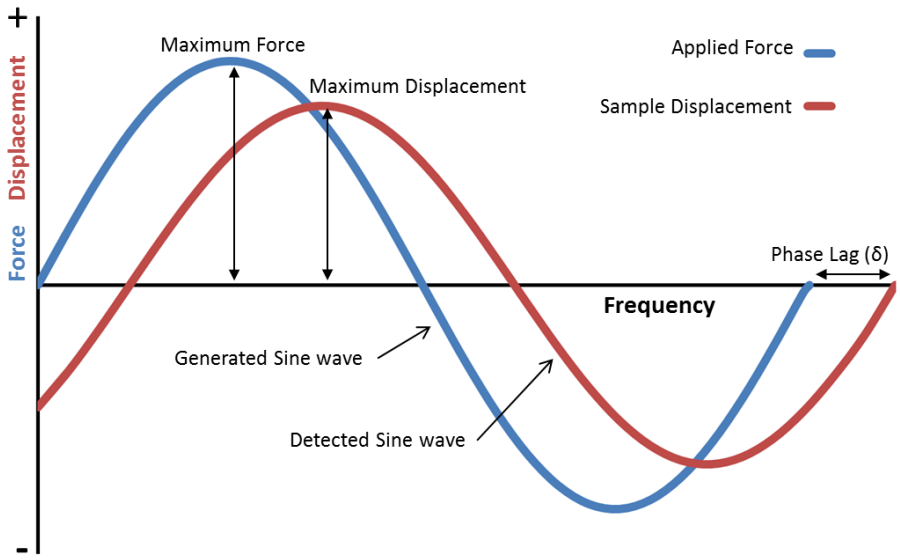

Figure 5.2.1 Diagrammatic representation of the sine wave applied to a sample by a DMA and the sample's response.

The storage modulus (E') can be said to be a measure of the material's stiffness or ability to return energy elastically when acting as a Hookean spring. In contrast the loss modulus (E'') can be described as the materials viscosity or ability to act as a Newtonean dashpot loosing energy to internal molecular motion. The combination of these two properties gives a polymer its viscoelastic behaviour at a given temperature.

As a force (energy) is applied a polymer instantaneously deforms elastically (spring like) through the stretching of atomic bonds, giving rise to the polymers storage component (E'). However, over time the viscous processes of creep or stress relaxation take place; in these processes energy is "lost" to internal molecular motion, giving rise to the polymers loss component (E''). The time scales for creep or stress relaxation are temperature dependent due to the thermodynamics involved in the internal molecular within the polymer.

Creep takes place when a constant force is applied to a polymer in its viscoelastic temperature range. An instantaneous displacement will occur due to the elastic response of the atomic bonds, however, over a period of time the displacement will increase due to molecular movement within the polymer. This

can be visualised using the Voigt-Kelvin model [49-51] (Figure 5.5.2 (a)). The model consists of a Hookean spring, representing the spring like response of the polymer's atomic bonds, and a Newtonean dashpot, to represent molecular motion. In the model the spring and dashpot are connected in parallel, therefore, as a force is applied a deformation, resisted by the spring (E), takes place at a rate governed by the viscosity of the dashpot (η). The model then continues to deform (creep) until the restoring force of the spring matches that of the applied force.

Stress relaxation is the converse of creep. An abrupt fixed displacement is applied to the polymer resulting in a measureable load, due the elastic resistance of the polymer's atomic bonds. Over time the internal motion of the polymer's molecules un-coiling or flowing over each other causes a reduction in stress without a change in displacement. The Maxwell model[49-51] (Figure 5.5.2 (b)) visualises this principle of stress relaxation; an instantaneously applied deformation is initially taken up by the extension of the spring (E). As the deformation is maintained, the load is decreased over time by motion within the dashpot (η) thus allowing the spring to shorten.

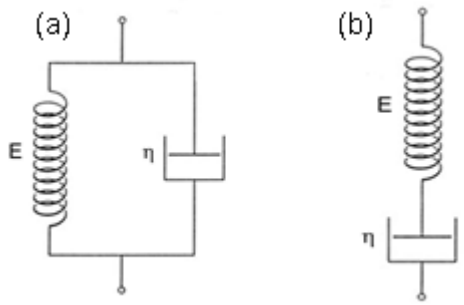

Figure 5.2.2 Diagrammatic representation of the Voigt -Kelvin model for viscoelastic creep (a) and the Maxwell model for stress relaxation (b) adapted from [52]

The modulus values E*, E' and E'' measured by DMA, allow for better characterisation of a material than Young's modulus from a stress-strain curve, and the two should not be compared. The DMA modlui measure the polymers ability to return energy (E'), lose energy (E'') and the ratio of E"/E' (tan δ). When plotted, tan δ allows transitions to be easily spotted as peaks, the height of

which are indicative of the amount of material involved in the transition and, as such is a useful tool.

To allow the testing of different materials and their behaviour to different kinds of applied stress, most DMA instruments are able to operate in multiple sample configurations (Figure 5.2.3) depending on the sample type, size and stiffness. One downside to DMA is that it is sensitive to sample geometry, shape and the force used to clamp the samples, and so care must be taken in the preparation of the samples and their mounting onto the DMA if reliable repeatable results are to be achieved.

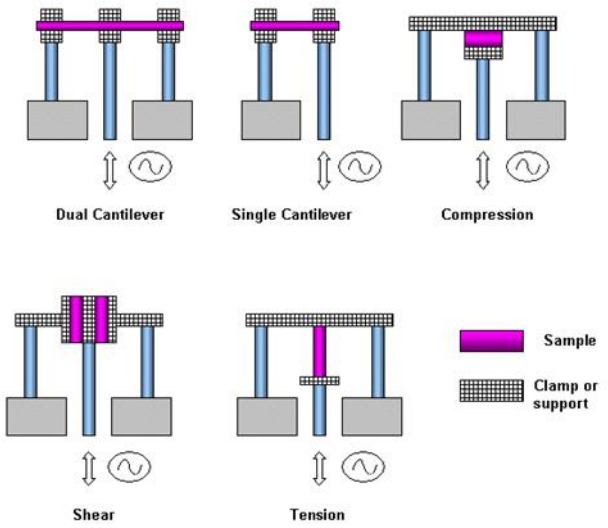

Figure 5.2.3 Diagrammatic representation of typical DMA sample configurations, from Introduction to Dynamic Mechanical Analysis (1)[53]

DMA is widely used in polymer science to investigate the effects of temperature on modulus. The DMA is set to heat the sample at a set ramp rate whilst a stress is applied at a single frequency (strain rate) and the modulus is recorded at regular intervals. However, some DMAs at low heating rates can test several frequencies during the temperature scan to study strain rate behaviour in conjunction with that of temperature. DMA is very sensitive to polymer transitions and Figure 5.2.4 shows a diagrammatic representation of the storage modulus of a polymer against temperature for a semi-crystalline polymer. Several step changes in the modulus can be seen as temperature increases;

these relate to changes in the molecular motion (transitions) within the polymer chains at the corresponding temperature. The two major transitions seen are melt temperature (T_m), corresponding to the crystalline melt of the polymer, and T_g, the glass transition, as main chain rotation causes the change from a glass to a rubber. Further secondary transitions β and γ are also shown in Figure 5.2.4; these correspond to side group rotation, and bending and stretching of atomic bonds respectively. For this study, DMA was used to temperature scan the irradiated samples and identify changes in mechanical behaviour caused by the effects of radiation.

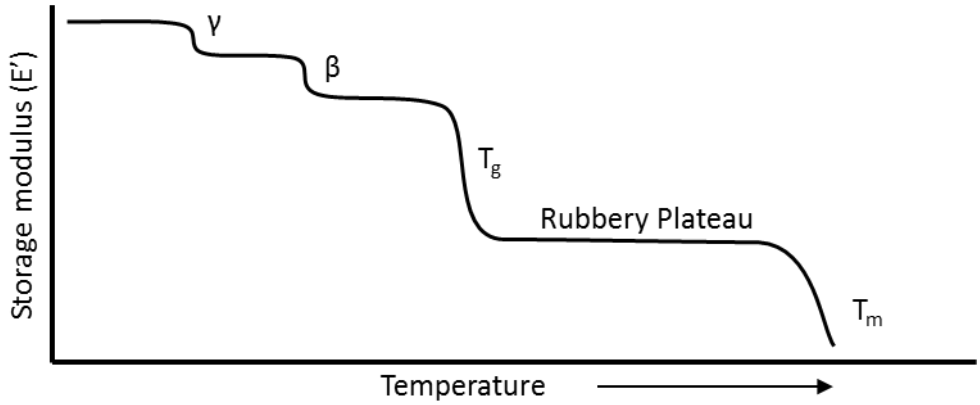

Figure 5.2.4 Idealised DMA temperature scan of a semi-crystalline polymer showing some of the various transitions.

5.2.1 DMA of polymer samples.

Sample bars of FK-800 were tested using a Perkin Elmer DMA 800 over a temperature range of -150 to 100 °C. The sample geometry used was single cantilever; the samples used were 2 x 5 mm with a 5 mm free length, and clamped in the glassy state with a torque of 0.25 Nm. Once cooled to -150 °C the samples were given a 5 minute stabilisation before being heated at 2 °C per minute. Three frequencies were used; 1, 5, and 10 Hz. An amplitude of 0.05 mm was used and a maximum force was set at 10 N. Sample data were collected and complex storage and loss moduli calculated for each frequency at 30 second intervals and exported into an Excel spreadsheet.

5.3 Brazilian disc test

The Brazilian disc test[11; 54-56] is a biaxial mechanical test used to study the tensile properties of brittle solids. PBXs such as TCV, are highly filled polymer composites with solid crystal loading in the region of 90 – 95 % by mass; the high solid loading makes mechanical response difficult to predict[11], and different from most filled polymer composites. The typical inter-crystal binder thickness in a highly filled PBX is only a few tenths of a micron[11], limiting the ability of pressed PBX samples to elastically deform and causing them to fail in a brittle manner. Due to its inelasticity, or ability to deform plastically, the mechanical properties of pressed PBXs are governed by they fail and not how they deform. The three main mechanisms governing PBX failure are crystal fracture, cavitation within the binder and failure of the binder crystal interface.

The explosive crystals within a PBX are relatively weak; therefore, flaws or inclusions in the crystal can cause it to fail under tensile stress. The failed crystal can further act as a point of stress localisation causing cracks to propagate though the binder and other crystals, resulting in the eventual failure of the whole sample.

Cavitation failure is the process of tensile stress localisation building at microscopic voids in the polymer until a micro-crack is formed in the binder. The ultimate tensile strength of the pure polymeric binder may be many times the stress required to cause cavitation in the same binder when formulated into a PBX[57]. In the PBX the sub micrometre polymer thicknesses allow the micro-cracks to propagate along the polymer crystal interface leading to the eventual failure of the material.

When failure of the binder crystal interface takes place on a local level, a build-up of stress takes place causing further interface failure around the crystal. The continued de-bonding can result in crack formation and propagation throughout the material. This crack formation can lead to the eventual failure of the pressed PBX. The stress required for de-bonding of the polymer is inversely proportional to the square root of the crystals radius[56], therefore, lager crystals will de-

bond first. Changes in the strength of the binder crystal interface can also be caused by changes in the mechanical and chemical properties of the binder.

The Brazilian disc test was developed during the 1940s to study the tensile properties of rock and concrete samples, before being adopted for use with explosive samples. The Brazilian test lends itself well to the study of highly filled PBX samples due to the ease and relative safety with which the samples can be produced by die pressing without the need for further machining, and the small mass (~0.6 g) of explosive required. For this study, Brazilian testing of irradiated and pristine PBX pellets was conducted by Dr David Williamson at the Cavendish Laboratories, Cambridge University.

The Brazilian test is a biaxial test with disc-shaped samples loaded in compression to induce a tensile stress across the centre of the sample. Sample size can vary, but for use with explosives the samples are pressed cylinders 10 mm in diameter and 4 mm high with a mass of approximately 0.6 g. The samples have the advantage over uniaxial tensile load samples that they do not require machining into complex shapes and can be much smaller, reducing the hazard when working with explosives. A diagram of a sample in a set of anvils is shown in Figure 5.3.1. As the two anvils compressively load the sample, a tensile stress is induced across the centre of the sample, causing failure along the central axis. Curved anvils are used to stop stress concentrations forming at the anvil contact points, causing premature sample failure at the anvil.

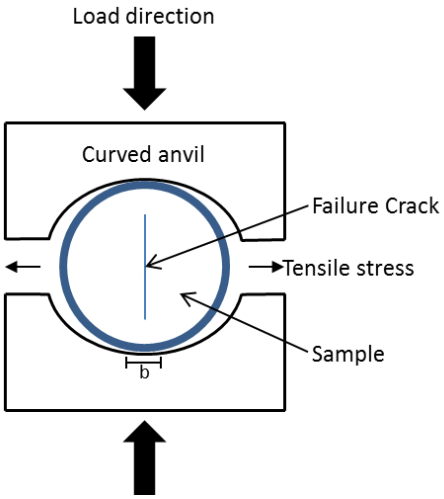

Figure 5.3.1 Diagram of the Brazilian test with b indicated. A tensile stress is generated in the sample by loading the top and bottom in compression.

It has been shown by Palmer et al.[58], that the ratio of half the sample anvil contact width (b) and the disc radius (R) is critical to sample failure mode. For b/R ratios of up to 0.27 the tensile strength is linearly dependent on the anvil curvature; of 0.27 and above the anvil curvature has no effect on the results. Tensile stress (σ) at the sample centre can be calculated using equation 5.3.1 where P is the applied load in newtons, D and t are the sample diameter and thickness in mm, and b/R is the anvil contact ratio.

$$\sigma = \frac{2P}{\pi D t}\left[1 - \left(\frac{b}{R}\right)^2\right] \qquad \textbf{(5.3.1)}$$

Strain measurements are difficult to record; due to the small sample size the attaching of strain gauges to the surface of the sample can affect the recorded sample strength. A method of digital image correlation has been developed whereby the sample is coated in a random speckle pattern of paint, the surface of the sample is filmed during the experiment, and the images can be analysed and the movement of specific specks tracked. Due to its complexities no measure of strain was made by the Cavendish Laboratories during the tests for this study.

5.3.1 Brazilian testing of irradiated explosive samples

Pressed cylinders of irradiated and pristine TCV were tested using a screw-drive Instron materials testing machine. The anvils had a b/R ratio of 0.27 and the Instron crosshead speed was set at 0.065 mm min^{-1}. To ensure that the PBX binder was above its glass transition to reflect possible future in service conditions, the TCV samples were tested at 40 °C. Five cylinders of PBX for each radiation dose were provided to the Cavendish Laboratories, although only three were tested unless excessive scatter was seen in the data.

5.4 Differential scanning calorimetry (DSC)

Differential scanning calorimetry (DSC) is one of the most widely used and rapid thermal analysis techniques; descriptions of the technique can be found in references [43; 59]. Traditionally, DSC measures the difference in energy input required to keep a sample and a reference - or blank - at the same temperature as both are subjected to a controlled change in temperature.

As a material undergoes a phase transition or decomposition, energy can be taken into the system (endothermic) or released (exothermic), and these changes in heat capacity can be quantitatively measured along with the temperature at which they occur.

A stylised diagram of a polymer DSC thermogram is shown in Figure 5.4.1. The diagram shows the step change in heat capacity as the polymer changes from a glass to rubber through its glass transition region. Figure 5.4.1 also shows the exothermic peak characteristic of a polymer crystallisation, although this may not be seen for all semi-crystalline polymers. The final event seen is the endothermic polymer crystal melt; the melt transition and crystallisation peak would not be seen for a wholly amorphous polymer with just the glass transition being seen.

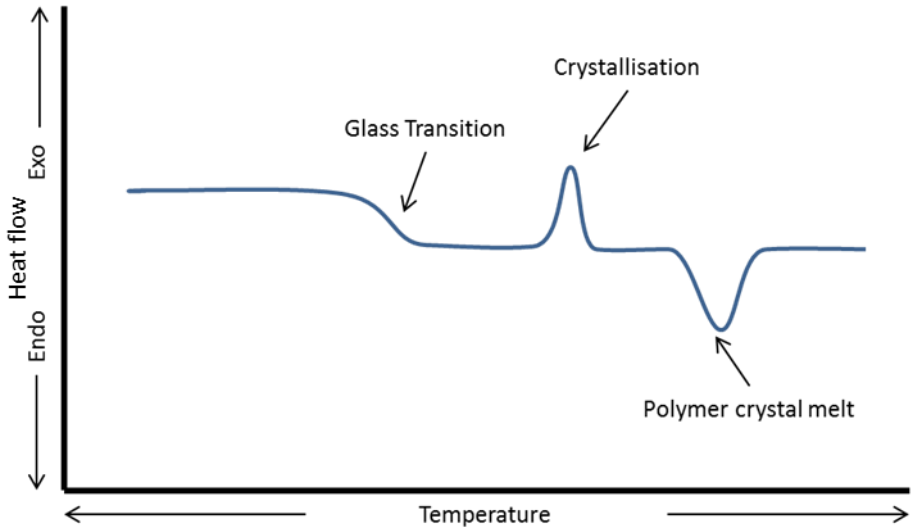

Figure 5.4.1 Diagrammatic representation of the DSC trace of a semi-crystaline polymeric material. The step change of a glass transition and the exothermic and endothermic peaks of crystallisation and melt are indicated.

The amount of energy required to melt the crystals within a polymer is related to the percentage crystallinity (X_c) of the polymer and can be calculated by integrating the area of the crystalline melt endotherm, known as the latent heat of fusion (ΔH_{fus}). The percentage crystallinity can be estimated using DSC from equation 5.4.1, where $\Delta H_{fus}{}^0$ is the latent heat of fusion for the 100% crystalline polymer. The $\Delta H_{fus}{}^0$ can be calculated using low molecular oligomers of the polymer of interest which are able to fully crystallise[60]. However, when $\Delta H_{fus}{}^0$ is not available for a polymer, changes in latent heat can be used to compare the crystallinity of different sample but not to give a definitive X_c.

$$X_c = \frac{\Delta H_{fus}}{\Delta H_{fus}^0} \times 100 \qquad \textbf{(5.4.1)}$$

Experiments using very small samples of explosive materials may be carried out by DSC and these runs can be used to investigate thermal properties such as the onset of thermal decomposition, peak decomposition temperature - which can be related to stability - and also to calculate the energy released during thermal decomposition.

There are two methods of conducting DSC scans*, power consumption DSC* and *heat flux DSC*. Power consumption DSC uses two ovens, one for the sample and one for the reference; the difference in power required to keep both the sample and the reference at the same temperature during the temperature scan is recorded and plotted. For this study all the equipment used was heat flux DSC. In heat flux DSC both the sample and reference are housed in a single furnace where the temperature can be raised or lowered at a constant and controlled rate. There are multiple sensors recoding the temperature of both the reference and the sample and recording any change. When a transition takes place in the sample, a temperature difference is formed between the sample and reference and this measured change is converted into a heat flow by the equipment which is then displayed against temperature or time.

5.4.1 DSC characterisation of polymer samples

A Mettler Toledo DSC1 combined with the STARe software was used to measure T_g, T_m and the ΔH_{fus}.

Six samples of FK-800 were tested for each total dose at each dose rate and irradiation atmosphere. Two samples were cut from each of the three polymer bars irradiated in one sample vial. The samples were approximately 15 mg in mass and heated at 10 °C per minute in 40 µl aluminium pans under a nitrogen atmosphere with an empty pan as the reference. Samples were heated from start temperatures of -25 °C to 150 °C before being cooled back to the start temperature at 10 °C min^{-1}, and then heated to 150 °C at 10 °C min^{-1}.

T_g was measured as the inflection point of the step change in the thermogram, peak value of the crystalline melt endotherm was taken as the T_m, and the integral of the crystalline melt endotherm was taken as ΔH_{fus}. To enable calculation of the percentage crystallinity for FK-800, the 100% crystalline latent heat of fusion (ΔH_{fus}^0) for poly-CTFE was used as previously described by Hoffman[61].

5.4.2 DSC characterisation of explosive samples

Both a Mettler Toledo DSC 30 and 822 running the STARe software were used to test explosive samples. Approximately 1.5 mg of explosive was run in a 40 µl aluminium pan against an empty reference pan. The pan lids had holes in them to release any pressure build-up from decomposition products formed during the temperature scan. Duplicate samples of TATB, and TCV were run from 30 to 450 °C at 10 °C min^{-1} under nitrogen atmosphere and the onset and peak temperatures of decomposition were measured and recorded.

Decomposition energies were found to be variable for the initial TATB samples; this was found to result from the sublimation and subsequent escape from the DSC pan of TATB before decomposition. To stop the sublimation affecting the decomposition energies, samples of irradiated and pristine TATB were run with a layer of sand covering the explosive sample. The sand was used to allow the sublimation of the TATB onto the sand and not to be lost from the pan. Samples were run from 30 to 450 °C at 10 °C min^{-1} under nitrogen atmosphere and the decomposition energy was measured by integration of the exothermic peak.

5.5 Thermogravimetric analysis (TGA)

Thermogravimetric analysis (TGA)[3; 62] is a technique in which the mass of a sample is accurately weighed and recorded as its temperature is changed (dynamic) or kept constant (isothermal). Explosive samples were analysed by isothermal TGA to assess thermal stability of the samples and dynamic TGA was used to analyse decomposition.

The TGA used for both isothermal and dynamic experiments was a Mettler Toledo TG50 thermo balance capable of weighing samples to 0.01 mg.

5.5.1 Isothermal TGA analysis of explosive samples

Approximately 30 mg of explosive was placed in a ceramic crucible and placed on the TGA balance. The sample was heated to 120 °C and kept under isothermal conditions in an atmosphere of air for 15 hours to investigate the thermal stability of the explosive.

5.5.2 Dynamic TGA of explosive samples

Samples of ~2.5 mg of explosive were heated in a ceramic crucible at a ramp rate of 10 °C min^{-1} under a constant flow of nitrogen gas. The temperature was raised from 30 °C to 450 °C to investigate changes in the thermal decomposition temperature of the explosive and the mass of non-combusted material.

5.6 Density

Changes in density can indicate changes to the internal structure of a solid sample. An increase in density can result from phase changes in crystalline solids, or a large increase in crystallinity within a polymeric system. A decrease may be caused by expansion of the sample caused by crystal phase changes, phase changes in the polymeric system, or from the formation of voids within a solid caused by off-gassing.

For this study, density measurements were made using the Archimedes principle. The Archimedes principle states that a solid immersed in a liquid is subjected to the force of buoyancy and the value of the buoyancy force is equal to the mass of liquid displaced by the volume of the solid[63] . This allows us to calculate density using equation 5.6.1.

Equation 5.6.1 is sufficient for working to an accuracy of one to two decimal places only; no correction is made for changes in the buoyancy of air. 1 cm^3 of air has a mass of approximately 1.2 mg, so when a sample is measured in air it is affected by the buoyancy force of the air it displaces, and this effect should be corrected for. This leads to equation 5.6.2 where ρ(a) equals the density of air under standard conditions (0.0012 g cm^{-3}).

$$\boldsymbol{\rho = \frac{W(a)\,\rho(fl)}{W(a) - W(fl)}} \qquad \textbf{(5.6.1)}$$

Where:
ρ = Density of solid
ρ(fl) = Density of the immersion liquid
W(a) = Mass of the solid in air
W(fl) = Mass of the solid immersed in liquid

$$\boldsymbol{\rho = \frac{W(a)\,[\rho(fl) - \rho(a)]}{W(a) - W(fl)} + \rho(a)} \qquad \textbf{(5.6.2)}$$

A Sartorius balance was used in conjunction with a Sartorius YDK 01 density determination kit as shown in Figure 5.6.1. The liquid used was distilled water with a small amount of Triton X-100 surfactant to ensure wetting of the sample surface.

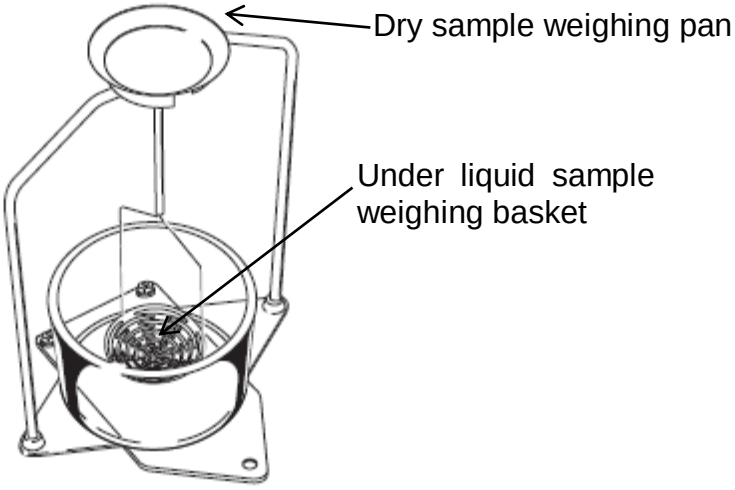

Figure 5.6.1 Diagram of the Sartorius density determination kit without the measuring balance. Adapted from [63]

Density measurements of the polymer dogbones and explosive cylinders were taken before and after irradiation. The samples were first weighed in air and then under water; the temperature of the water was measured every sixth sample and the corrected water density was used to calculate the sample density. The densities of all the samples before and after irradiation were used to look for radiation-induced changes.

5.7 Gas chromatography-mass spectroscopy (GC-MS)

Headspace GC-MS is a very sensitive technique where small amounts of gas surrounding a sample are analysed for chemical composition. The headspace gases of both the polymer and PBX samples were analysed after irradiation to detect and identify radiation-induced decomposition products. GC-MS is

essentially two processes coupled in series to separate and then identify mixtures of unknown compounds.

Gas chromatography (GC)[44; 64] is a well-established separation technique for gases or stable vaporised mixtures and consists of three components; injection, separation, and detection. Once the unknown mixture is volatilised at low pressure and injected onto the column, it is carried by the gaseous mobile phase which is usually helium. The mixture interacts with the column stationary phase, and by a process of adsorption and elution as the mixture passes along the column, the mixture is separated according to its affinity to the stationary phase. An important part of GC is the ability to change the temperature of the column during the GC run; this enables a wide range of compounds to be eluted within a reasonable time frame. Detection can be by one or more ionisation and detector techniques and the results are reported as intensity vs. retention time on a chromatogram.

Mass spectroscopy (MS)[65-67] allows the determination of the mass of a sample based on the spectrum formed from the mass of its fragments after ionisation. Gaseous samples are first ionised using a high energy stream of electrons to break up and ionise the sample, resulting in a number of radical cation fragments being formed. These fragments are then sorted by mass before being detected. There are several different methods of sorting the fragments but the most commonly used in GC-MS – and used in this study – is a quadrupole mass spectrometer.

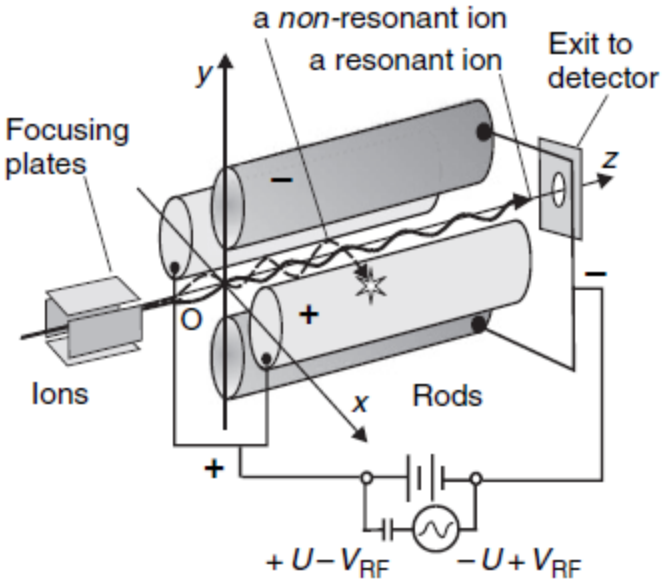

Figure 5.7.1 Diagrammatic representation of a quadrupole mass analyser, reproduced from Chemical Analysis[66]

A quadrupole mass analyser, shown diagrammatically in Figure 5.7.1, consists of four parallel circular rods with each opposing rod electrically connected and charged in pairs either positively or negatively. As the ions travel along the centre of the quadrupole towards a detector at the far end, an AC voltage is superimposed over the DC field. By varying frequencies or voltages, instability in the flight path of the ions is generated related to their mass to charge ratio (m/z). Only ions of a certain m/z will reach the detector for a given ratio of voltages or frequency and other ions will collide with the rods. Voltage ratios or frequencies can be scanned to enable a mass spectrum to be generated.

5.7.1 Headspace gas collection

Because the sample vials used to irradiate the samples were made entirely of glass and flame-sealed, there was no way of directly sampling the gases from the vials. A method was developed using a 20 ml Chromacol headspace vial which had been adapted to have two glass tubes attached, both with in-line ground glass gas taps (Figure 5.7.2). The gas collection kit was attached to the sample vial by flexible gas tubing before the whole kit was evacuated using a high-vacuum pump. Once the gas collection kit had been evacuated, the gas

tap to the vacuum line was closed and the glass break arm on the sample vial broken. After 3 minutes, the gas tap between the headspace vial and the sample vial was closed. To allow a sample to be drawn, pressure between the inside of the gas collection kit and the outside had to be equalised. Pressure equalisation was achieved by injecting helium into the vial before a sample was drawn; helium was chosen because as the mobile phase for the GC-MS it would not affect the results.

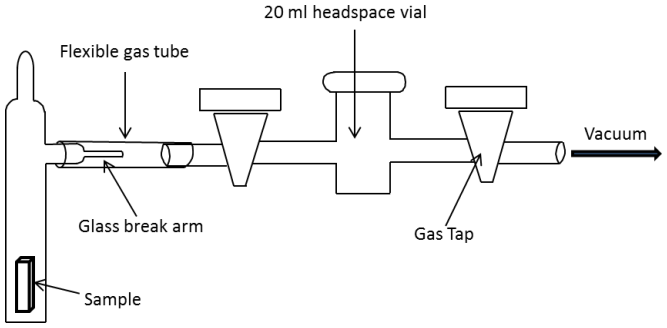

Figure 5.7.2 Diagrammatic representation of headspace gas collection kit. The headspace vial and gas tubing were evacuated and closed off before the glass break arm was broken to collect gasses from the sample vial.

5.7.2 Headspace gas analysis

Headspace gases of both polymer and PBX samples were analysed post-irradiation using a Thermoquest Trace GC coupled to a Fisons Instruments MD800 MS to look for radiation-induced decomposition products. The GC used a Chromopack PoraPLOT Q fused silica porous–layer open tubular (PLOT) column (25 m x 0.25 mm). The MS used electron impact ionisation and quadrpole mass sorting with 4 scans per second. The Chromopack PoraPLOT Q GC column was chosen because of its ability to separate CO_2, O_2, N_2, Ar, N_2O, CO and NO as well as other gases. The column was not able to detect NO_2 (a common decomposition product of explosives) because of its absorption onto the column and beakdown into NO which would be measured instead of NO_2[39]. The sample injection size was 0.05 ml and a 50/50 by volume gas split was used. The start temperature was -80 °C and the end temperature was 150 °C with a ramp rate of 60 °C; start and end temperatures were both held for 3 minutes.

5.8 High performance liquid chromatography (HPLC)

High performance liquid chromatography (HPLC)[68; 69] is an analytical technique used to separate mixtures dissolved in a liquid mobile phase. During this study HPLC was used to analyse radiation-induced decomposition in irradiated TATB samples.

HPLC uses several components connected in series. A flow diagram showing the main components is shown in Figure 5.8.1; the solvent rack will hold all of the different solvents used to make up the mobile phase without the need for premixing. Once the solvents are drawn from the bottles, they pass through a degasser before being mixed to form the mobile phase in the pump. The analytical pumps used in HPLC have to able to sustain highly accurate flow rates between 0.1 and 10 ml min^{-1} at pressures in excess of 400 bar; the high pressures are caused by back pressure from the highly packed stationary phase in the separation column. A high pressure injector is used in conjunction with an auto sampler to inject a precise amount of sample into the mobile phase at the head of the column.

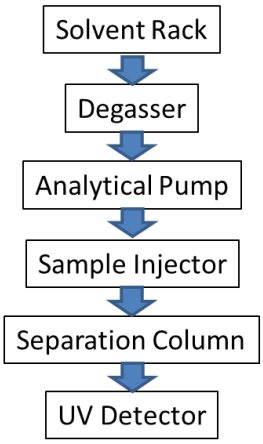

Figure 5.8.1 Flow diagram of the main units of a HPLC

The HPLC separation column is the most important single part of a HPLC system as this is where the physical separation takes place. Interchangeable columns are normally housed in a unit capable of maintaining a constant temperature as this can have an effect on the separation times within the column. The column itself is normally a stainless steel tube 3 - 15 cm in length

and used to hold the stationary phase between two porous end plugs. Many inorganic materials have been used as stationary phases in the past, although the majority have used silica gel formed into spherical particles. The silica gel is highly polar, and the sample mixture is separated by the repeated adsorption and retention, based on polarity of the fractions, onto the gel surface as it passes through the column. Silica gel columns suffer aging issues and retention times can be affected by the age of the column.

Modern HPLC columns use reversed phase polarity partition chromatography columns; these columns still use silica as the base material but have other components covalently bonded to the silanol groups. Bonded silica columns no longer separate by adsorption, now behaving as stationary liquids instead. The stationary phase acts as a solvent immiscible with the mobile phase, this allows separation based on partition coefficient instead of adsorption. The use of different covalently-bonded phases allows HPLC columns to be designed to separate specific types of mixtures, such as aromatics. Identification of fractions eluted from the column is achieved with the use of a diode array detector capable of detecting the whole UV spectrum as the column elute passes through it. The results are then presented using a computer to give either absorbance vs. retention time for a single UV wavelength, or absorbance of the whole UV spectrum for a specific retention time.

5.8.1 HPLC of irradiated TATB

Approximately 5 mg samples of pristine and irradiated TATB were dissolved in 100 ml of dimethyl sulfoxide (DMSO) to make a solution of ~50 ppm. The samples were diluted further with the HPLC mobile phase to give a ~25ppm for injection.

HPLC was conducted using a Waters 2695 HPLC; the mobile phase was composed of 45% / 55% by volume acetonitrile/water with a flow rate of 1.4 ml min^{-1}. The injection volume was 10 µl and the column temperature was a constant 30 °C. The separation column - which is specially designed to separate aromatic compounds - was a 4.6 x 100 mm Phenomenex™ Kinetex™

phenyl-hexyl column with a particle size of 2.6 µm. UV spectra were recorded using a Waters 996 photodiode array detector.

5.9 Liquid chromatography - mass spectrometry (LC-MS)

Liquid chromatography - mass spectrometry (LC-MS)[66; 70] techniques use a HPLC connected to a MS (described elsewhere in Sections 5.8 and 5.7) via an interface. The job of the interface is to separate the elute from the mobile phase as it comes off the HPLC. There are several different interface techniques but, only the negative electro spray ionisation technique used during this study will be discussed here.

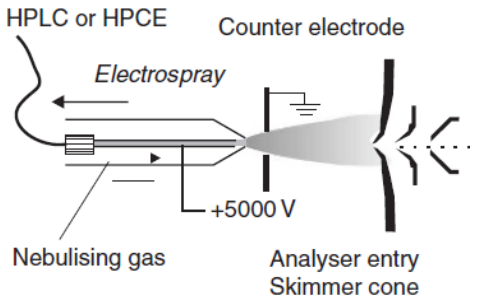

Figure 5.9.1 Diagrammatic representation of an electrospray ioniser reproduced and adapted from Chemical Analysis[66]

During negative electrospray ionisation (Figure 5.9.1) the liquid output from the HPLC passes along a stainless-steel capillary tube at a flow rate of up to 1 ml min^{-1}. The tip of the capillary tube has a high voltage of up to 5 kV applied to it which disperses the liquid as an aerosol of highly charged droplets. The spraying process is assisted by a co-axially introduced nebulising gas which flows around the outside of the capillary tube; the gas both helps direct the spray towards the MS and evaporate the mobile phase. After all the solvent has evaporated, some of the charged sample ions pass through a skimmer cone into an intermediate vacuum region, and from there to the mass spectrometer held under high vacuum.

5.9.1 LC-MS of irradiated of Irradiated TATB

LC-MS of both pristine and irradiated TATB samples was conducted at AWE plc Aldermaston by Paul O'nion. The experiments were conducted to attempt identification of peaks seen by HPLC alone.

Samples of TATB irradiated and pristine, were supplied dissolved in DMSO to a concentration of 50 ppm. The irradiated sample had been irradiated to 100 kGy at a rate of 1.8 kGy hr^{-1} in air, before being stored in the dark at ambient temperatures before testing. HPLC was conducted using the same parameters as described in Section 5.8.1 with a reduced flow rate of 1 ml min^{-1}. Negative electrospray ionisation mass spectroscopy was used with a capillary temperature of 300 °C and a voltage of 4 kV. The scanning range of the MS detector was 60 - 1000 m/z.

5.10 Gel permeation chromatography (GPC)

GPC[43; 71] (also known as size exclusion chromatography) is used to separate macromolecules based on hydrodynamic volume (size). By using a standard of known molecular mass it is possible to make a calibration curve for a GPC column and so measure the molecular mass of an unknown sample against the standard.

GPC uses a similar equipment set up to HPLC (Section 5.8). However, GPC uses a larger and different type of column. A representation of a GPC column is shown in Figure 5.10.1. The Figure shows how the stationary phase consists of porous particles; the pores range in size so that molecules of different hydrodynamic volumes can pass through them. The mobile phase with the sample dissolved in it is pumped through the column at a precisely controlled flow rate. The sample interacts with the stationary phase via a process of adsorption and elution; molecules with a smaller volume undergo a greater number of these interactions with the stationary phase by passing through the pores of the particle, slowing their path through the column. Larger molecules which are too large to pass through the pores of the stationary phase flow around the gel particles undergoing less interactions with the stationary phase

and are eluted off the column first. A refractive index detector is most commonly used to measure the amount of material being eluted from the column at a particular time, which is then plotted on a chromatogram. The refractive index detector works by continuously measuring the difference between the flow from the column and a reference of mobile phase. A beam of light is passed through the cell containing both the reference and column elute; as the sample passes though the cell, the change in refractive index causes a change in the angular displacement of the beam, with the amount of displacement relating to the amount of sample present in the column elute.

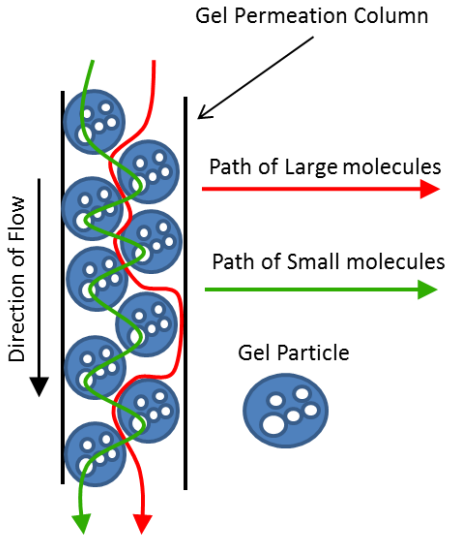

Figure 5.10.1 Diagrammatic representation of a GPC column. The green arrow represents the path of small hydrodynamic chains passing through the pores of the gel particles and being retarded. The red line shows the faster path of large molecules around the gel particles.

To determine the molecular mass of a sample by GPC, reference materials of known molecular mass must first be run through the column using the exact conditions that are to be used for the samples. The retention time of the reference materials are recorded and used to form a calibration curve which the sample can then be measured against. Because polymers have a range of molecular masses, the polymer's mass is normally quoted as an average. The two most important and most commonly reported are the number average (M_n) and mass average (M_w) masses. M_n is the numerical mean mass of the

polymer; however M_w represents the average mass of a polymer chain if a single chain was randomly chosen from the polymer. A diagrammatic representation of a typical polymer's molecular mass distribution indicating the position of M_n and M_w is shown in Figure 5.10.2. The equation for the M_n is shown in equation 5.10.1 and M_w is shown in equation 5.10.2 where M_i is the molecular mass and N_i is the number of molecules.

$$M_n = \frac{\sum M_i N_i}{\sum N_i} \quad \textbf{(5.10.1)}$$

$$M_w = \frac{\sum M_i^2 N_i}{\sum M_i N_i} \quad \textbf{(5.10.2)}$$

The sample's molecular-mass dispersity ($Đ_M$) is calculated by dividing M_w by M_n to give a measure of how wide the molecular mass distribution is where a uniform polymer would have a value of 1.

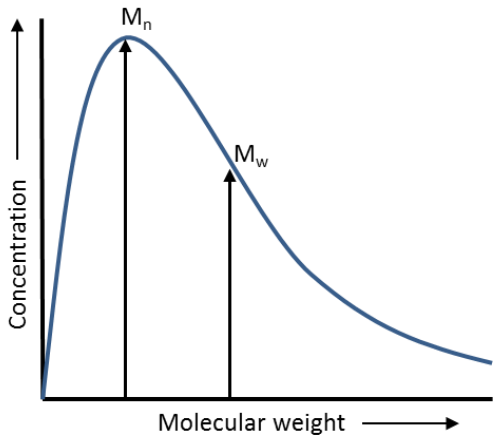

Figure 5.10.2 Diagrammatic representation of the molecular mass distribution of a typical polymer. Adapted from[72]

5.10.1 GPC of polymer samples

Samples of approximately 100 mg of irradiated and pristine FK-800 were cut from the polymer bars and tetrahydrofuran (THF) was added to make a solution with a concentration of 9 mg ml^{-1}. The samples were allowed to dissolve for a minimum of 16 hours before analysis.

GPC analysis was performed using a Viscotek VE1121 GPC solvent pump, a Kontron Instruments DEG-104 degasser, Waters 717 Plus auto-sampler and Waters 2410 refractive index detector. THF at a flow rate of 1 ml min^{-1} and temperature of 35 °C was used as the mobile phase. Two Polymer Laboratories PLgel 10 µm mixed phase B columns, 300mm x 8 mm columns connected in series were used to separate injected volumes of 100 µl. Ten EasiCal PS1™ narrow molar mass polystyrene standards in 10 ml THF were used to calibrate the columns, covering a molar mass range of 580-7,500,000 g mol^{-1}. All GPC molar masses reported are reported as polystyrene equivalent.

5.11 Fourier transform infra-red spectroscopy

Polymer samples were analysed for chemical changes using attenuated total reflectance (ATR) Fourier transform infra-red spectroscopy (FT-IR)[65; 73]. Infra-red spectroscopy is based on the principle that atomic covalent bonds are not rigid. In fact they can be described as spring-like; because of this spring-like behaviour they are able to stretch, twist and rock with a defined frequency dictated by the atoms and type of covalent bond involved. When infra-red light encounters a bond of a certain vibrational frequency, the photon energy at a frequency equal to that of the bond vibration is transferred to the bond and the bond's vibrational amplitude is increased whilst its frequency remains constant.

Early infra-red spectroscopy relied on scanning through the infra-red spectrum one frequency at a time and recording the amount of light absorbed at a particular frequency by the sample against a reference beam; today's modern FT-IR equipment operates in a different way. FT-IR uses a single beam as opposed to the split sample and reference beam originally used. The beam of infra-red passes through a Michelson Interferometer which is used to manipulate the beam to contain a mixture of frequencies to be detected. The whole beam absorbance is detected by the detector before the beam is modified to contain a different set of frequencies. This process takes place many times and a computer processor uses the Fourier transform to calculate the absorbance of each frequency which is then subtracted form an initial blank scan, multiple scans can be run in a short period of time and combined to give

more accurate results. FT-IR can be combined with additional add-on equipment - such as ATR - to study solids which are too thick for transmittance of a beam to be possible.

ATR is a quick and effective method of looking at samples too thick or not suitable for transmittance FT-IR and has become commonly used. ATR uses mirrors to divert the infra-red beam through a crystal which has a sample in close contact with its surface (Figure 5.11.1); the beam is passed along the crystal and if the angle of incidence is greater than the critical angle the evanescent wave will penetrate the sample and be reflected. The succession of several attenuated reflections along the crystal leads to a spectrum comparable to that achieved using transmittance techniques

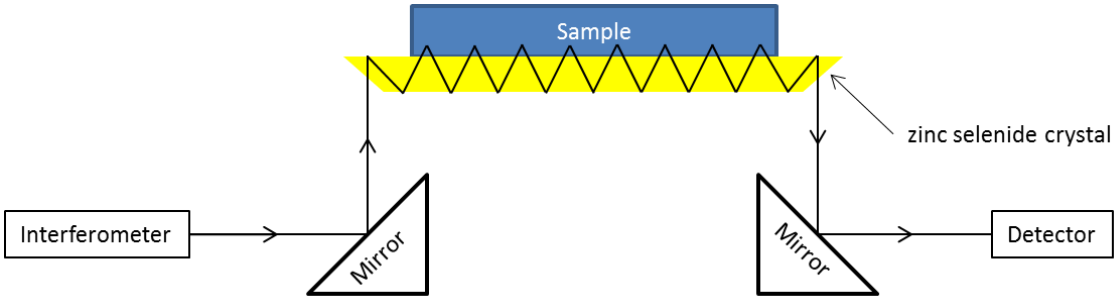

Figure 5.11.1 Diagrammatic representation of how an ATR attachment for an FT-IR works. The beam traveling from the interferometer to the detector is reflected along a crystal and interacts with the sample at its surface.

5.11.1 FT-IR Characterisation of FK-800 samples

Three bar samples of FK-800 were aligned end to end along the length of an ATR crystal to maximise the sample surface area to be analysed. The equipment was a Bruker Vector 22 mid-range FT-IR and a Specac ATR with a zinc selenide crystal. Sixty-four scans were taken of each sample and used to form the IR absorbance spectra.

5.12 X-ray diffraction

X-ray diffraction which is describe in detail in [43; 44; 74] can be used to look at crystal and amorphous structures within polymers. For this study, X-ray

scattering was used to determine the estimated percentage crystallinity of the irradiated FK-800 samples.

X-rays are high frequency (~10^{18} Hz) electromagnetic waves with wavelengths comparable to those of interatomic distances in crystal. The X-rays interact with the electrons surrounding an atom causing them to oscillate with the same frequency therefore elastically scattering the incident X-rays. The Bragg equation can be used to express the conditions required for X-ray diffraction and relies upon the concept that scattering from the scattering objects must be in phase for a diffraction maximum to occur. Miller indices (*hkl*) can be used to describe a crystal plane that cuts a unit cell along the **a** axis into *h* parts, the **b** axis into *k* parts and the **c** axis into *l* parts. For scattering to occur from a plane (*hkl*), Bragg realised all the lattice points in that plane must scatter in phase, as well as those in subsequent (*hkl*) planes. This geometry is described in Figure 5.12.1

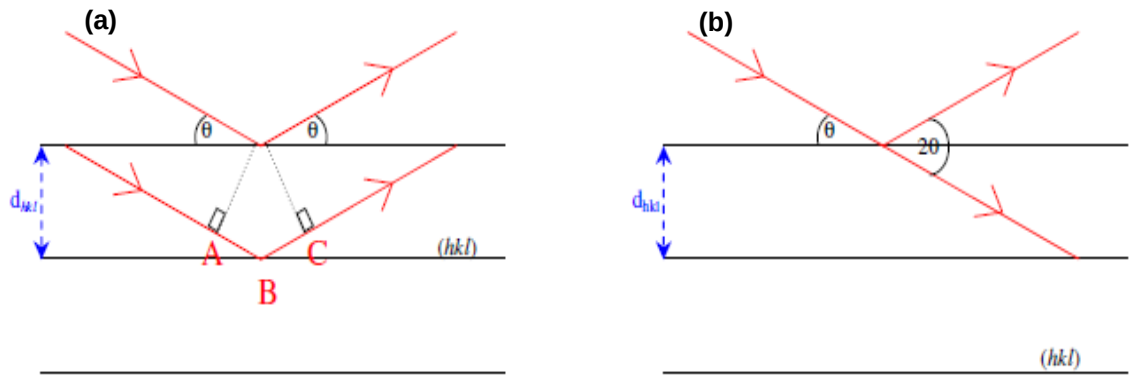

Figure 5.12.1 A diagrammatic representation of Bragg diffraction showing (a) the path difference between X-rays reflected from planes (*hkl*) a distance d_{hkl} apart and (b) how the incident beam is scattered through angle 2θ. Adapted from [75]

When the incident X-ray beam is diffracted from two successive (*hkl*) planes a distance d_{hkl} apart (Figure 5.12.1), the path difference between the two beams is equal to distance ABC, which equals $2d_{hkl} \sin \theta$, where d_{hkl} is the distance between crystal planes and θ is the incident angle. In practice, the nth order reflection from an (*hkl*) plane is the same as the 1st order reflections from the

(n*h*, n*k*, n*l*), so the result is the Bragg Law for a diffraction peaks, Equation 5.12.1

$$\lambda = 2\mathrm{d}_{hkl}\ \sin\theta \qquad \textbf{(5.12.1)}$$

Polymers are very rarely 100% crystalline and are a mixture of random amorphous material and ordered crystals. The disordered structure of the amorphous region where atoms are in randomly positioned in relation to each other will cause scattering in all directions. In contrast in crystalline regions where the atoms are arranged periodically in a repeated structure which causes the scattering to be confined to particular angles

The Bragg law allows us to identify the two differing regions within the polymer because, when the X-ray beam interacts with the randomly located atoms of the amorphous region, the beam is randomly scattered, giving rise to a large halo on the spectra (Figure 5.12.2). By contrast, when the beam interacts with an ordered crystalline region the beam diffraction is no longer random leading to sharp peaks in the spectra on top of the amorphous halo as shown in Figure 5.12.2.

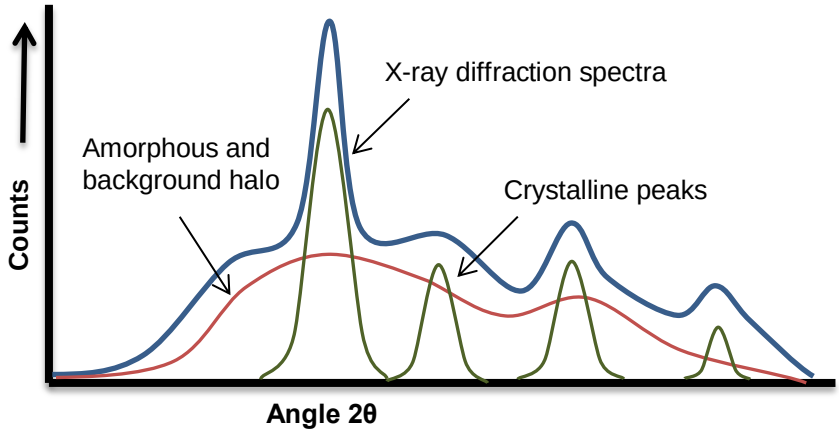

Figure 5.12.2 Diagrammatic representation of X-ray diffraction pattern for a semi-crystalline polymer. The full spectra is shown in blue, and the de-convoluted amorphous halo and crystalline peaks are shown in red and green

The percentage crystallinity can be calculated by Ruland's method using Equation 5.12.2, where X_c is the percentage crystallinity, I_c is the integrated

area of the crystalline peaks and I_a is the integrated area of the amorphous peaks.

$$X_c \approx \frac{I_c}{I_c + I_a} \times 100 \quad \textbf{(5.12.2)}$$

5.12.1 X-ray scattering of FK-800 samples

X-ray diffraction was carried out by Dr Annette Glauser at AWE plc Aldermaston Samples of pristine and irradiated FK-800 10 mm by 20 mm by 2 mm were mounted on poly(methyl methacrylate) (PMMA) holders and analysed at room temperature using a Bruker D8 Advance X-ray diffractometer. The 2θ angles scanned were from 5 ° to 50 °, with a step size of 0.0017 °, and a step time of 4 seconds. Baseline subtraction was carried out using the Brucker software DIFFRACPLUS EVA, and integrations were performed using Microsoft Excel.

5.13 Small scale explosive powder safety tests

Small scale explosive powder safety tests were conducted by the Cranfield University Energetics Hazard Test House. The tests were carried out to ensure that the irradiated explosive materials produced were safe to handle for further analysis. Testing consisted of drop weight, electric spark discharge and mallet friction tests adapted from the UK Ministry of Defence, Energetic Materials Testing and Assessment Policy committee's (EMTAP) Manual of Tests[76]. Testing was carried out on samples of TATB and TCV irradiated in air to total doses of 50 and 200 kGy.

5.13.1 Drop weight impact

When handling a material in general use, incidences of impact, such as dropping of the sample, can easily occur. Because of this samples are tested for sensitiveness to impact. The drop weight impact test used in this study test was a reduced Rotter impact test[3; 76] (EMTAP test 1a). The tests used were reduced from a 50 shot test to a 10 shot test due to limited supplies of irradiated material. For the Rotter impact test, a 5 kg weight is dropped onto a brass cap containing 30 mm^3 of explosive mounted on an anvil. The anvil and cap

arrangement is placed in an air tight housing attached via tubing to a gas burette. The burette is used to indicate the production of gas during the test. When the weight is dropped a “go” is recorded if greater than 1 ml of gas is measured with the burette (0.5 ml with secondary evidence such as smoke) or on removal from the anvil housing, sooty deposits or sample discolouration are seen. The drop height is raised and lowered based on the Bruceton Staircase technique for 50 shots and a height at which a 50% probability of sample ignition is established.

Results are presented as a comparative Figure of Insensitiveness (F of I) which is calculated against a standard material from equation 5.13.1; the standard in this case is RDX with a F of I of 80.

$$F\ of\ I\ Sample = \frac{Median\ drop\ height\ Sample}{Median\ drop\ height\ Standard}\ .F\ of\ I\ Standard \qquad \textbf{(5.13.1)}$$

5.13.1.1 Drop weight Impact testing of irradiated explosives

The reduced shot test used in this study was the Rotter Langlie 10 shot test using the Langlie search tree method of determining the mean. Samples of irradiated TATB and TCV were tested via the Rotter Langlie method with start heights based on the full Rotter results from pristine samples of each material.

5.13.2 Electric spark discharge

It is possible for a human to build up a static charge which can then be discharged by touch. Because of this potential for a static discharge whilst handling an explosive the electric spark discharge test (EMTAP test 6)[76] has been developed. The test provides a means of distinguishing between materials which require added safety precautions when handling. The test is carried out at three energy levels; 4.5, 0.45 and 0.045 J, with the full test consisting of 50 tests per energy level starting at the highest. The energy levels used were selected based on the lowest energy level (0.045 J) equalling double the quoted electrostatic charge that can build up on a person (~0.02 J)[76]. The two higher levels are 10 and 100 times the lowest energy to build in a margin of safety. A “go” for this test is signified by noise, visual flash, blackening or consumption of

the sample. A material requires only a single “go” at an energy level to be classified at that level.

5.13.2.1 Electric spark testing of irradiated explosives

A reduced electric spark test of 10 samples per energy level was used in this study. Holes with a diameter of 6.35 were drilled into a polythene strip with a thickness of 3.2 mm. One side of the strip was coated with self-adhesive copper foil before each hole was filled level and covered using copper foil, the two strips of foil forming a top and bottom electrode. Starting at the 4.5 J level a current was passed through each sample in turn. If a material had a single “go” at an energy level the next level down was then tested. The results are reported as “No ignitions at 4.5 J”, “Ignitions at 4.5 J but not at 0.45 J”, “Ignitions at 0.45 J but not at 0.045 J” or “Ignitions at 0.045 J”

5.13.3 Mallet friction test

Ignition caused by friction is a real and present risk when working with explosives; ignition results from the explosive crystals either rubbing together or rubbing against an abrasive surface leading to the formation of hot spots. Because of the friction risk in everyday handling and use of explosives, the mallet friction test (EMTAP test 2)[76] is used to test explosive under a range of friction conditions. The full mallet friction test uses 100 mm^3 of explosive placed on an anvil and then struck 5 times with a glancing blow by an operator using a mallet. Several different anvils and mallet tips made of different materials are used for the test and 10 repeats of each combination are carried out. The combinations, in order of harshness, are wood mallet on softwood anvil, wood-on-hardwood, wood-on-yorkstone, nylon mallet on steel anvil and steel mallet on steel anvil. The results are recorded by an observer and “ignitions” are said to have occurred if spark or flame are seen, a crack is heard, and for the wood mallet, only burning can be smelt.

The recorded results are presented for each combination as 0% for no “ignitions” in the 10 cycles, 50% for up to 6 “ignitions” in 10 cycles, and 100%

for more than 6 “ignitions” in 10 cycles. Due to the large amount of explosive required in the mallet friction test an abridged version was used for this study.

5.13.3.1 Mallet friction test of irradiated explosives

The limited mallet friction test for this study consisted of the steel on steel test. Steel on steel is regarded as the harshest conditions and most likely to cause an “ignition”. The sample was prepared and tested in the same way as it would be for the full test described above, but only steel on steel was used.

6 The effects of ^{60}Co gamma radiation on FK-800

Due to the hazard implications of working with an energetic material, this study started by investigating the FK-800 polymer binder and then exploring if the changes observed in the binder carried across into the PBX.

When used in a PBX it is important that the physical properties of the polymeric binder remain consistent when exposed to environmental factors to ensure the PBX responds as expected throughout its life cycle. Tensile load testing and DMA were used to study changes in the mechanical properties of the FK-800 samples. In addition to the mechanical properties, the polymer's transition from the glassy to the rubbery state (T_g) was also studied using DSC and DMA**.**

6.1 Mechanical properties

The methods used for the tensile load and DMA tests are described previously in Section 5. The stress extension curves recorded by the Instron material testing machine for all FK-800 samples are shown in Figure 6.1.1 and 6.1.2

Six samples were tested in each data set except for the 200 kGy at 1.8 kGy hr^{-1} air, which consisted of three samples due to breakages during handling. Figure 6.1.1 and 6.1.2 show the individual samples overlaid; the different total radiation doses have been offset by 175 mm showing the differences with increasing radiation dose. The data has been normalised to sample dimensions to give a stress in MPa, however, no compensation has been made for changes in cross sectional area during necking. The scatter evident in the data is caused by the inherent problems of testing polymers by this method; as the cross sectional area decreases during necking the sample can become susceptible to premature failure due to defects or nicks at the sample edge.

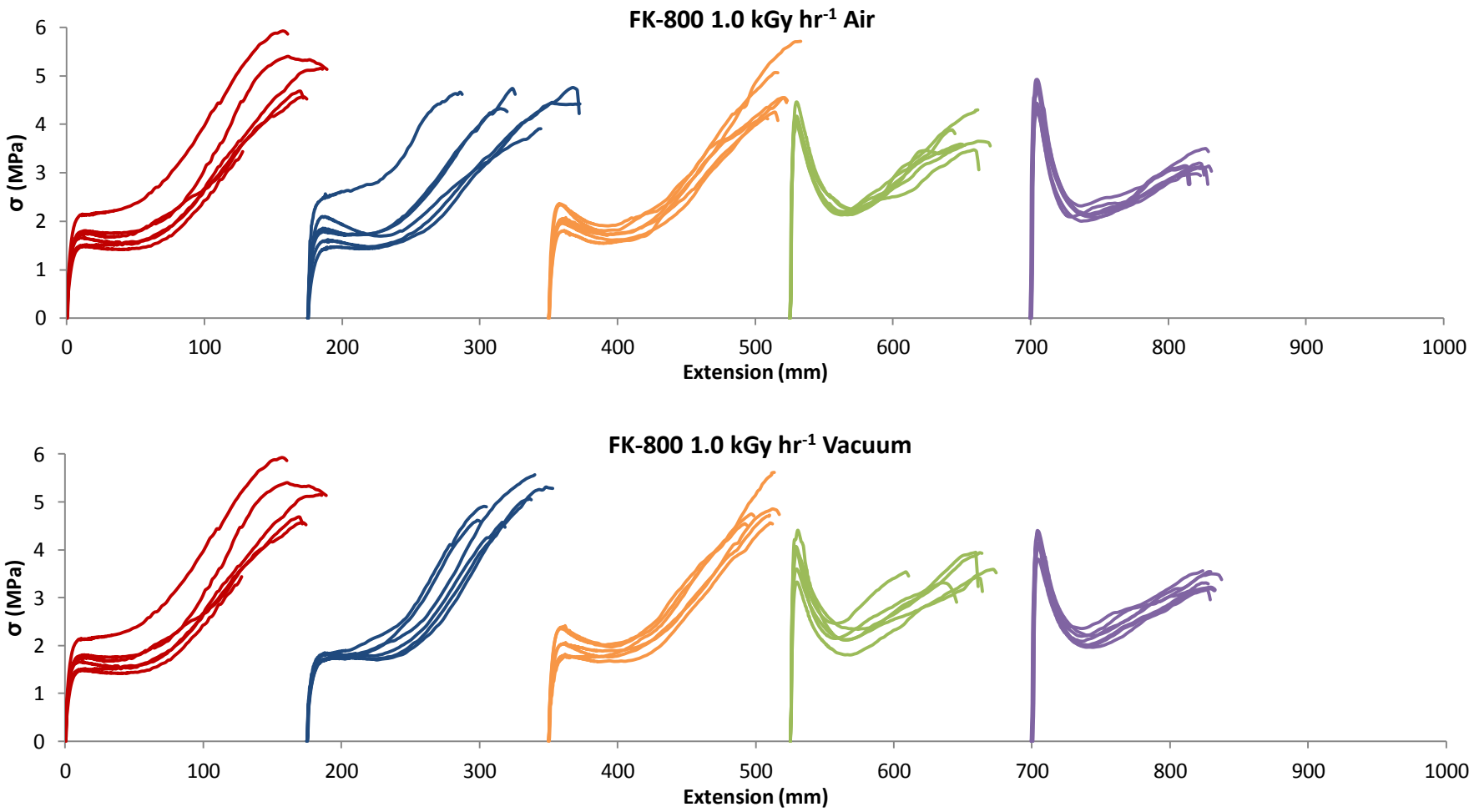

Figure 6.1.1 Stress Vs. extension curves for all the samples FK-800 tested at 1.0 kGy hr^{-1}. Each graph shows a different test atmosphere. Total radiation doses shown: Pristine — 10 kGy — 20 kGy — 50 kGy — 100kGy —

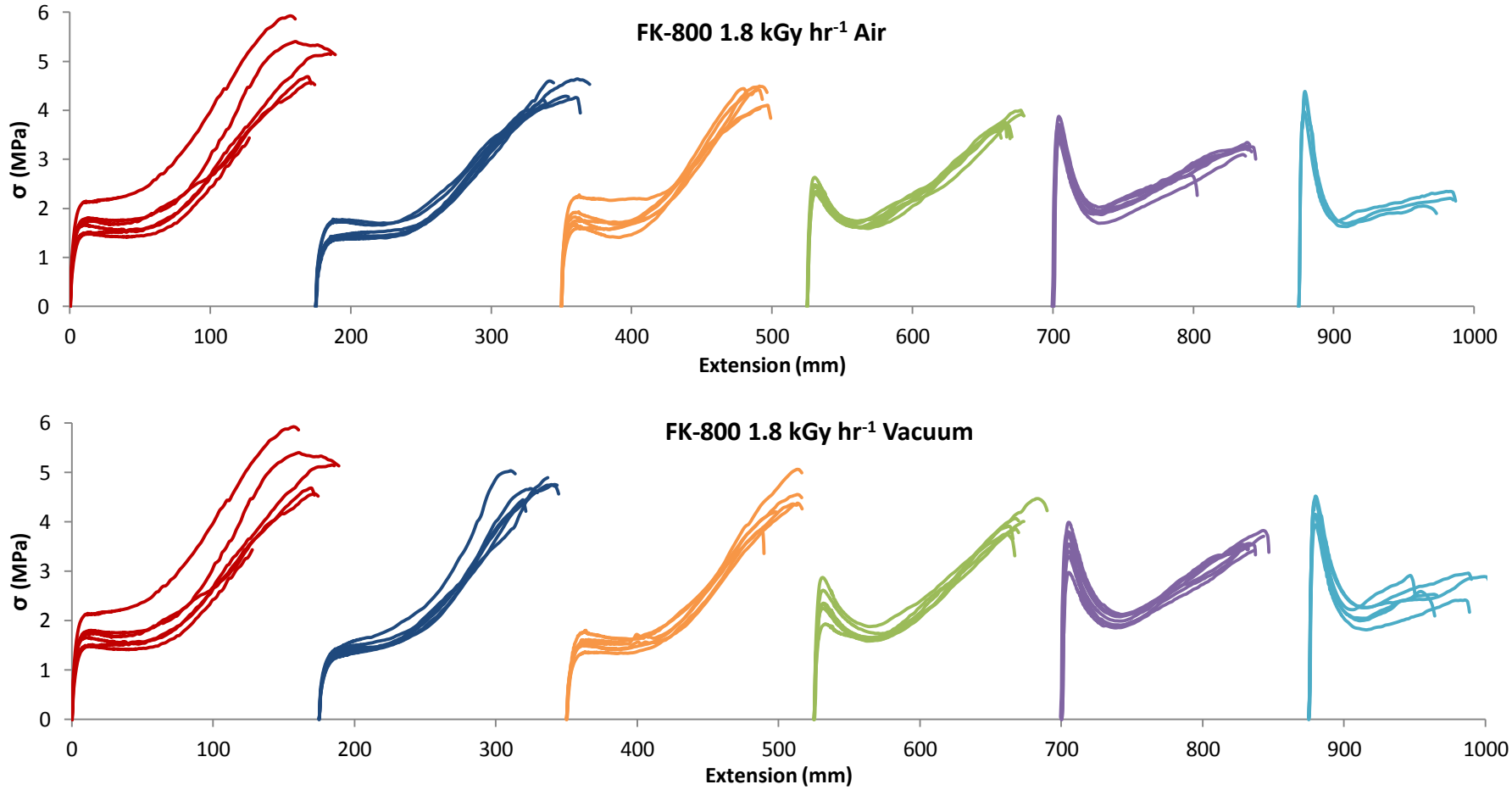

Figure 6.1.2 Stress Vs. extension curves for all the samples FK-800 tested at 1.8 kGy hr^{-1}. Each graph shows a different test atmosphere. Total radiation doses shown: Pristine 10 kGy 20 kGy 50 kGy 100kGy 200 kGy

In contrast to Figure 5.1.1 the FK-800 samples in Figures 6.1.1 and 6.1.2 show only limited extension for a large increase in stress in the initial linear phase of the stress extension curve, indicating that the samples have a low Young's modulus. The higher dose samples show a sharp yield indicating that the changes taking place at the yield are over a very short time frame and unlike the stylised Figure 5.5.1, which shows a large region of plastic flow between the yield and the rising stress caused by strain hardening, the pristine FK-800 samples show almost no plastic flow before a large amount of strain hardening is seen before failure It is clear from this data, that there has been an increase in load at yield and a reduction in ultimate tensile strength with increasing radiation dose. Additionally it is also interesting to note from that for samples irradiated at 1.0 kGy hr^{-1} to total doses of 50 kGy and 100 kGy, the samples' failure load is less than the load at yield. This change is also true for the 1.8 kGy hr^{-1} irradiated samples at doses of 100 and 200 kGy but not 50 kGy A more detailed data from the tensile load tests is shown in Figures 6.1.3 to 6.1.6

Young's modulus (E) against radiation dose has been plotted in Figure 6.1.3 shows. E can be seen to increase with radiation dose, from a mean of 6.0 MPa for the pristine sample, to a maximum mean of 23.2 MPa for the 100 kGy sample irradiated in air at 1.0 kGy hr^{-1}. No significant evidence is seen for irradiation atmosphere dependence, although some dose rate dependence is evident. At 50 kGy there is an 8.5 MPa difference between the samples irradiated at 1.8 kGy^{-1} under vacuum and the samples irradiated under the same conditions at 1.0 kGy hr^{-1}. The E data shows an initial sharp rise before with irradiation before the rate of increase flattens indicating a saturation effect is taking place at higher doses. An increase in E would indicate that a crosslinking effect is taking place within the polymer resulting in the need for a larger stress to cause permanent deformation to the samples.

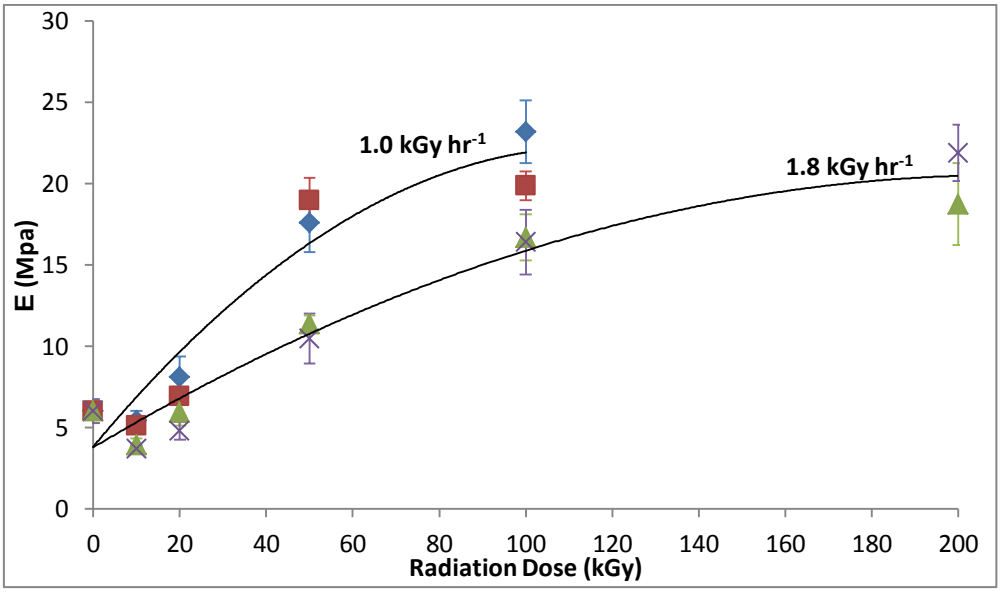

Figure 6.1.3 FK-800 mean Young's modulus against radiation dose. Radiation dose rate and sample atmosphere: 1.0 kGy hr^{-1} Air (♦) 1.0 kGy hr^{-1} Vacuum (■) 1.8 kGy hr^{-1} Air (▲) 1.8 kGy hr-1 Vacuum (X). Trend lines have been added for the two dose rates.

The mean yield stress (σ_y) for the FK-800 samples is shown in Figure 6.1.3*. As with the E data, there is an increase in σ_y with increasing radiation dose and again no irradiation atmosphere dependence is seen. Dose rate dependence is shown in the data with the largest increase in σ_y seen in the samples irradiated at 1.0 kGy hr^{-1} with a maximum 2.88 MPa increase at 100 kGy whilst a maximum 2.54 MPa increase is seen between the pristine and 200 kGy samples at 1.8kGy hr^{-1}. At both dose rates the data follows the same trend as previously seen in the E data of initially σ_y increases sharply with dose before the increase per dose unit flattens out. This is again indicative of saturation taking place at higher radiation doses. Changes in a polymer's σ_y are related to changes in crystallinity within the polymer which is explored further in Section 6.3.

* All error bars on figures in this thesis represent the 95% confidence interval.

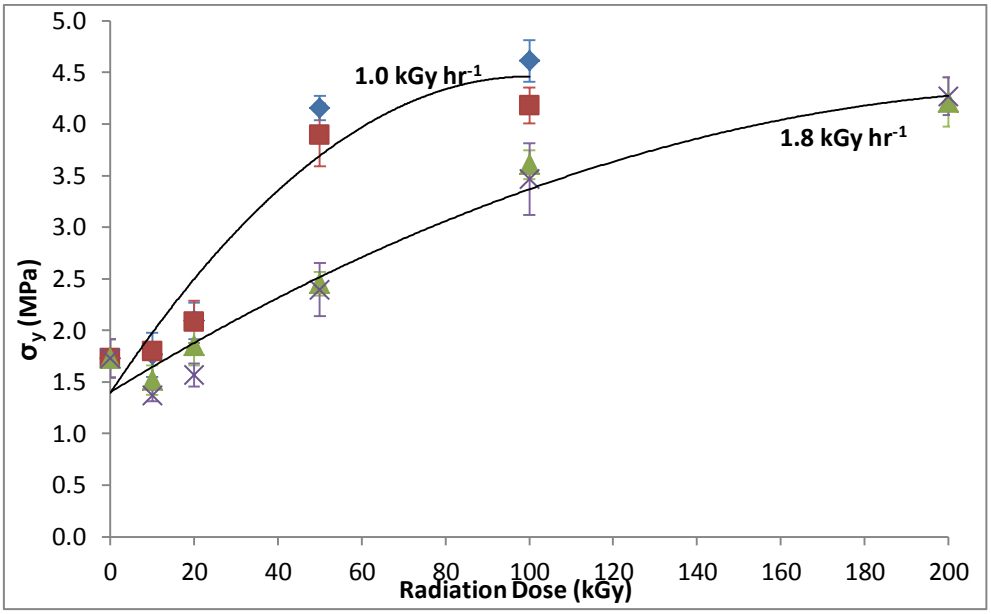

Figure 6.1.4 FK-800 mean yield stress against radiation dose. Radiation dose rate and sample atmosphere: 1.0 kGy hr^{-1} Air (♦) 1.0 kGy hr^{-1} Vacuum (■) 1.8 kGy hr^{-1} Air (▲) 1.8 kGy hr^{-1} Vacuum (X). Trend lines have been added for the two dose rates.

The data for the 1.0 and 1.8 kGy hr^{-1} E and σ_y can be fitted to the general expression Equation 6.1.1, where A is either E or σ_y at a given dose rate, B is an offset equal to the value for pristine material; C is the radiation induced changes proportional to dose and D is a correction for saturation. The values for A, B, C and D are given in Tale 6.1.1 along with the R^2 values for the fitting of the equation to the data. The associated trend lines have also been plotted in Figures 6.13 and 6.14. The inclusion of a correction for saturation indicates that at higher radiation doses, the change in the samples properties per kGy of absorbed radiation decreases.

$$A = B + C\Phi + D\Phi^2 \qquad \textbf{(6.1.1)}$$

Values for E and σ_y at higher radiation doses than those recorded in this study would be expected to flatten out following Equation 6.1.1 but not to drop off after their maximum as the calculation would suggest.

Table 6.1.1 Values for expressions A, B, C and D for equation 6.1.1 and the corresponding R2 value for the equation.

A	B	C	D	R^2
$E_{(1.0\ kGy\ hr^{-1})}$	3.8302	0.3192	-0.0014	0.93
$E_{(1.8\ kGy\ hr^{-1})}$	3.7836	0.1585	-0.0004	0.97
$\sigma_{y\ (1.0\ kGy\ hr^{-1})}$	1.3925	0.0613	-0.0003	0.94
$\sigma_{y\ (1.8\ kGy\ hr^{-1})}$	1.3999	0.025	-0.00005	0.97

Ultimate tensile strength (σ_s) - defined as the true stress at failure during tensile load testing - is shown for the irradiated FK-800 samples in Figure 6.1.5. There is an initial increase in σ_s seen in all sample sets before decreasing at higher doses. The largest decrease in σ_s is in the 200 kGy 1.8 kGy hr^{-1} vacuum samples with a decrease of 9.1 MPa from 25.3 to 16.3 MPa. A large amount of error is present in the data because as the samples fail within the reducing cross-sectional area of the necking region, any inconsistencies in the polymer sample in that region - such as small gas bubbles - can cause premature failure of the sample. No significant atmosphere or dose rate dependence can be ascertained from the σ_s data in Figure 6.1.5.

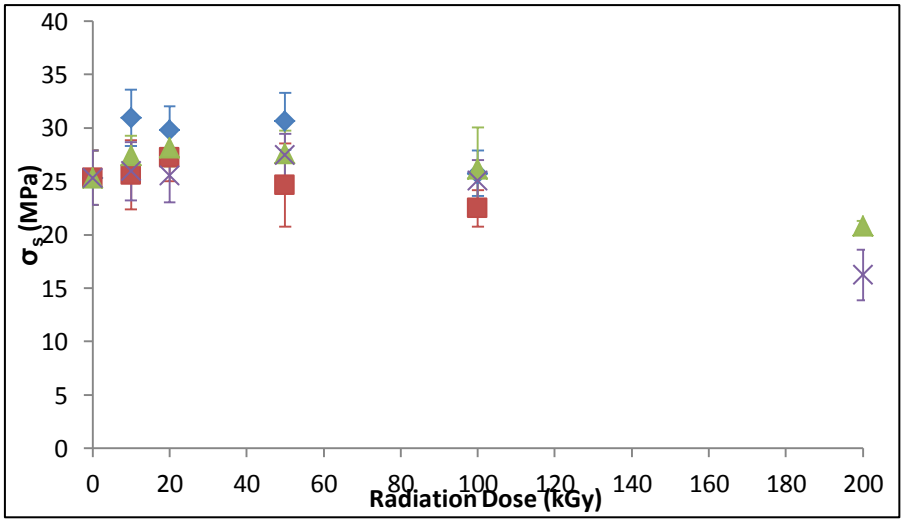

Figure 6.1.5 FK-800 mean ultimate tensile strength against radiation dose. Radiation dose rate and sample atmosphere: 1.0 kGy hr^{-1} Air (♦) 1.0 kGy hr^{-1} Vacuum (■) 1.8 kGy hr^{-1} Air (▲) 1.8 kGy hr^{-1} Vacuum (X).

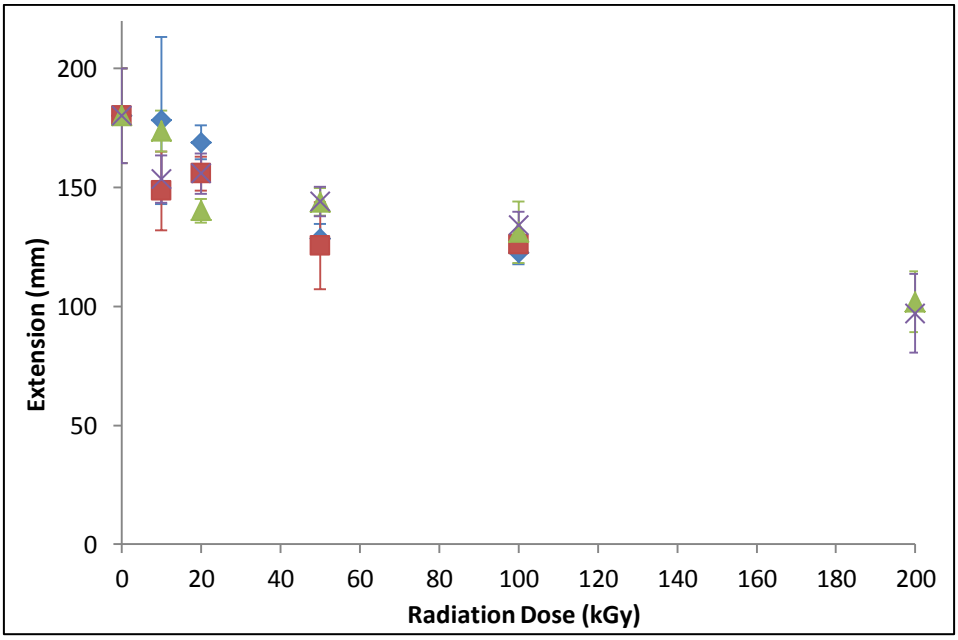

Figure 6.1.6 FK-800 mean extension at ultimate tensile stress against radiation dose. Radiation dose rate and sample atmosphere: 1.0 kGy hr^{-1} Air (♦) 1.0 kGy hr^{-1} Vacuum (■) 1.8 kGy hr^{-1} Air (▲) 1.8 kGy hr^{-1} Vacuum (X).

Figure 6.1.6 shows the sample extension at σ_s as recorded by the Instron universal testing machine. A mean decrease in elongation can be seen for all irradiated sample sets. No dose rate or irradiation atmosphere dependence is present in the data with all samples behaving similarly at each total dose. The largest change in the mean values was 54% for the 1.8 kGy hr^{-1} 200 kGy vacuum irradiated sample with a decrease in elongation of 83 mm from 180 to 97 mm.

In contrast to tensile load testing which tests samples beyond their elastic limits (initial linear region of the stress-strain curve) to destruction, DMA was used to repeatedly test the same sample within its elastic limit, whilst changing the temperature.

Figure 6.1.7 shows the results for one DMA test on a pristine sample of FK-800. The plot shows E', E'' and tan δ for the 1, 5 and 10 Hz frequencies tested from -150 to 100 °C. The samples show a large transition indicative of a T_g between 20 and 50 °C; this is indicated by a drop in E', a peak in E'' and a large peak in the tan δ. A beta transition can also be seen in Figure 6.1.7 between -120 and

0 °C, indicated by a hump in both E'' and tan δ along with a change in slope for E'.

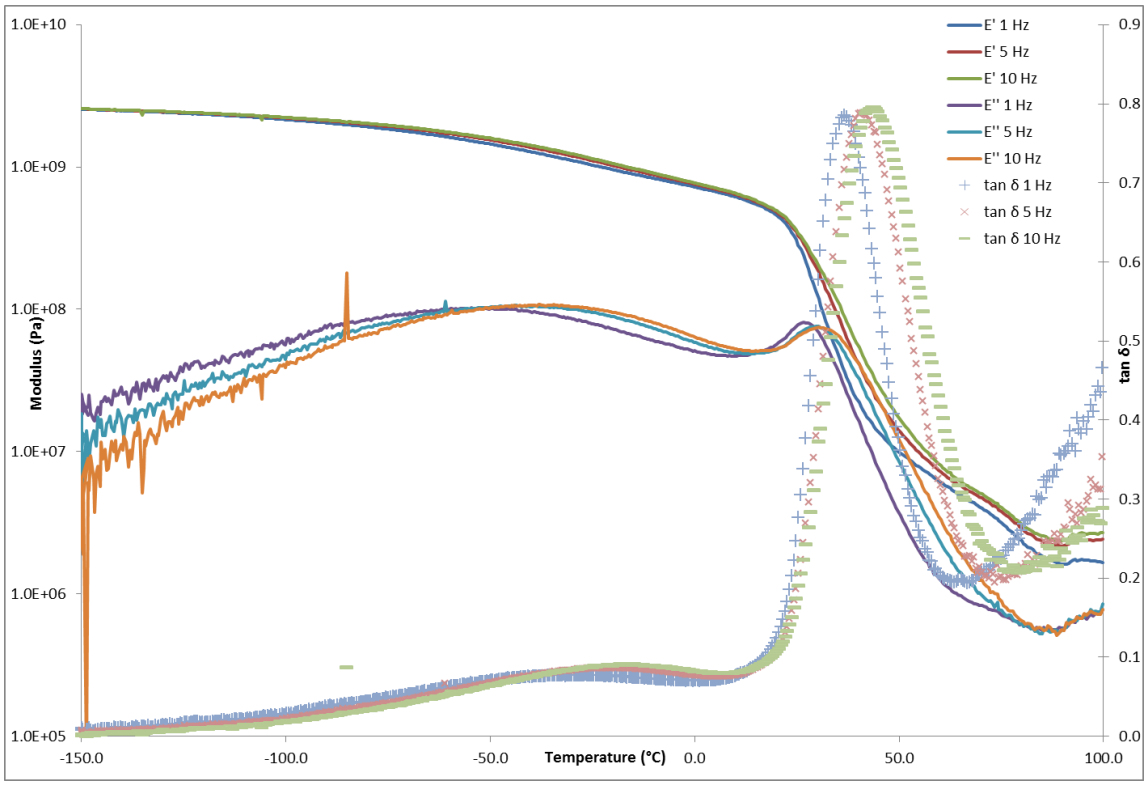

Figure 6.1.7 Log plot of the DMA results of a pristine FK-800 sample. The plot shows E', E'' and tan δ at all temperatures and frequencies tested.

During some of the DMA tests, artefacts resulting in a double peak around the E'' T_g maximum caused by the DMA equipment were seen; because of this, E'' was not a suitable measure for T_g and the tan δ peak value was used to compare samples instead. It was also discovered after initial testing that the DMA equipment had developed a fault prior to this study which had affected the results. A decision was made to start the testing over using back-up samples, however, the vial containing the back-up samples for the 1.8 kGy hr^{-1} air samples irradiated to 200 kGy had become damaged in storage and these data set was not tested due to the time implications of producing new samples.

During the DMA experiments, no identifiable changes were seen in any sample at test temperature below -50 °C, there was also no difference in the trends seen in the 1, 5 and 10 Hz data during testing of the FK-800 samples. Therefore, only the 0, 10, 20, 50 and 100 kGy data from -50 °C and at 1 Hz will be presented and discussed here.

Figures 6.1.8 to 6.1.11 show the DMA E' results for pristine FK-800 and irradiated samples; three samples from each irradiation were tested and the results have been averaged for presentation using the robust statistics, median/MAD method as described in the RSC Analytical Methods Committee technical brief "Robust statistics: a method of coping with outliers"[77] .

The samples irradiated at 1.0 kGy hr^{-1} in air (Figure 6.1.8) show changes in the E' over the polymers plateau region after the T_g. At 10, 20 and 50 kGy the samples show a decrease in E' against the pristine between 30 and 80 °C, whilst the 100 kGy sample shows a stiffer E' between 30 and 70 °C before dropping off and crossing the pristine line around 80 °C. The increase in E' of the 100 kGy sample also leads to a smaller drop in modulus across the T_g region. The same trends seen in the 1.0 kGy hr^{-1} air samples are also seen in the samples irradiated at 1.0 kGy hr^{-1} under vacuum (Figure 6.1.9) with no atmosphere dependence shown between the two data sets.

The samples irradiated at 1.8 kGy hr^{-1} in air (Figure 6.1.10) show a similar trend to those irradiated at the lower dose rate, although the 50 kGy sample's E' values are very close to those of the pristine over the rubbery plateau region. The 100 kGy samples irradiated at 1.8 kGy hr^{-1} in air show the formation of a new step drop in E' at approximately -25 °C, as well as the increase in E' over the pristine samples through the plateau seen at the lower dose rate. The new step in E' could indicate the formation of a new transition in the polymer but no corresponding peak was observed in the tan δ results.

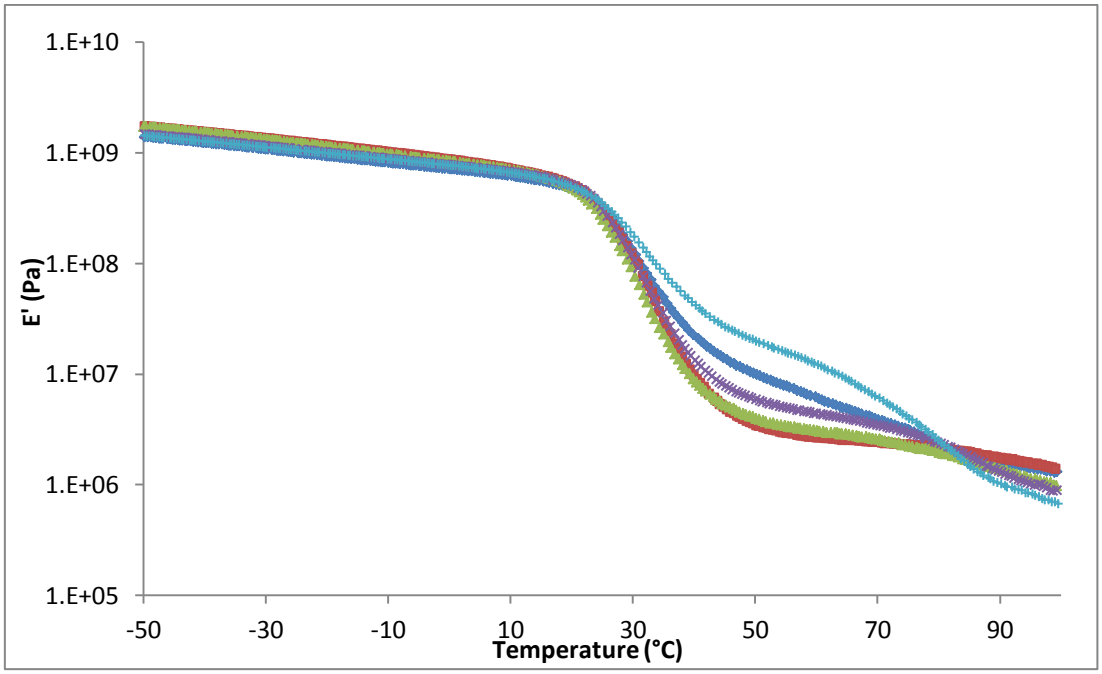

Figure 6.1.8 Log plot of the DMA median/MAD mean storage modulus (E') results for pristine (♦), 10 kGy (■), 20 kGy (▲), 50 kGy (X), and 100 kGy (+) FK-800 samples irradiated at 1.0 kGy hr^{-1} in air

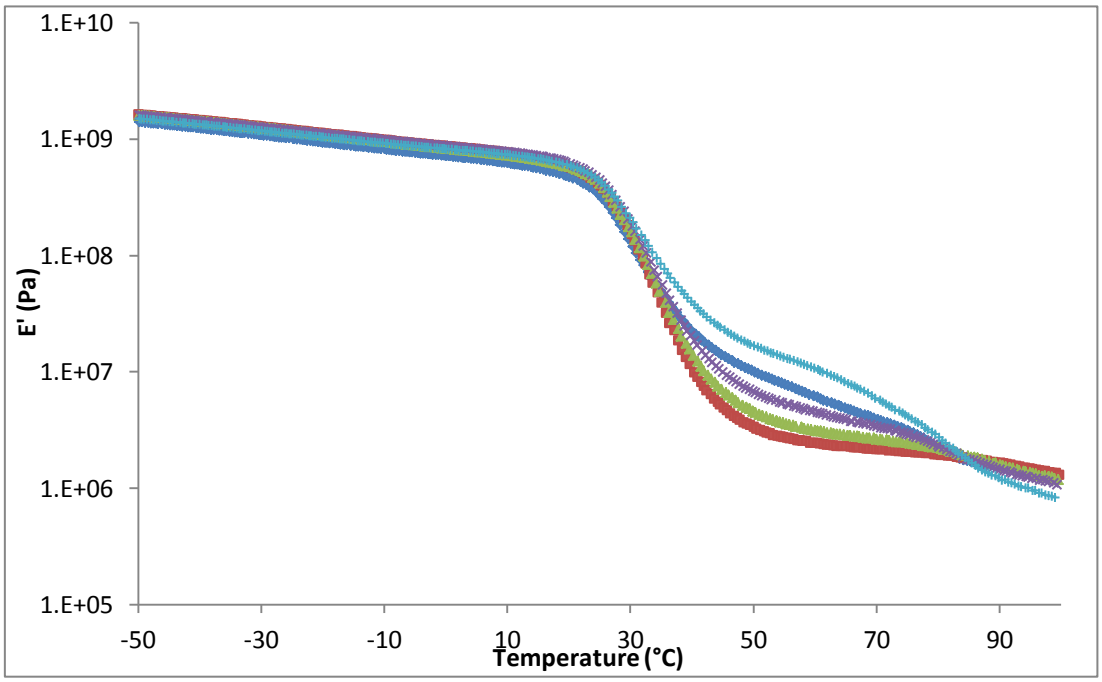

Figure 6.1.9 Log plot of the DMA median/MAD mean storage modulus (E') results for pristine (♦), 10 kGy (■), 20 kGy (▲), 50 kGy (X), and 100 kGy (+) FK-800 samples irradiated at 1.0 kGy hr^{-1} under vacuum

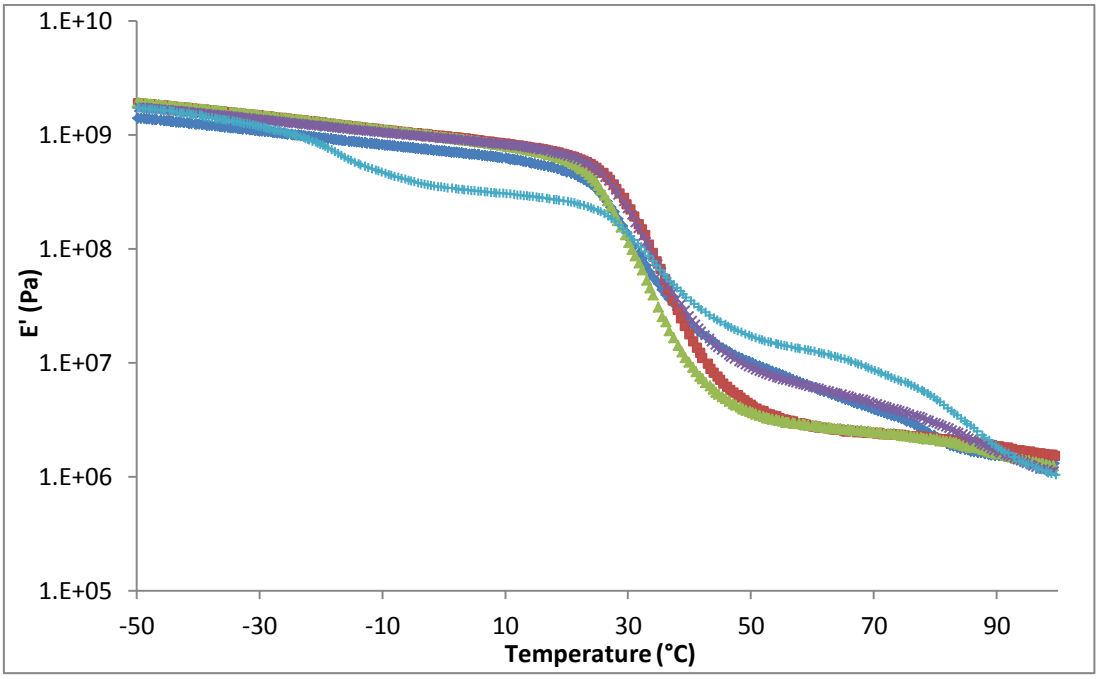

Figure 6.1.10 Log plot of the DMA median/MAD mean storage modulus (E') results for pristine (♦), 10 kGy (■), 20 kGy (▲), 50 kGy (X), and 100 kGy (+) FK-800 samples irradiated at 1.8 kGy hr^{-1} in air

The E' results for the 1.8 kGy hr^{-1} vacuum irradiated samples (Figure 6.1.11) follow the same trends seen in the 1.0 kGy hr^{-1} sample sets. Some irradiation atmosphere dependence was noted at the higher dose rate with the 100 kGy vacuum samples not showing the possible sub T_g transition seen in the air-irradiated sample set. Evidence does exists for a sub T_g transition at 200 kGy for samples irradiated at 1.8 kGy hr^{-1} under vacuum (Figure 6.1.12) but these data were not included in the median/MAD plots because of the inconsistency in the results of the three samples tested. Only sample 3 in Figure 6.1.12 gives a whole set of data indicating a possible below T_g transition similar to that seen in the 100 kGy 1.8 kGy h^{-1} air samples. In the two other samples tested from the 200 kGy under vacuum irradiation set, both show breaks in the data indicating that the samples had become too fragile for testing under the experimental conditions used.

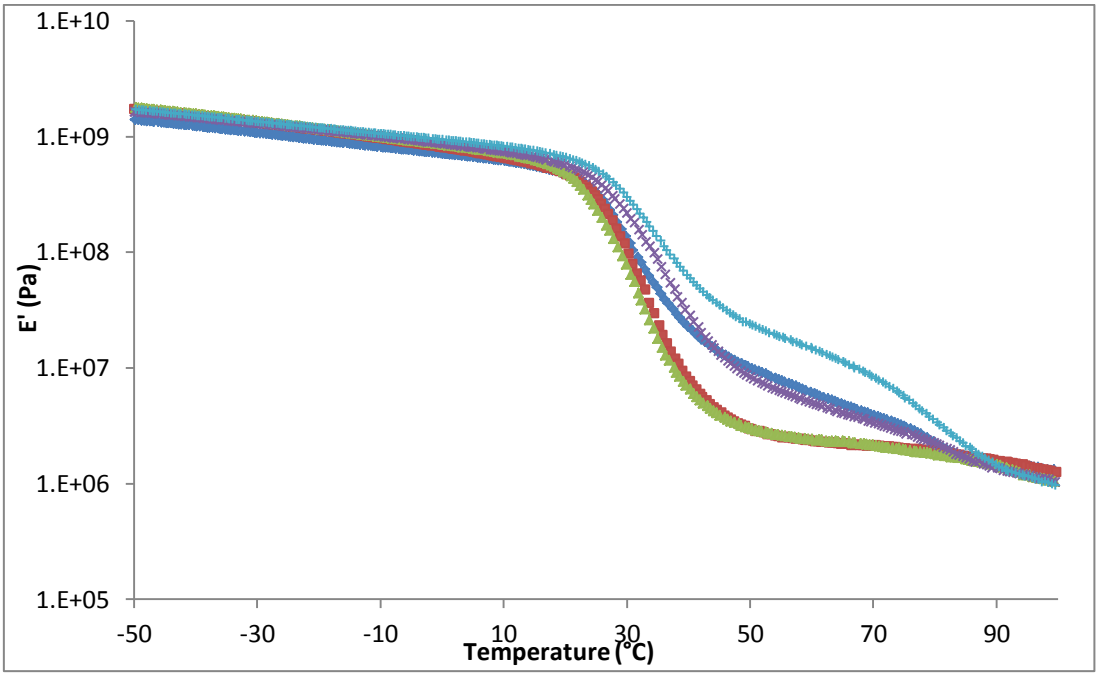

Figure 6.1.11 Log plot of the DMA median/MAD mean storage modulus (E') results for pristine (♦), 10 kGy (■), 20 kGy (▲), 50 kGy (X), and 100 kGy (+) FK-800 samples irradiated at 1.8 kGy hr^{-1} under vacuum

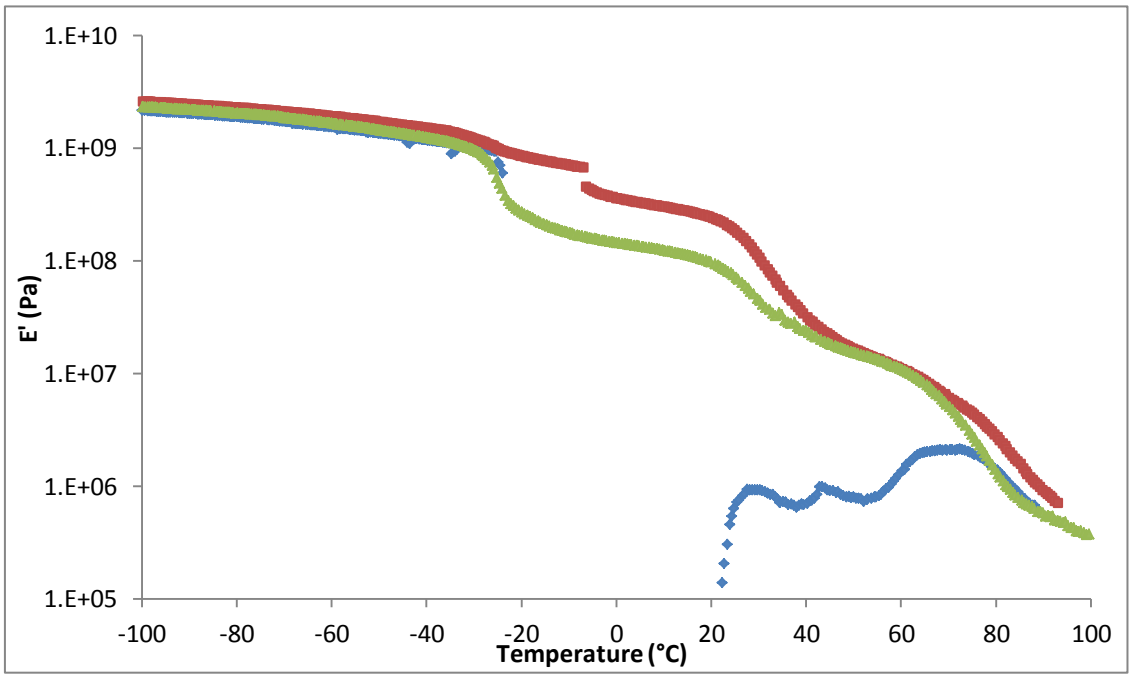

Figure 6.1.12 Log plot of the DMA storage modulus (E') 1 Hz results for FK-800 samples irradiated to 200 kGy at 1.8 kGy hr^{-1} under vacuum. Sample 1 (♦), sample 2 (■), sample 3 (▲)

To quantify the changes in E' seen across the rubbery plateau of the irradiated samples, the E' values at 50 °C were recorded and plotted against each other (Figure 6.1.13). The E' data at 50 °C show little to no dose rate or atmosphere dependence; all data sets show a drop in E' of ~5 MPa between the pristine and 10 kGy data points, before recovering to values similar to the pristine material at 50 kGy. At 100 kGy there is an approximately three fold increase in the mean E' over the pristine material with an increase from 8 to ~24 MPa, although, at 100 kGy the 95% confidence error has significantly increased. The increase in the error size indicates a large spread in values across the three individual samples. The results shown in Figure 6.1.13 show that the FK-800 samples irradiated to 100 kGy are significantly stiffer at 50 °C than the pristine or lower dose irradiated samples. The increase in stiffness of the 100 kGy samples quickly falls away at temperatures above 70 °C returning to E' values close to those of the other samples by 85 °C (Figures 6.1.8-11).

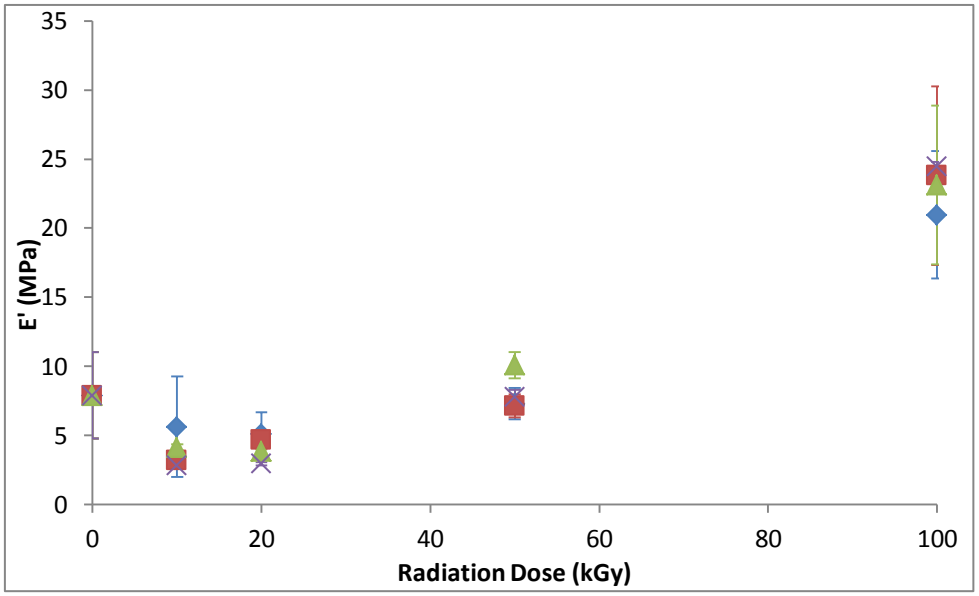

Figure 6.1.13 DMA mean storage modulus (E') values at 50 °C for samples irradiation conditions: 1.0 kGy hr^{-1} Air (♦) 1.0 kGy hr^{-1} Vacuum (■) 1.8 kGy hr^{-1} Air (▲) 1.8 kGy hr^{-1} Vacuum (X)

Tan δ, Figures 6.1.14 - 17, can be used to both identify transitions as peaks in the data, and also to give an indication of the relative intensity of the transition against another sample.

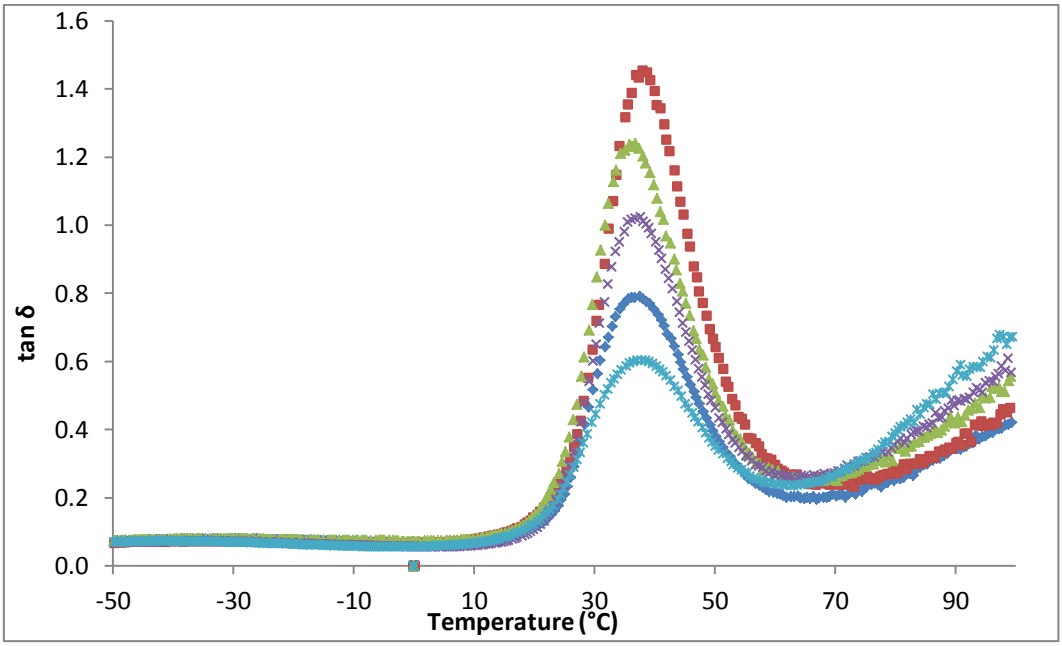

Figure 6.1.14 DMA median/MAD mean tan δ results for pristine (♦), 10 kGy (■), 20 kGy (▲), 50 kGy (X), and 100 kGy (ж) FK-800 samples irradiated at 1.0 kGy hr^{-1} in air

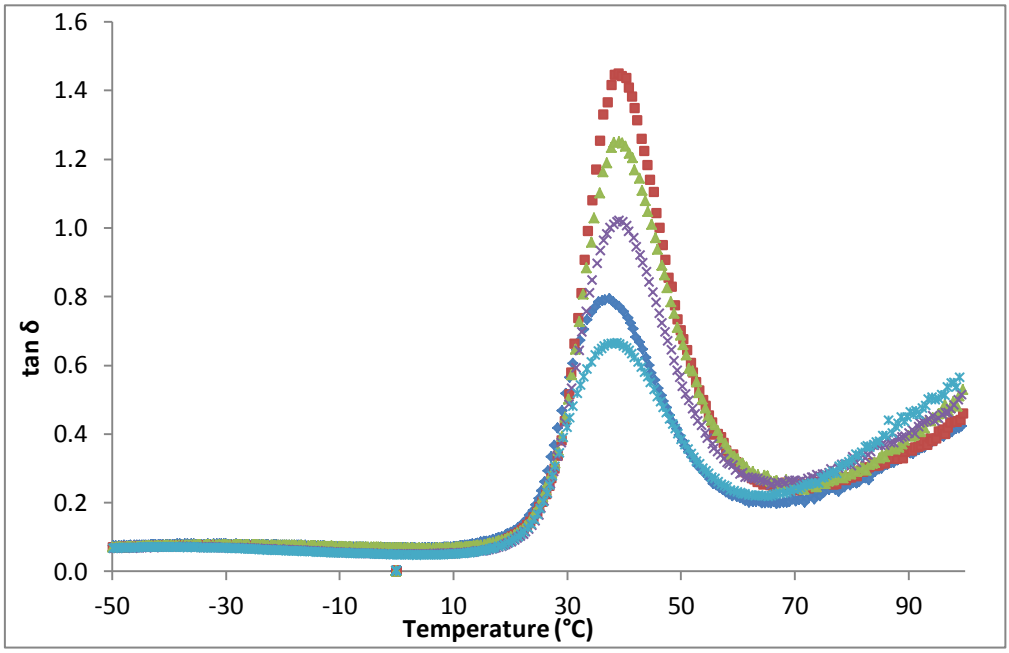

Figure 6.1.15 DMA median/MAD mean tan δ results for pristine (♦), 10 kGy (■), 20 kGy (▲), 50 kGy (X), and 100 kGy (ж) FK-800 samples irradiated at 1.0 kGy hr^{-1} under vacuum

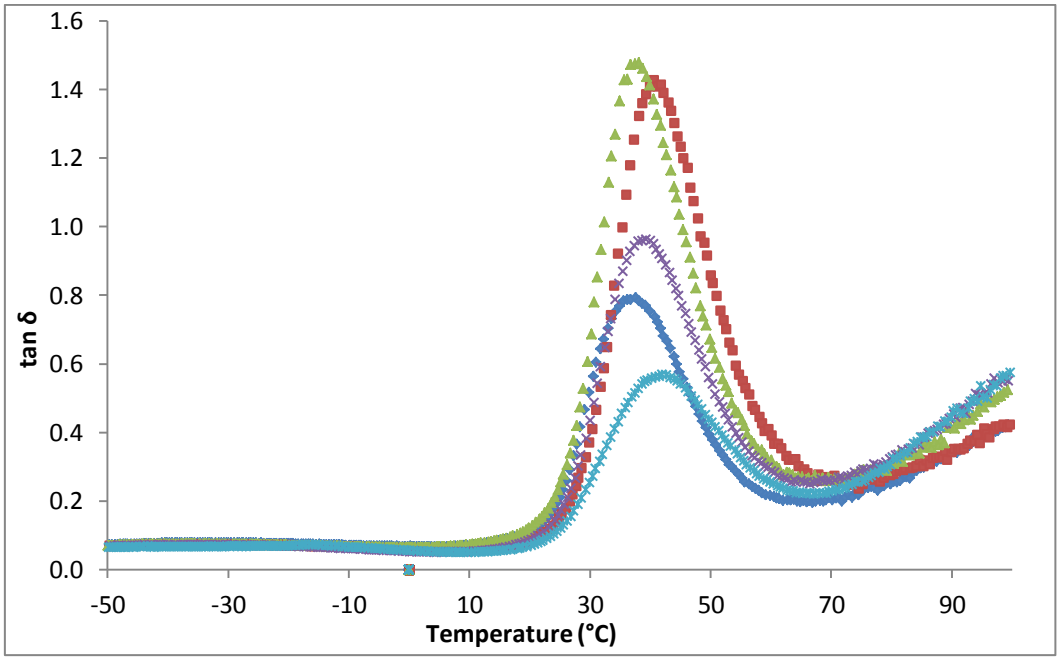

Figure 6.1.16 DMA median/MAD mean tan δ results for pristine (♦), 10 kGy (■), 20 kGy (▲), 50 kGy (X), and 100 kGy (ж) FK-800 samples irradiated at 1.8 kGy hr^{-1} in air

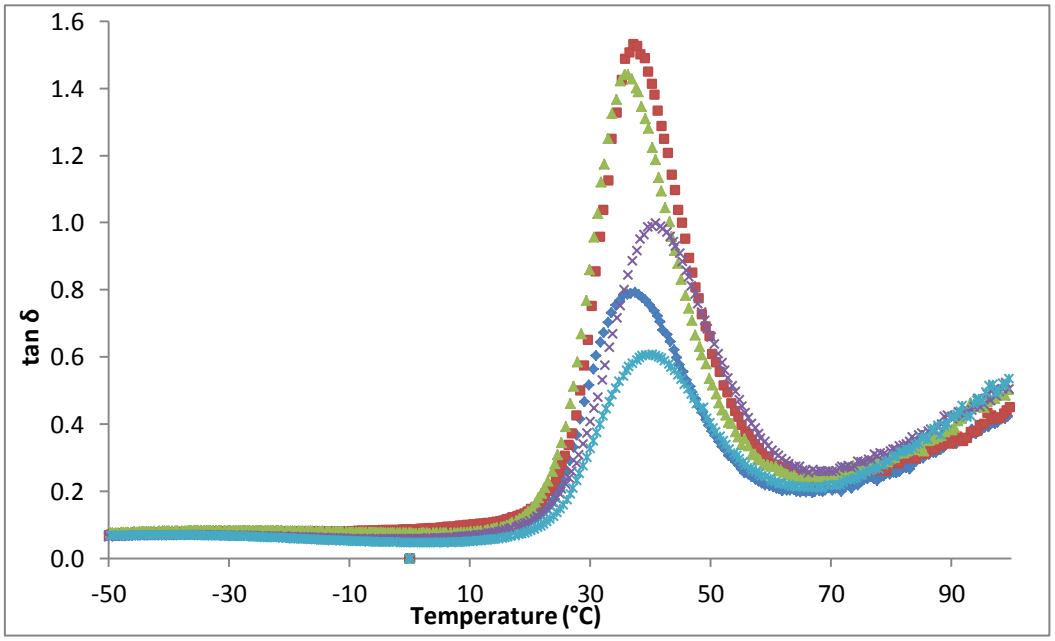

Figure 6.1.17 DMA median/MAD mean tan δ results for pristine (♦), 10 kGy (■), 20 kGy (▲), 50 kGy (X), and 100 kGy (ж) FK-800 samples irradiated at 1.8 kGy hr^{-1} under vacuum

Each set of results shows the same trend with the 10, 20, and 50 kGy peak heights being higher than those of the pristine material, and the 100 kGy peak lower than the pristine in all the sample sets. This is indicating that the T_g intensity is greatest in the samples irradiated to 10 kGy and so more of the sample is undergoing the transition in those samples. The changes in tan δ are directly related to the lower E' values seen in Figures 6.1.8 to 6.1.11 and follow the same trend. From approximately 65 °C the tan δ values for all the samples start to rise but do not reach a peak. This rise is related to the start of the polymer's crystalline melt but to protect the equipment the samples were not run through their melt.

The changes in the tan δ peak heights relate to changes in the amount of material undergoing the transition, an increase in the peak height can be related to chain scissions or a reduction in crystallinity both resulting in increased polymer chain mobility. The inverse is also true with a decrease in tan δ peak height resulting in a reduction in chain mobility caused by either chain crosslinking or increases in crystallinity.

6.2 Glass transition temperature (T_g)

Changes in the polymers' T_g were measured using DSC and DMA. Only the trends in the two sets of data can be compared with each other; the absolute values cannot be compared due to the two differing measurement techniques. DSC measures the heat capacity change as the polymer changes from a glass to a rubber at T_g, whilst DMA measures the change in mechanical properties over the same region. Because it is measuring mechanical properties the glass transition temperature reported by DMA is affected by both strain rate and thermal ramp rate therefore values cannot be directly compared between the two techniques.

The T_g results of the DSC first run (before thermal cycling) showed a lowering of T_g at higher irradiation doses. However, a large amount of scatter and error in the data due to made it unsuitable for comparison. Therefore, the T_g was measured on a second run after thermal cycling of the sample to remove any

thermal history which may affect the samples[78]. The second scan was measured after the samples were put through a controlled temperature cycle up to 150 °C, before being returned to the start temperature at a constant cooling rate of 10 °C. The thermal cycle was used to reset the samples' crystallinity and remove any influence from the sample's thermal history. Figure 6.2.1 shows the T_g temperatures obtained from the DSC second scan and shows a drop in T_g temperature with increasing radiation dose. A maximum drop of 2.9 °C from 28.3 to 25.3 °C at 200 kGy for both the 1.8 kGy air and vacuum irradiated samples. No irradiation atmosphere or dose rate dependence can be inferred from the results shown in Figure 6.2.1.

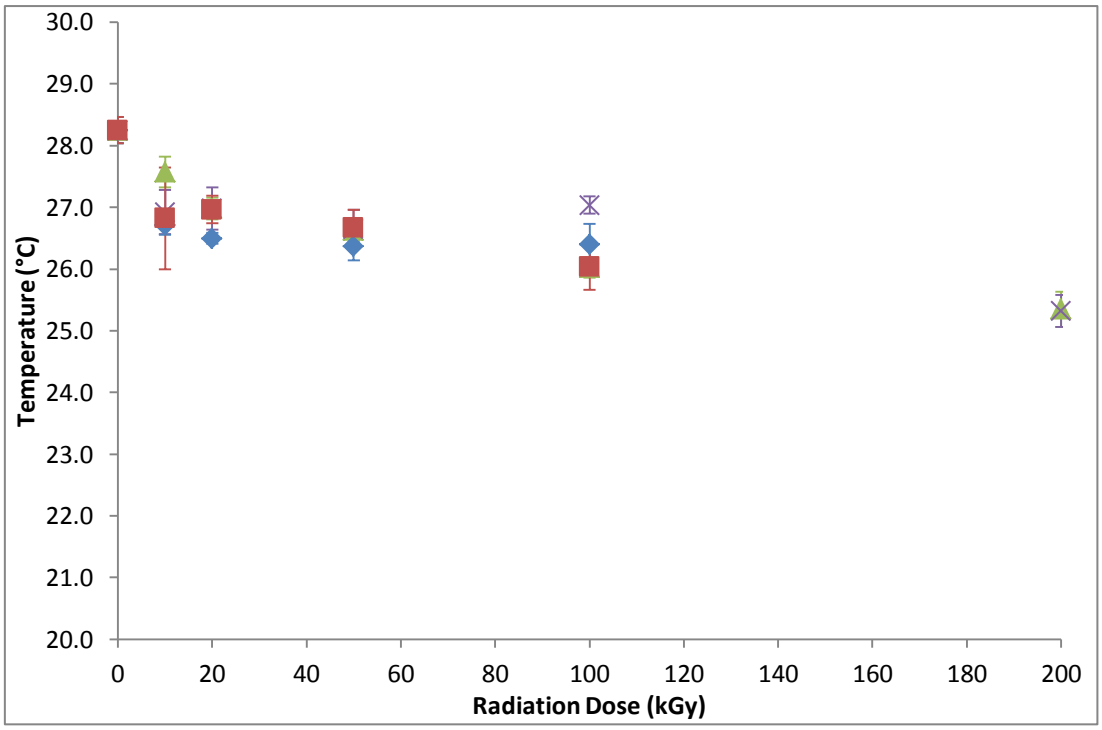

Figure 6.2.1 DSC second scan mean glass transition temperature (T_g) for pristine and irradiated FK-800. 1.0 kGy hr^{-1} Air (♦) 1.0 kGy hr^{-1} Vacuum (■) 1.8 kGy hr^{-1} Air (▲) 1.8 kGy hr^{-1} Vacuum (X)

In contrast to the DSC results, the DMA T_g measurements were recorded on the first temperature cycle of the sample without an attempt to reset the sample's thermal history. For the DMA samples the T_g was measured as the temperature at the tan δ peak and the results are presented in Figure 6.2.2. There is no dose rate or irradiation atmosphere dependence shown in the T_g data. Some spread

in the data can be seen at 10 kGy, but, when the error is taken into account no significant difference between irradiation conditions is seen at this dose, or at any of the other radiation doses tested. There is a slight upward trend in the T_g in all sample set with a maximum increase of 2.3 °C from 37.8 to 40.1 °C between the pristine and 100 kGy samples irradiated at 1.8 kGy hr^{-1}. A 2.3 °C increase in the T_g is small but, combined with the changes in the tan δ peak heights, could indicate that changes in the polymer are taking place, affecting its glass transition behaviour when measured by a mechanical method.

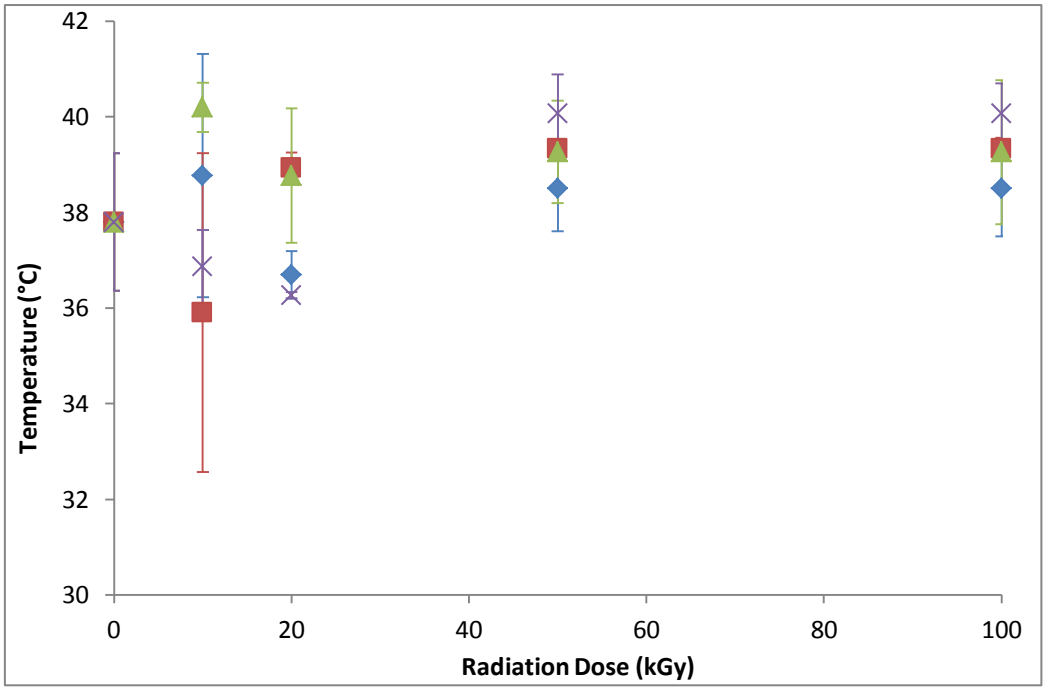

Figure 6.2.2 DMA tan δ mean glass transition (T_g) temperatures for FK-800. 1.0 kGy hr^{-1} Air (♦) 1.0 kGy hr^{-1} Vacuum (■) 1.8 kGy hr^{-1} Air (▲) 1.8 kGy hr^{-1} Vacuum (X)

6.3 FK-800 Crystallinity

The most obvious change in the stress - strain behaviour of the irradiated FK-800 samples is the large increases seen in the stress at yield and corresponding increase in Young's modulus. Yield behaviour of polymers is related to the crystallinity of the polymer and the yield process itself is governed by the deformation or transformation of part or all of the polymer's crystals[79]. To investigate changes in the crystallinity of the irradiated samples, DSC was

used to calculate the percentage crystallinity based on the heat of fusion for 100 % crystalline poly-CTFE. The use of this method for samples of Kel F-800 was discussed by Hoffman[61] who based the method on the assumption that, because CTFE makes up 75 % of the Kel F-800, only it would be involved in forming crystals.

Percentage crystallinity was calculated using the heat of fusion from the DSC first scan and the latent heat of fusion for 100 % crystalline poly-CTFE (-43.09 J g^{-1})[61]. Figure 6.3.1 shows how the crystallinity of the irradiated samples increases with radiation dose. All sample sets are seen to rise rapidly from a mean crystallinity of 0.6 % in the pristine samples to between 5.7 and 7 % at 100 kGy. The rate of increase in crystallinity shows a linear trend up to 100 kGy, before flattening between 100 and 200 kGy in the 1.8 kGy hr^{-1}. No dose rate or atmosphere dependence can be deduced from these results and all the data can be fitted to a trend line (Equation 6.3.1) with the general terms of Equation 6.1.1 and an R^2 value of 0.99. The equation includes a term for saturation indicating that as crystallinity increases the crystallinity increase per kGy decreases due to reduced chain mobility caused by the formation of crystals. As with the mechanical properties results, the rate of crystallisation would be expected to decrease following Equation 6.1.3 and stop at a maximum crystallinity rather than decreasing as the expression would indicate.

$$\%\, Crystallinity = 0.4056 + 0.0747\ \Phi - 0.0002\ \Phi^2 \qquad \textbf{(6.3.1)}$$

The evidence for the polymer crystallinity increasing with radiation dose is further supported by increases in the density of the polymer after irradiation. Figure 6.3.2 shows an increase in mean density in all sample sets with the highest density increase in the highest total dose samples for each dose rate/atmosphere combination. The data show a maximum mean increase in density of 0.9% for the 100 kGy, 1.0 kGy hr^{-1} air samples from 1.996 to 2.104 g cm^{-3}. The data would be expected to plateau as a maximum density is reached. Dose rate and atmosphere dependence is evident in the density data; however, this may result from differences in temperature during the density

measurements affecting the trends. The temperature variations could not be avoided due to the location of the test equipment.

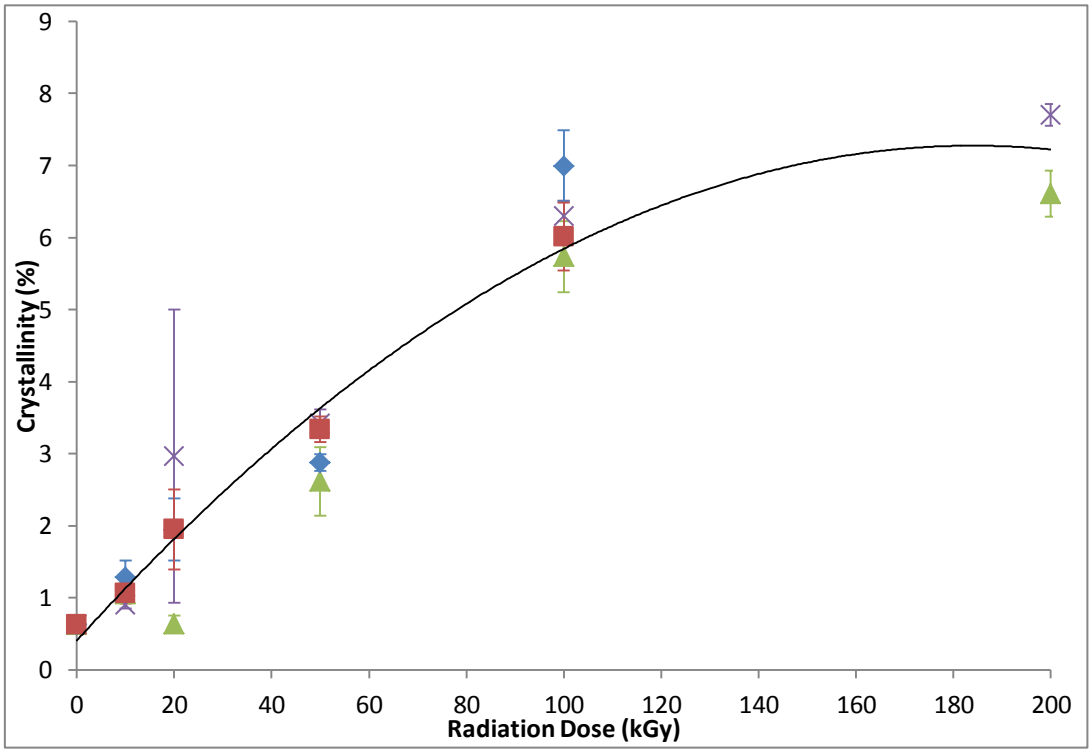

Figure 6.3.1 Mean DSC first scan percentage crystallinity for pristine and irradiated FK-800. 1.0 kGy hr^{-1} Air (♦) 1.0 kGy hr^{-1} Vacuum (■) 1.8 kGy hr^{-1} Air (▲) 1.8 kGy hr^{-1} Vacuum (X). A trend line has been added based on all results.

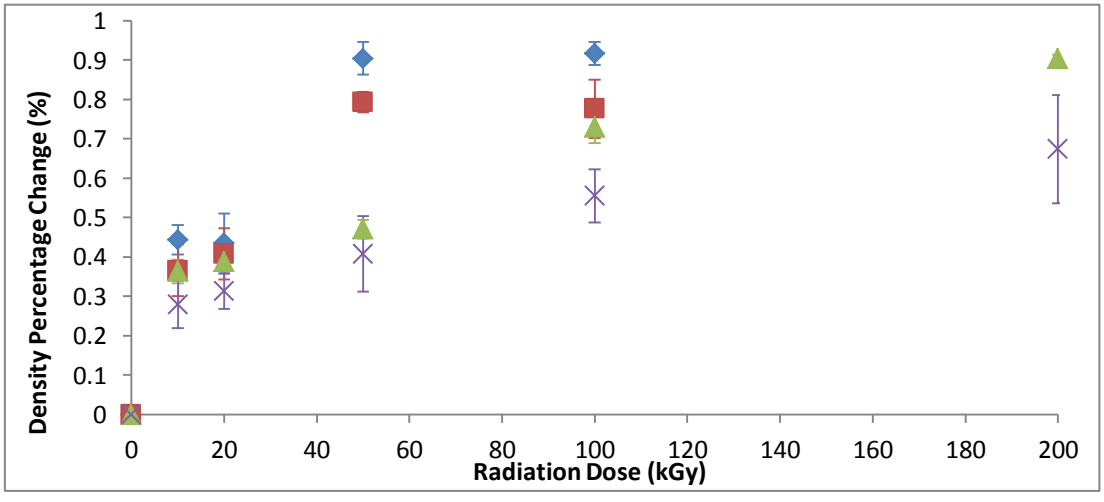

Figure 6.3.2 Mean percentage change in density of the FK-800 dogbone samples after irradiation. 1.0 kGy hr^{-1} Air (♦) 1.0 kGy hr^{-1} Vacuum (■) 1.8 kGy hr^{-1} Air (▲) 1.8 kGy hr^{-1} Vacuum (X)

To confirm the DSC percentage crystallinity values, X-ray diffraction tests were conducted on samples of FK-800 irradiated in air and under vacuum to doses of 10, 50 and 100 kGy at 1.8 kGy hr^{-1}. The percentage crystallinity for the samples tested by X-ray diffraction is shown in Table 6.3.1.

The X-ray diffraction data were processed by assuming that the pristine material had no crystallinity and measuring the difference in area between the pristine and the irradiated samples to give I_c (Equation 5.12.1), represented by the area between the blue and red lines in figure 6.3.3. I_c was then divided by $I_c + I_a$ measured as the area under the irradiated sample spectrum (red line in Figure 6.3.3), and finally multiplied by 100 to give a percentage. The 0% pristine assumption was made because a good and consistent baseline could not be established on the X-ray diffraction spectra to allow calculation of absolute values. It can also be seen from the DSC thermograms (Figure 8.1.7) that the pristine sample shows only a very small crystal melt at 115 °C, indicating it has very little crystallinity.

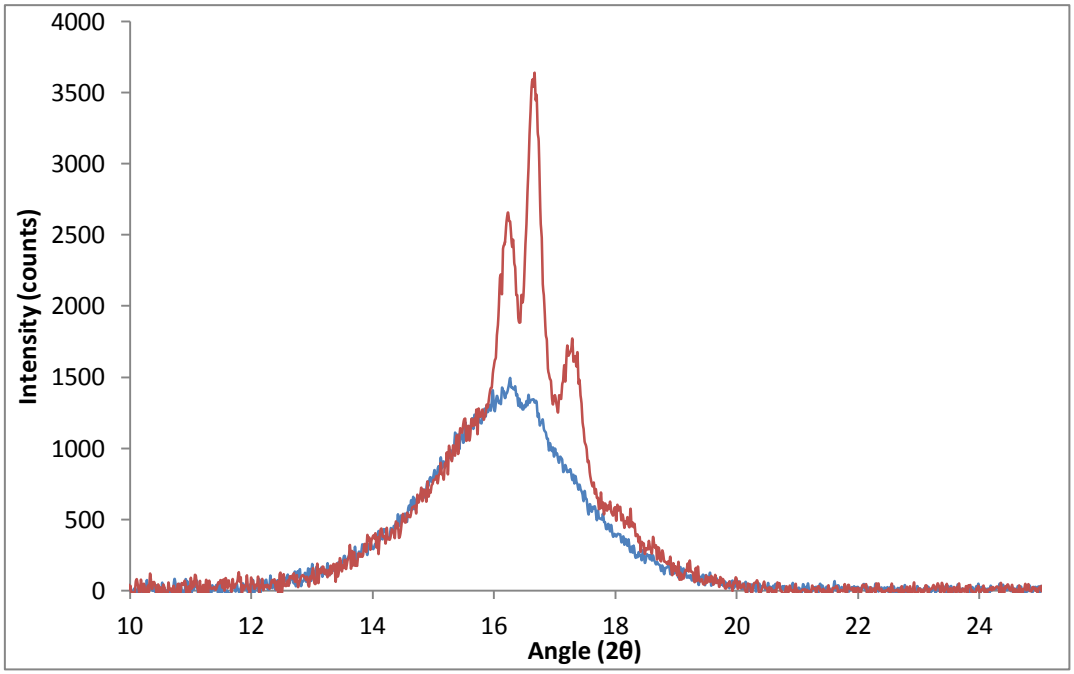

Figure 6.3.3 X-ray diffratogram for angles 10 to 25 2θ for Pristine — and 100 kGy air irradiated — samples of FK-800

Table 6.3.1 X-ray diffraction estimated percentage crystallinity for irradiated FK-800 assuming an amorphous pristine

Radiation Dose (kGy)	Air Irradiated Crystallinity (%)	Vacuum Irradiated Crystallinity (%)
Pristine	~0%	~0%
10	6.5%	1.9%
50	10.5%	8.2%
100	12.0%	12.1%

The X-ray diffraction data for samples irradiated in air show a rapid rise of 6.5 % at 10 kGy but then the rate of increase in crystallinity slows with only a doubling of the percentage crystallinity to 12 % for a 10 times increase in radiation dose. In contrast to the air-irradiated samples, the crystallinity in the samples irradiated under vacuum increases at a close to constant rate before reaching a maximum equal to that of the air-irradiated samples. The X-ray diffraction results suggest a difference in crystallisation rate between the samples irradiated in air and under vacuum. Although a large atmosphere dependence has been seen in the rate of crystallisation, it must be noted that the results consist of only one sample at each radiation dose and so no indication of any error can be identified.

It is clear from the X-ray diffraction data that the values for the percentage crystallinity obtained by DSC underestimate the actual crystallinity of the samples. It can therefore be inferred that although the majority of crystals would form in the regions of CTFE the VDF component of FK-800 must be playing a part in the co-polymer's crystals.

6.4 FK-800 polymer molecular mass

GPC was used to study changes in the polymer's mass caused by irradiation. Samples of irradiated polymer were tested along with pristine material and the results are presented as a percentage change from the pristine.

Initially the GPC chromatograms were processed using an automated method; peak measurements were automatically taken as peaks lifted 1 % above the baseline to 1% before the peak touched down. Using the automated method

gave consistent results which were not affected by inconsistencies in the baseline. When the results were analysed against the GPC chromatograms, it was observed that not all of the polymer's low molecular mass chains were being accounted for. Figure 6.4.1 shows two GPC chromatograms for pristine and irradiated FK-800, with the point at which the automated peak measuring stopped indicated. Figure 6.4.1 a clearly shows that even in pristine FK-800, when the automated 1% stop is used the peak does not return to the baseline at that point, with the FK-800 curve having a low molecular mass tail. After irradiation the low molecular mass tail can be seen to increase in size (Figure 6.4.1 b), indicating the formation of more low molecular mass chains.

As a result of the automated peak measuring not being able to include the curve's tail consistently, an automated start for the peak integration was taken from 1% above the baseline and a manual baseline extension and stop were used for the integrations. The results for percentage change in M_n, M_w and $Đ_M$ using the manual integration method are shown in Figures 6.4.2 to 6.4.4.

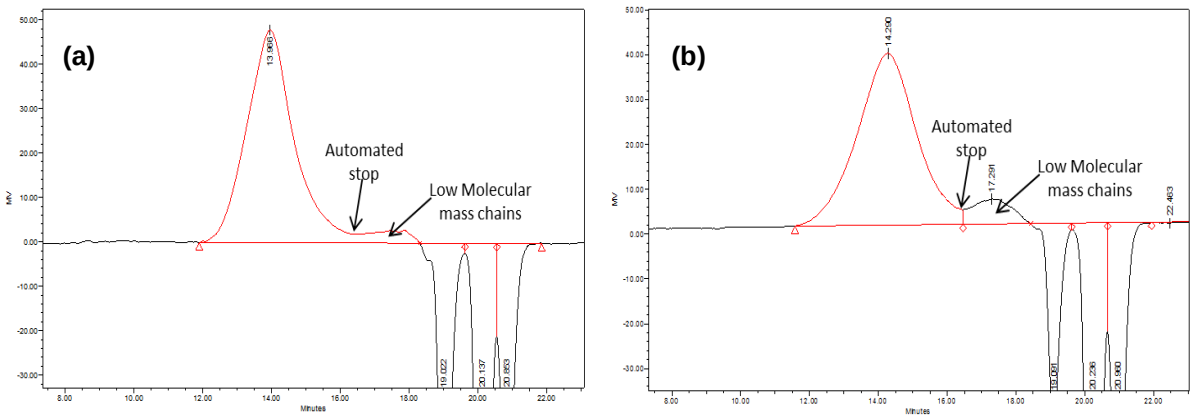

Figure 6.4.1 GPC chromatograms of pristine (a) and 200 kGy irradiated (b) FK-800

The percentage change results for M_n are shown in Figure 6.4.2. The results show a drop in M_n in all sample sets above 50 kGy with the largest average drop of 50% seen in the 200 kGy 1.8 kGy hr^{-1} vacuum irradiated samples. The lower dose rate samples sets show a drop in M_n for all irradiation doses. The 1.8 kGy hr^{-1} air results show an average increase in M_n at 10 and 20 kGy but have large amounts of error in the 0, 20 and 200 kGy samples. If the error was taken into account, all irradiated samples could show a mass loss. The mean

M_n values for the 1.8 kGy hr^{-1} show atmosphere dependence; however, due to the large amount of error in the M_n data there may be an effect but it cannot be confirmed from these data alone.

The large error seen in some of the M_n results is due to issues with the GPC equipment during testing. During the course of this study the GPC's degasser was replaced and other issues were caused with a build-up of residue inside the GPC column. The resulting noise and baseline distortion (Figure 6.4.1 b shows an upward slanted baseline) meant that during the manual integration of the FK-800 peaks some error of the exact end point crept in. With these issues affecting the calculation of the number of low molecular mass polymer chains, the values for M_n and $Đ_M$ were affected to a greater extent than the values for M_w.

Figure 6.4.3 shows the mean percentage change in M_w for the irradiated FK-800 samples. In contrast to the M_n results, the M_w results show an increase in mass over the pristine for all irradiation conditions up to 100 kGy, except the 10 kGy samples irradiated in air at 1.8 kGy hr^{-1} which show a small decrease. The maximum mean increase in M_w observed was 19% at 50 kGy for the 1.8 kGy hr^{-1} vacuum irradiated samples. The trend for all irradiation conditions shows M_w increasing before peaking at 50 kGy and then dropping off with the 200 kGy at 1.8 kGy hr^{-1} in air and vacuum samples showing a drop in M_w over the pristine sample. No dose rate dependence is identifiable, although a clear atmosphere dependence can be seen in the 50 and 100 kGy sample sets. The samples irradiated under vacuum show a larger increase than the air samples with a maximum difference of 12% between the 1.8 kGy hr^{-1} samples at 50 kGy.

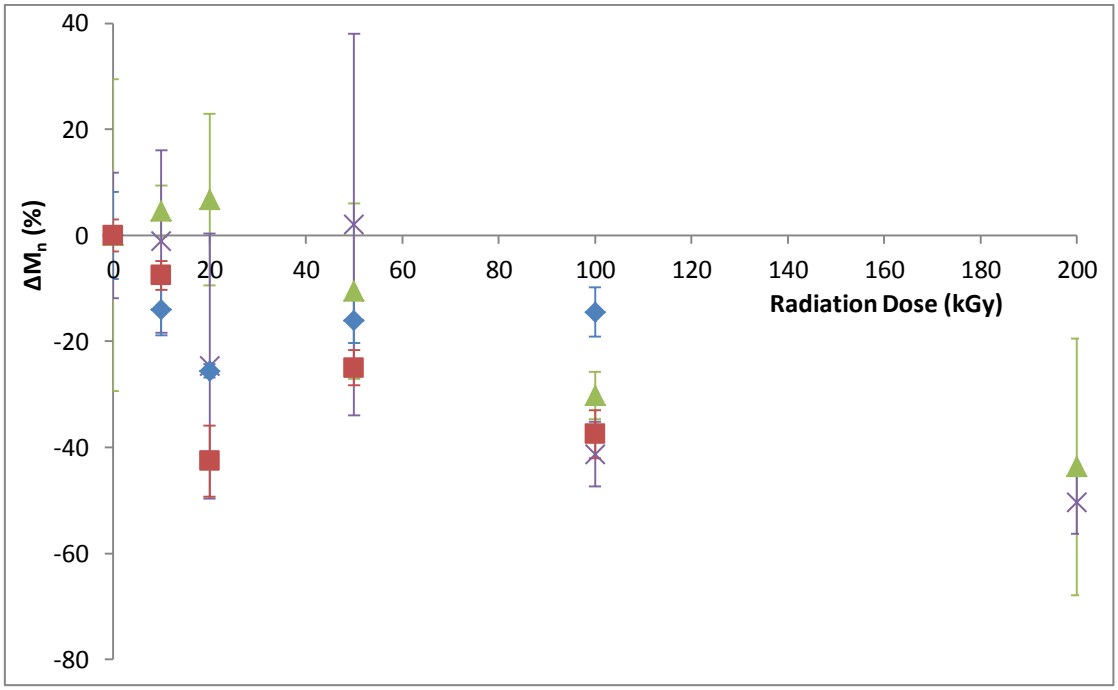

Figure 6.4.2 Mean percentage change number average molecular mass (M_n) for pristine and irradiated FK-800. 1.0 kGy hr^{-1} Air (♦) 1.0 kGy hr^{-1} Vacuum (■) 1.8 kGy hr^{-1} Air (▲) 1.8 kGy hr^{-1} Vacuum (X)

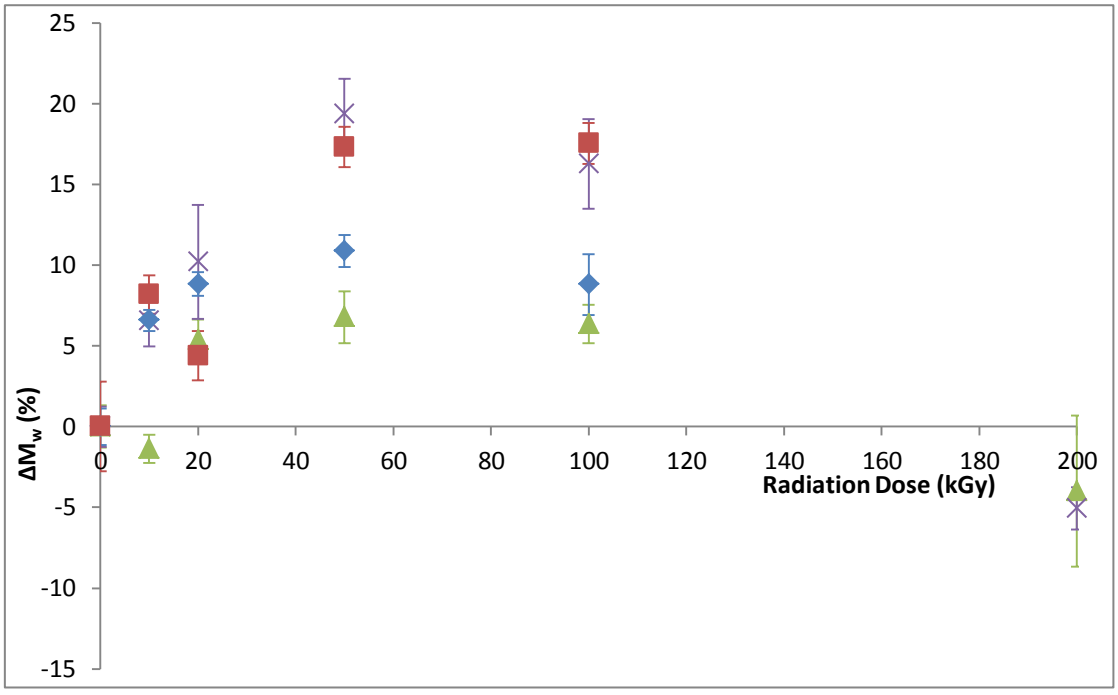

Figure 6.4.3 Mean percentage change in mass average molecular mass (M_w) for pristine and irradiated FK-800. 1.0 kGy hr^{-1} Air (♦) 1.0 kGy hr^{-1} Vacuum (■) 1.8 kGy hr^{-1} Air (▲) 1.8 kGy hr^{-1} Vacuum (X)

A decrease in M_n whilst M_w increases indicates that the samples' molecular mass dispersity ($Đ_M$) is increasing (Figure 6.4.4). The increase in $Đ_M$ coupled with the large decreases in M_n and smaller increases in M_w indicate that much of the change is predominantly due to the formation of low molecular mass chains in the irradiated samples. The $Đ_M$ data show a large amount of scatter and error but a general trend towards an increase in dispersity can clearly be seen.

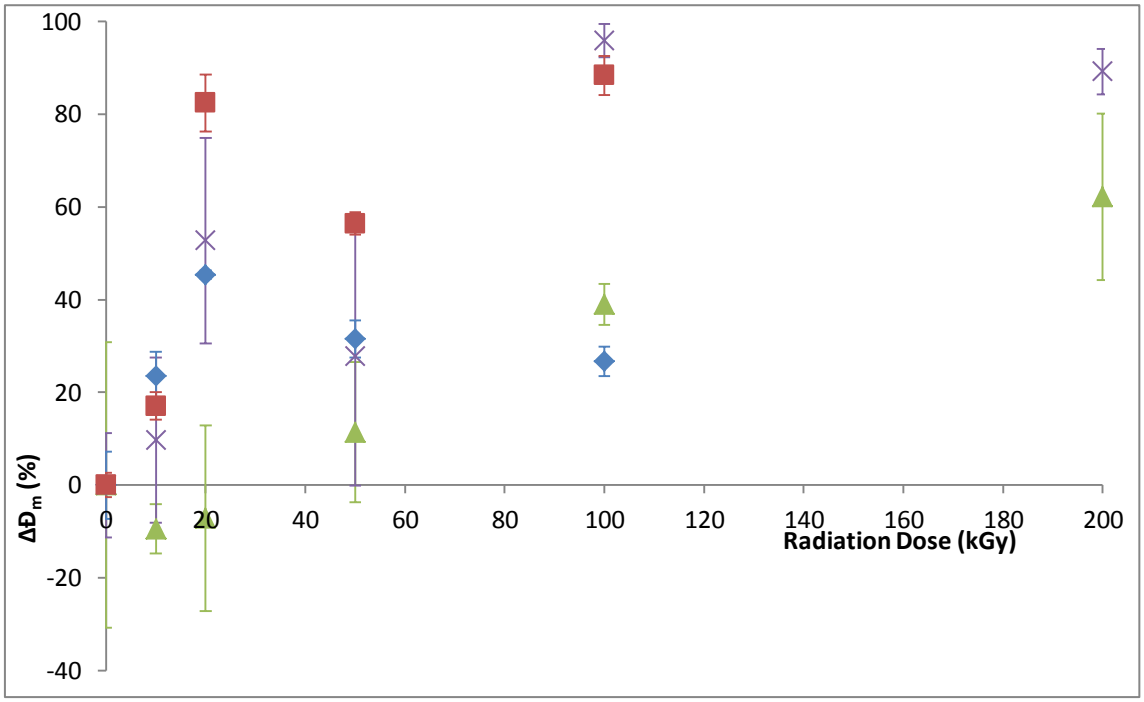

Figure 6.4.4 Mean percentage change in molecular-mass dispersity ($Đ_M$) for pristine and irradiated FK-800. 1.0 kGy hr^{-1} Air (♦) 1.0 kGy hr^{-1} Vacuum (■) 1.8 kGy hr^{-1} Air (▲) 1.8 kGy hr^{-1} Vacuum (X)

The molecular mass analysis has indicated the formation of small molecular mass chains which would result from radiation induced chain scission. Chain scissions in of the polymer back bone will lead to weakening of the polymer contradicting the mechanical properties results. To further understand the processes involved in the formation of small chains, chemical analysis was carried out to identify the chemical mechanisms.

6.5 Chemical analysis

GC-MS was used to identify and measure volatile decomposition gases given off by the polymer samples during irradiation. To allow for comparison between GC-MS runs, the results need to be normalised against a known factor. For the air-irradiated samples argon was used as an internal standard because of its constant 0.98% concentration in air. However, the vacuum-irradiated samples did not contain air, therefore, no internal standard was available and to normalise these samples, the number of detections of the molecule of interest has been divided by the total number of detections for that sample.

The results of the headspace gas analysis are shown in Tables 6.5.1 to 6.5.4. An increase in carbon dioxide is seen in all sets of results, along with the detection of carbon monoxide and a range of fluorine-containing compounds. The fluorine-containing compounds specifically identified were, difluorodimethylsilane ($SiF_2(CH_3)_2$), chlorodifluoromethane (CHF_2Cl), dichlorodifluoromethane (CF_2Cl_2), chlorotrifluoromethane (CF_3Cl) and tetrafluoromethane (CF_4). For the samples irradiated in air, the average CO_2 content normalised against Ar was 0.42 based on three runs of air on different dates. This value has been subtracted from the CO_2 values in Tables 6.5.1 and 6.5.2, so that these tables only show the increase in CO_2 for comparison. During analysis, some oxygen and nitrogen were detected in the vacuum-irradiated samples, although at much reduced levels compared to the air-irradiated samples. It is likely that the oxygen and nitrogen detected in the vacuum samples resulted from the methods of gas collection and sample injection used, and not from the pre irradiation vial sealing process. At higher doses, small quantities of nitrous oxide (N_2O) were detected in the air-irradiated samples. This is not likely to have resulted from a reaction involving the FK-800, but is likely to have resulted from radiation-induced reactions in the air atmosphere inside the vials.

Table 6.5.1 Headspace gas analysis results for the FK-800 samples irradiated at 1.8 kGy hr^{-1} in air. Results shown are GC-MS peak area relative to argon. CO_2 results have been adjusted to show increase only

Dose (kGy)	CO_2	CO	$SiF_2(CH_3)_2$	CHF_2Cl	CF_2CL_2	CF_3Cl	CF_4
10	0.30	-	-	-	-	-	-
20	0.76	-	-	-	-	-	-
50	1.70	0.26	0.17	-	-	-	-
100	3.98	0.74	1.19	-	0.01	-	-
200	5.62	1.08	3.68	0.01	0.02	0.01	-

The results for the 1.8 kGy hr^{-1} air-irradiated samples are shown in Table 6.5.1. They show that there has been an increase in the levels of CO_2 detected even at the lowest total dose of 10 kGy. The increase in CO_2 shows a linear relationship with dose and the equation of the trend line is shown in Equation 6.5.1. The trend line has an R^2 value 0.96 indicating good correlation between the predicted and actual values.

$$CO_2/Ar\ ratio = 0.0306\ \Phi \qquad \textbf{(6.5.1)}$$

No fluorine-containing compounds are detected until the 50 kGy irradiation, at which point a small amount of $SiF_2(CH_3)_2$ is detected along with CO. In contrast, the lower dose rate samples irradiated in air (Table 6.5.2), do not show an increase in CO_2 at 10 kGy but do show a very small amount of $SiF_2(CH_3)_2$. The 100 and 200 kGy samples irradiated at 1.8 kGy hr^{-1} also includes small amounts of CHF_2Cl, CF_2Cl_2, CF_3Cl and CF_2Cl_2 which are not seen at the lower dose rate.

Table 6.5.2 Headspace gas analysis results for the FK-800 samples irradiated at 1.0 kGy hr^{-1} in air. Results shown are GC-MS peak area relative to argon. CO_2 results have been adjusted to show increase only

Dose (kGy)	CO_2	CO	$SiF_2(CH_3)_2$	CHF_2Cl	CF_2CL_2	CF_3Cl	CF_4
10	0.00	-	0.05	-	-	-	-
50	0.74	0.12	0.13	-	-	-	-
100	1.56	0.18	0.39	-	-	-	-

The samples irradiated under vacuum at 1.8 kGy hr^{-1} (Table 6.5.3) show increases in the concentration of CO_2, CO and $SiF_2(CH_3)_2$, but do not show any linear relationships. CHF_2Cl, CF_2Cl_2 and CF_3Cl detected in the highest dose air samples were not detected in the 200 kGy vacuum irradiated sample. This may have been due to the method of gas extraction used for the vacuum irradiated samples reducing the concentration of the gases present. In contrast to the 1.8 kGy hr^{-1} vacuum samples, the 1.0 kGy hr^{-1} samples show small amounts of CF_4 in the 50 and 100 kGy samples which are not seen in any other sample set.

Head space analysis has identified fluorine containing compounds given off as gases when FK-800 is irradiated. This is evidence that the polymer is undergoing radiolysis through the breaking of bonds.

Table 6.5.3 Headspace gas analysis results for the FK-800 samples irradiated at 1.8 kGy hr^{-1} under vacuum. Results shown are GC-MS peak area relative to total number of detections

Dose (kGy)	CO_2	CO	$SiF_2(CH_3)_2$	CHF_2Cl	CF_2CL_2	CF_3Cl	CF_4
10	0.05	-	-	-	-	-	-
20	0.00	-	-	-	-	-	-
50	0.19	0.02	0.01	-	-	-	-
100	0.10	0.02	0.02	-	-	-	-
200	0.20	0.04	0.09	-	-	-	-

Table 6.5.4 Headspace gas analysis results for the FK-800 samples irradiated at 1.0 kGy hr^{-1} under vacuum. Results shown are GC-MS peak area relative to total number of detections

Dose (kGy)	CO_2	CO	$SiF_2(CH_3)_2$	CHF_2Cl	CF_2CL_2	CF_3Cl	CF_4
10	0.04	-	0.01	-	-	-	-
50	0.07	-	0.31	-	-	-	0.02
100	0.09	0.01	0.75	-	-	-	0.05

ATR FT-IR analysis of the irradiated FK-800 samples was conducted in an attempt to further identify chemical changes in the polymer upon radiolysis. However the data was found to be mostly inconclusive. This was due to the use of ATR, it was difficult to obtain repeatable spectra and when the spectra

obtained were compared by “stretching” the spectra, the data could not be deemed reliable. Bearing in mind that the data could not be fully trusted, there was some evidence of the formation of bands at ~1650 and ~1715 cm^{-1} in the air irradiated samples, and there was evidence of these peaks increasing in size with increasing radiation dose. The vacuum-irradiated samples showed evidence of an increasing band at 1650 cm^{-1}, but, did not have a peak at 1715 cm^{-1}. Bands in these regions have been seen previously when poly-VDF and poly-ethylene-tetrafluoroethylene were electron beam irradiated[80]. The two bands are attributed to C=C (~1650 cm^{-1}) and C=O (~1715 cm^{-1}) stretches. The C=C bonds form due to abstraction of fluorine and hydrogen from the polymer backbone resulting in unsaturation of the backbone and the formation of new chain ends during chain scission. The C=O band is caused by the reaction of oxygen with a main chain radical and a $H^{\cdot}$ radical to form a hydroperoxide[80].

The chemical analysis concluded the study of the FK-800 polymer, further discussion of the results and their implications can be found in Section 8. Section 7 presents the results from the study of the explosive TATB and the PBX TCV containing both TATB and the FK-800 polymer.

7 The effects of ^{60}Co gamma radiation on TATB and TCV

The study of the effects of gamma radiation on the FK-800 polymer binder revealed marked changes take place in both the mechanical properties and chemical structure of the polymer. Following the FK-800 study, an investigation was conducted on irradiated TCV exploring if changes in the binder, which only contributes 5 % by mass to the TCV, were affecting the properties of the irradiated TCV. Alongside the tests on TCV, tests were carried out on TATB to confirm if changes noted in the TCV were due to the polymer binder, or the TATB filler.

7.1 Small scale hazard testing of TCV and TATB

To ensure the irradiated samples of TCV and TATB produced during this study could be handled and stored safely, small scale powder hazard tests and thermal analysis were conducted. Samples for the small scale tests were irradiated to 50 and 200 kGy at 1.8 kGy hr^{-1} in air, and stored at ambient temperatures in the dark until testing.

Table 7.1.1 Rotter - Langlie 10 shot drop weight impact and mallet friction (steel mallet on steel anvil) sensitiveness test results

Radiation Dose (kGy)	Rotter- Langlie F of I			Mallet Friction Steel		
	0	50	200		50	200
TATB	165	141	87	0%	0%	0%
TCV	140	125	117	0%	0%	0%

Table 7.1.1 shows the results of the Rotter-Langlie drop weight impact tests and steel mallet on steel anvil mallet friction tests. The impact tests show a drop in F of I for all of the irradiated samples indicating that the samples are becoming more sensitive to this test. The TATB sample irradiated to 200 kGy shows a drop in F of I from 165 to 87. This is a very significant drop, and the final result is comparable to that of the conventional high explosive RDX which has an F of I of 80. Although the drop in F of I in the TCV samples is not as large as the TATB sample, there is still a definite downward trend indicating the PBX is

becoming more sensitive to impact. In contrast to the drop weight impact test, no change in sensitiveness to friction was noted in the mallet friction results.

10 sample electric spark discharge tests were conducted on the irradiated explosives and the results are shown in Table 7.1.2. The results show the material becoming significantly more sensitive to ignition by electrical spark with irradiation. The 50 kGy samples in both explosives show a jump from no ignitions at 4.5 J to ignitions at 0.45 J but not at 0.045 J. This change in response means that antistatic precautions need to be considered when handling the material. In contrast to the 50 kGy and 200 kGy TATB samples, the 200 kGy TCV sample appears to show lower sensitiveness to electric spark than the 50 kGy samples. This result is likely due to the reduced number of tests carried out for this study and not changes in the material reducing its sensitiveness. The full electric spark discharge test requires 50 samples to be tested at each energy level, with only one ignition required to classify the material at a level. Therefore, it may simply be the case that the 200 kGy TCV did not go through enough tests for an ignition to happen at 0.45 J.

Table 7.1.2 Electric spark discharge sensitiveness results for irradiated TATB and TCV

Dose (kGy)	Electric spark discharge sensitiveness		
	0	50	200
TATB	No ignitions at 4.5 J	Ignitions at 0.45 J but not at 0.045 J	Ignitions at 0.45 J but not at 0.045 J
TCV	No ignitions at 4.5 J	Ignitions at 0.45 J but not at 0.045 J	Ignitions at 4.5 J but not at 0.45 J

Basic thermal stability tests (Table 7.1.3) were conducted on the irradiated samples to check for excessive changes in the onset of decomposition and excessive mass loss at elevated temperature. A drop in the decomposition onset temperature was noted for all irradiated samples with no difference in the onset between the TATB and TCV samples in any test. This indicates that it is the TATB explosive affecting the decomposition onset of both materials, and the FK-800 binder is not having an effect.

Isothermal TGA results for the explosives show a small mass loss for all samples due to the loss of water after 15 hours at 120 °C. These tests were conducted to check the materials' thermal stability as part of the risk assessment process. A maximum of 3 % mass loss was set as a safety margin for this test. Some variation can be seen in the data; however, the results shown in Table 7.1.3 are for a single run only therefore, the variation may result from human error and not the samples.

Table 7.1.3 DSC and isothermal TGA stability testing of irradiated TATB and TCV

Radiation Dose (kGy)	DSC onset of decomposition (°C)			Isothermal-TGA mass loss (%)		
	0	50	200	0	50	200
TATB	382	375	371	0.39	0.39	1.20
TCV	383	375	371	0.31	2.04	0.26

Having shown that samples of both TATB and TCV could be irradiated up to 200 kGy without undue risk; irradiation of small cylinders for Brazilian disc mechanical testing and further powder samples was carried out.

7.2 Mechanical properties of TCV

Brazilian disc tests were conducted on pristine and irradiated samples of TCV at the Cavendish Laboratories, Cambridge University. The samples were tested at 40 °C to ensure the TCV's polymer binder was above its $T_{g,}$ ensuring parity with the FK-800 experiments. Due to restrictions in resources at Cambridge University, only one sample set was tested. The sample set consisted of three samples at each of 0, 10, 20, 50 and 100 kGy irradiated at a dose rate of 1.8 kGy hr^{-1} under vacuum. The samples were irradiated under vacuum because these conditions most closely match those TCV will experience in a service environment.

Figure 7.2.1 shows the Brazilian disc samples central tensile stress (calculated using the measured load and equation 5.3.1) against displacement with the different doses offset. The only difference in the sample sets which can be seen is a small increase in the central stress at failure with increasing radiation dose. When the sample traces are overlaid (Figure 7.2.2), the samples form a tight

group showing little difference in behaviour other than the changes failure stress.

By expanding Figure 7.2.2 to show only the region between 1.3 and 1.7 MPa (Figure 7.2.3), it can be seen that the 100 kGy samples show a small shift to the left of the pristine. This shift indicates that the 100 kGy samples were stiffer than the pristine material. It is also true to say that the softest sample (furthest to the right) was a pristine sample. However, the data contains a lot of scatter with only a general trend for the irradiated samples to behave stiffer than the pristine, and for stiffness to increase with increasing radiation dose.

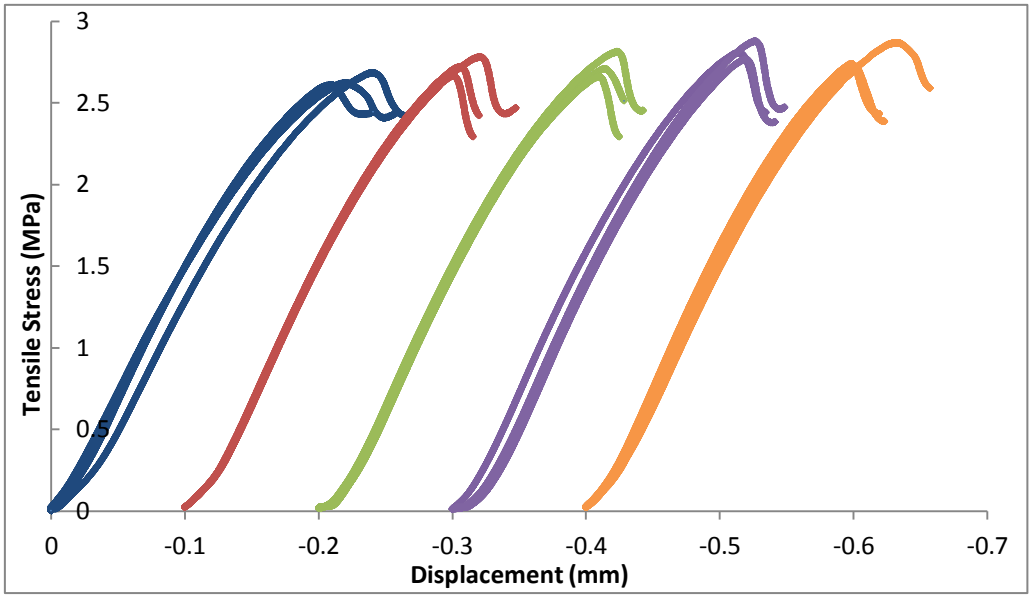

Figure 7.2.1 TCV Brazilian disc test central tensile stress vs. displacement curves for all the samples tested. Each radiation dose has been offset by 0.1 mm.

Pristine **10 kGy** **20 kGy** **50 kGy** **100kGy**

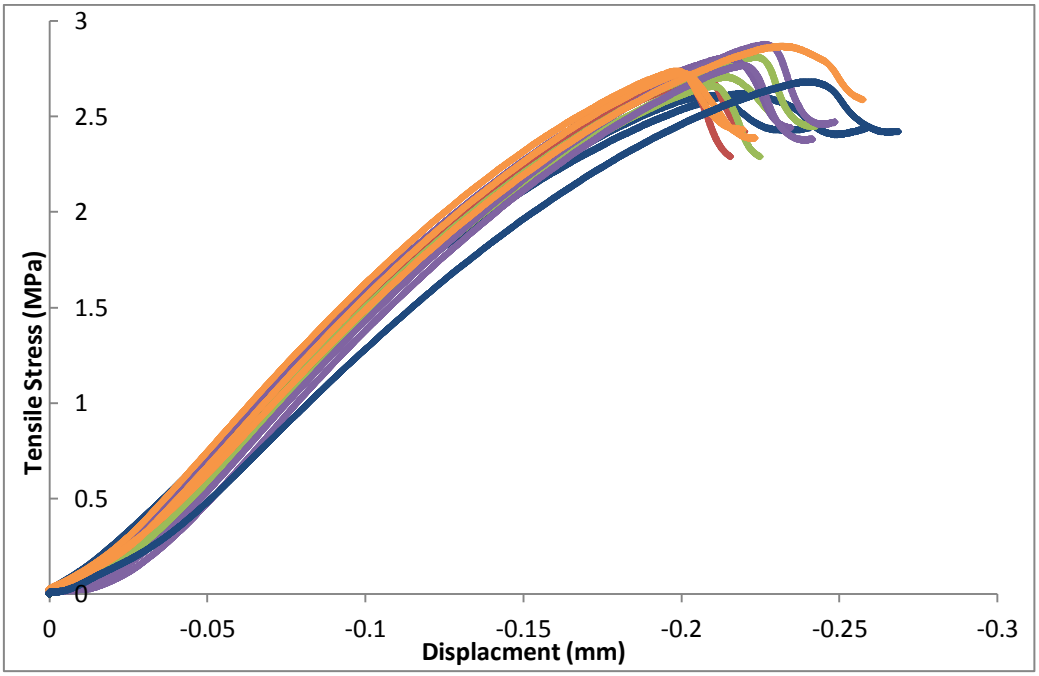

Figure 7.2.2 TCV Brazilian disc test central tensile stress vs. displacement curves for all the samples tested. Pristine — 10 kGy — 20 kGy — 50 kGy — 100kGy —

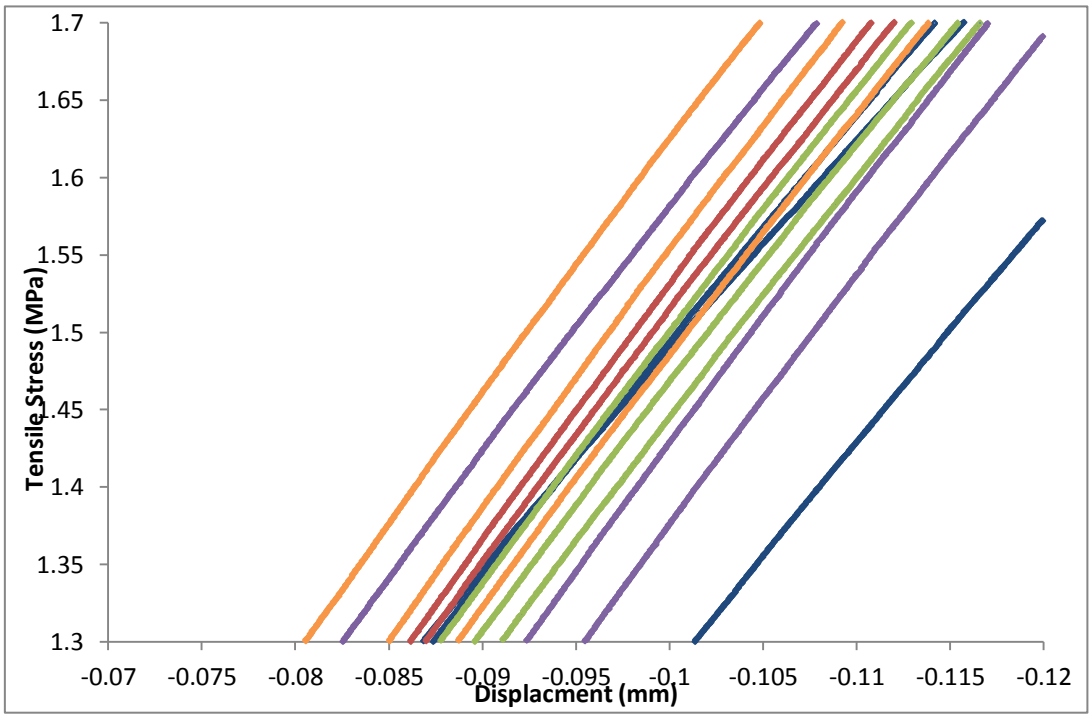

Figure 7.2.3 TCV Brazilian disc test central tensile stress vs. displacement curves for all the samples tested between 1.3 and 1.7 MPa. Pristine — 10 kGy — 20 kGy — 50 kGy — 100 kGy —

The mean central stress at failure has been plotted against radiation dose in Figure 7.2.4. The mean data show an increase of 0.2 MPa at 50 kGy with a slight drop in the mean for the 100 kGy. Although the 100 kGy mean stress at failure is less than the 50 kGy mean, there is significant enough error to indicate this may not be a true trend. All that can be confirmed from the data in Figure 7.2.4 is, the central stress at failure increases with irradiation, however, the increases seen are very small.

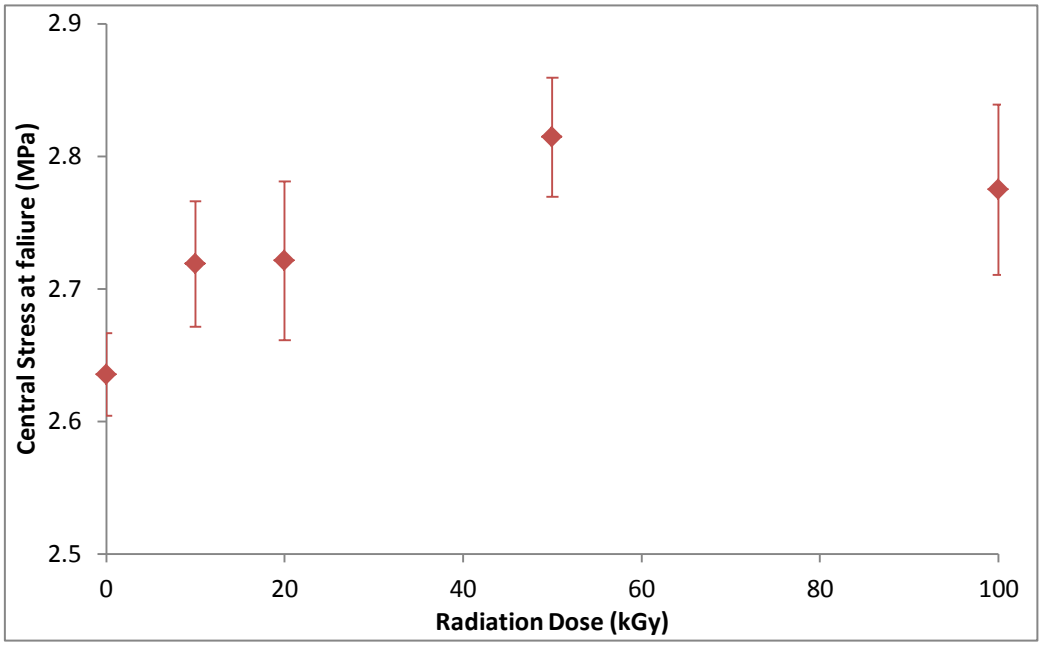

Figure 7.2.4 Mean Brazilian disc test central stress at failure for pristine and irradiated TCV samples

The Brazilian disc tests carried out on the TCV samples have shown that ^{60}Co irradiation up to a dose of 100 kGy under vacuum has little effect on the mechanical properties of the composition.

7.3 Thermal analysis of irradiated TCV by DSC

DSC analysis was used to identify changes in the thermal properties of the vacuum irradiated TCV samples. A lowering of the onset temperature of thermal decomposition was observed during the small scale hazard experiments (Table 7.1.3), indicating radiation-induced changes in the explosive materials' thermal stability were taking place. Further DSC analysis was conducted to investigate if

changes in the energy released during thermal decomposition were taking place. A covering of sand was included to stop the TCV sample escaping from the DSC pan during the test run due to sublimation of the TATB. By adding sand, the TATB could sublime onto the sand and still contribute to the experimental results.

Figure 7.3.1 shows the mean energy released by the TCV samples normalised to sample size against radiation dose. There is no significant change in the mean energy at radiation doses up to 100 kGy. It is however, interesting to note the increasing size of variability in the three repeat samples with increasing radiation dose. The variability can be seen in Figure 7.3.1, represented by the increasing size of the error bars. This may indicate that changes are taking place in the TCV, however further experiments would be required to confirm this.

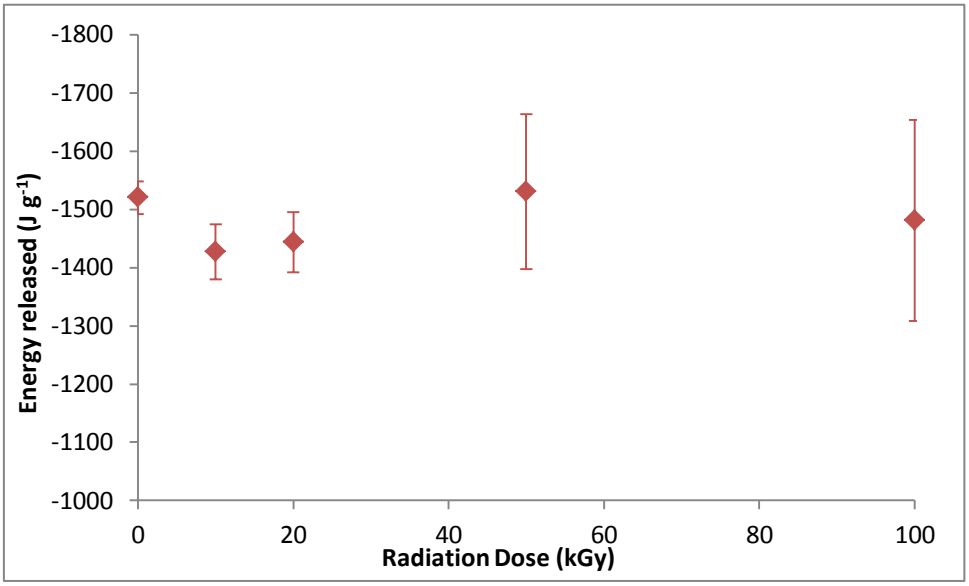

Figure 7.3.1 Mean energy released during thermal decomposition of pristine and irradiated TCV. Values have been normalised for sample mass

The vacuum-irradiated TCV samples showed little change in mechanical properties or energy released during thermal decomposition. However, a colour change was seen in all the TCV samples irradiated. Figure 7.3.2 is a picture of the Brazilian discs after irradiation. A very clear colour change from yellow in the pristine, to dark green at 100 kGy can be seen. This colour change has

been noted previously in all studies involving the gamma irradiation of TATB (Section 2.1.1) and is a result of changes in the TATB filler and not related to the binder in the FK-800 binder present in the TCV.

Figure 7.3.2 Picture showing the TCV Brazilian discs after irradiation at 1.8 kGy hr^{-1} under vacuum

The biggest changes noted in the TCV samples with gamma irradiation were the changes in the TCV's hazard properties (Tables 7.1.1 - 3), the colour change, and the reduction in the onset of thermal decomposition temperature. These changes were identified in both the TCV and TATB samples and it is therefore likely the radiation-induced changes result from changes in the TATB only, not the FK-800 binder. In an attempt to identify changes in the TATB which are affecting the irradiated materials HPLC and TGA were conducted on samples of irradiated TATB.

7.4 Dynamic thermogravimetric analysis of irradiated TATB

Dynamic TGA was conducted on duplicate samples of TATB irradiated to 0, 10, 50 and 100 kGy at 1.8 kGy hr^{-1} in air. The results (Table 7.4.1) show a lowering of the onset of decomposition from 358 °C to an average of 349 °C. This drop of ~9 °C indicates the thermal stability of the samples is changing with gamma irradiation and further supports the DSC results from the small scale hazard experiments (Section 7.1).

Table 7.4.1 Dynamic-TGA onset of thermal decomposition temperatures for pristine and irradiated TATB

Radiation Dose (kGy)	Onset of thermal decomposition (°C)	
	TATB Sample 1	TATB Sample 2
0	358	358
10	359	358
50	353	348
100	348	350

After the samples had been allowed to decompose by heating to 450 °C during the dynamic-TGA experiments, the % mass loss of each sample was calculated. The mass loss data shown in Table 7.4.2 indicate a lowering of the percentage mass loss in the irradiated samples against the pristine material. These results suggest that less oxygen is present to oxidatively decompose[3] the irradiated samples when heated under inert atmosphere. The increase in material remaining after the dynamic-TGA experiment indicates the presence of a radiation-induced decomposition product with a lower oxygen balance than TATB may have been formed. The decomposition product could possibly be the mono-nitroso derivative of TATB suggested by Manaa et al.[27]. However, this cannot be confirmed from the data set shown in Table 7.4.2 due the amount of error resulting from the small sample size used (~2.5 mg).

Table 7.4.2 Dynamic-TGA percentage mass loss for pristine and irradiated TATB

Radiation Dose (kGy)	Mass loss (%)	
	TATB Sample 1	TATB Sample 2
0	76.0	77.3
10	71.0	71.2
50	68.2	72.0
100	72.5	69.7

It is likely that the changes in the thermal properties and progressively deepening green colour of the irradiated TATB and TCV samples results from the formation of a radiation-induced decomposition species. Several studies[15; 25-27] have attempted to identify the “green” decomposition species but at this time no definitive identification has yet been made.

7.5 HPLC analysis of irradiated TATB

No data have at this time been published relating to the HPLC analysis of irradiated TATB. Separation and detection of the “green” decomposition species by HPLC could allow the concentration of the decomposition product to be measured against radiation dose. Separation of any new species by HPLC may also lead to the identification of the “green” species.

The HPLC method used to analyse the irradiated TATB has previously been described in Section 5.8.1. Duplicate runs of samples irradiated to 0, 10, 50, and 100 kGy at 1.8 kGy hr^{-1} in air were tested and their chromatograms recorded at 354 nm. Figures 7.5.1 and 7.5.2 show the chromatograms for the pristine and 100 kGy irradiated samples. An additional peak not present in the pristine sample can be seen in the 100 kGy sample at a retention time of 1.07 minutes. The unidentified peak in the 100 kGy sample was also identified in all the irradiated samples. This indicates that the unidentified peak results from a radiation-induced decomposition product of TATB.

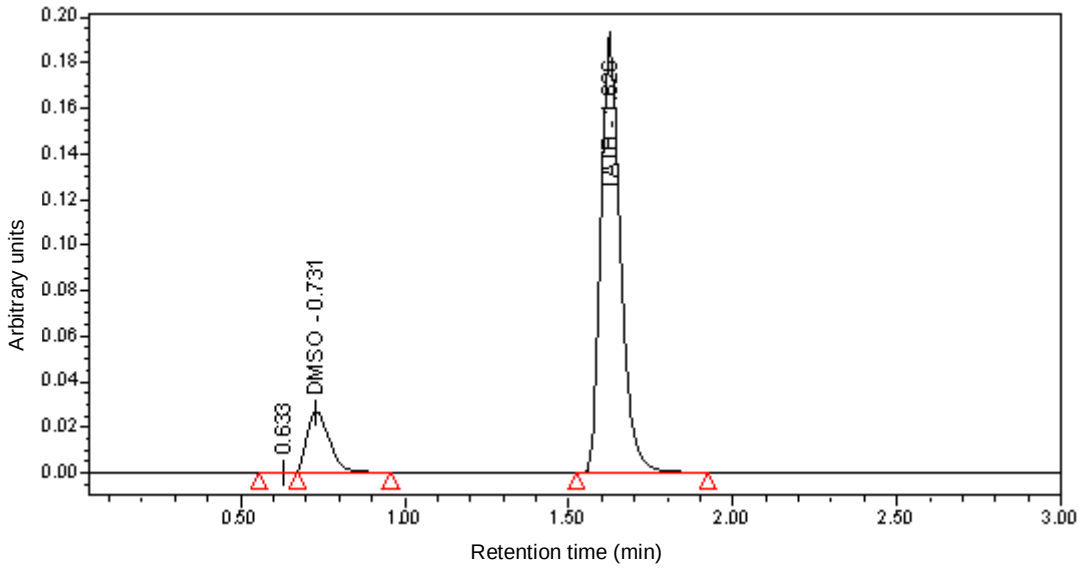

Figure 7.5.1 HPLC chromatogram for pristine TATB. Recorded at 354 nm

Expanded chromatograms for the pristine and irradiated TATB samples are shown in Figure 7.5.3. It can be seen that the unidentified peak at 1.07 minutes increases in size with increasing radiation dose, further supporting that the peak results from a radiation-induced decomposition product. Although the 1.07

minute peak could be detected in all the irradiated samples and was observed to increase in concentration, even at the highest radiation dose the concentration of the product was not high enough for the HPLC's diode array detector to record a full UV spectrum.

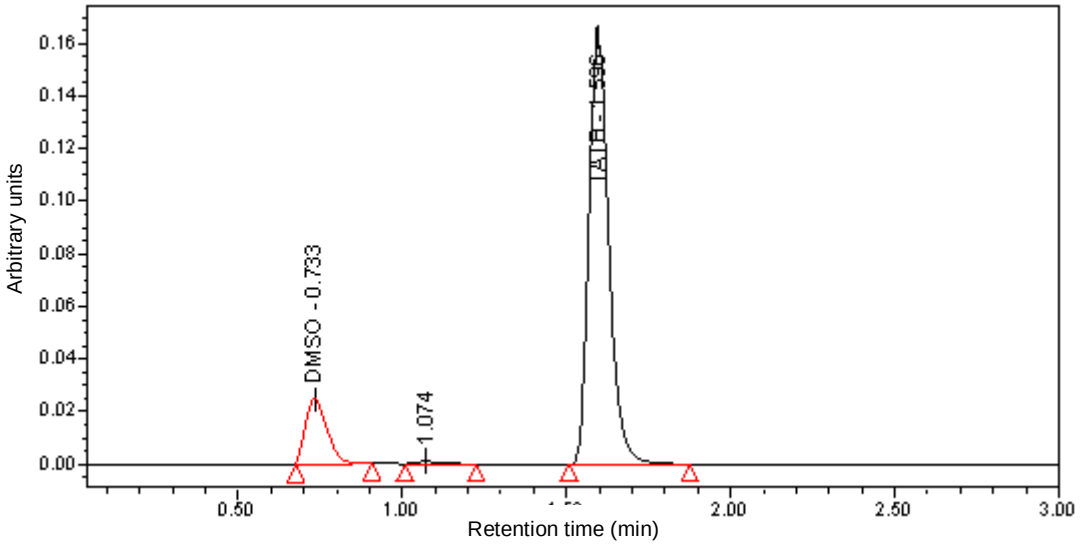

Figure 7.5.2 HPLC chromatogram for TATB irradiated to 100 kGy at 1.8 kGy hr^{-1} in air. Recorded at 354 nm

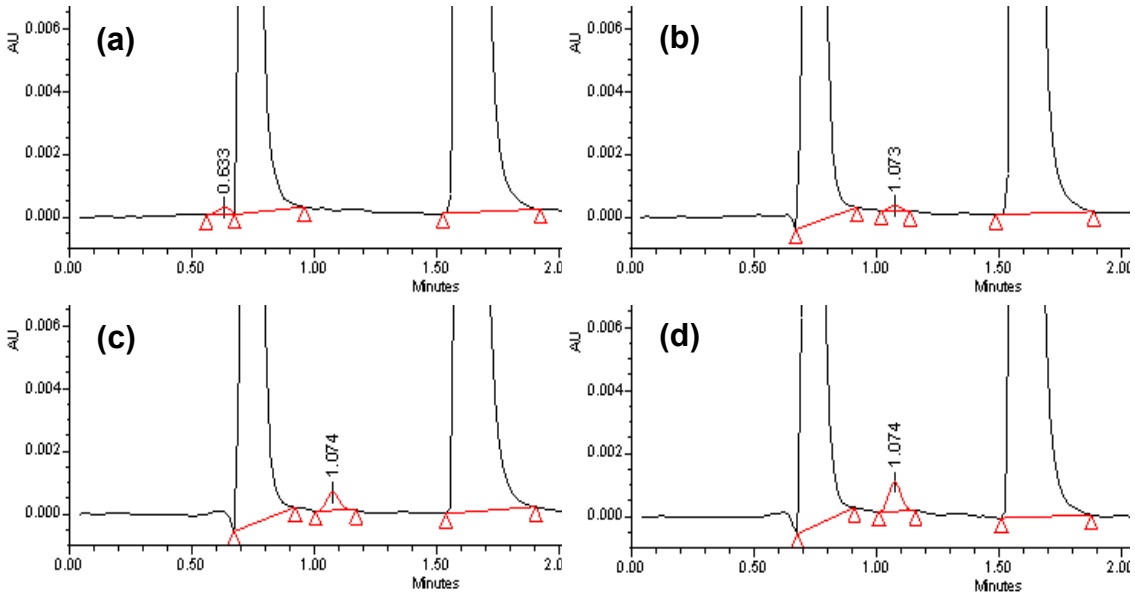

Figure 7.5.3 Expanded HPLC chromatograms recorded at 354 nm for the pristine and irradiated TATB samples. (a) pristine, (b) 10 kGy, (c) 50 kGy and (d) 100 kGy

The peak of the unidentified peak at 1.07 minutes was measured and plotted against radiation dose in Figure 7.5.3. To allow for comparison between samples, the unidentified peak area was normalised for comparison by dividing it against the TATB concentration in the injected sample in ppm. The duplicate samples were found to have good correlation with each other in all but the 100 kGy. This difference at 100 kGy may result from the up to 5 % error in irradiation dose received by the samples. This error is present in all the irradiations but becomes more apparent the higher the radiation dose. A trend line was fitted to the data (Equation 7.5.1) and was found to fit the data with an R^2 value of 0.99 indicating a very close fit.

$$Unidentified\ peak\ area = 2.188\Phi - 0.0078\Phi^2 \qquad \textbf{(7.5.1)}$$

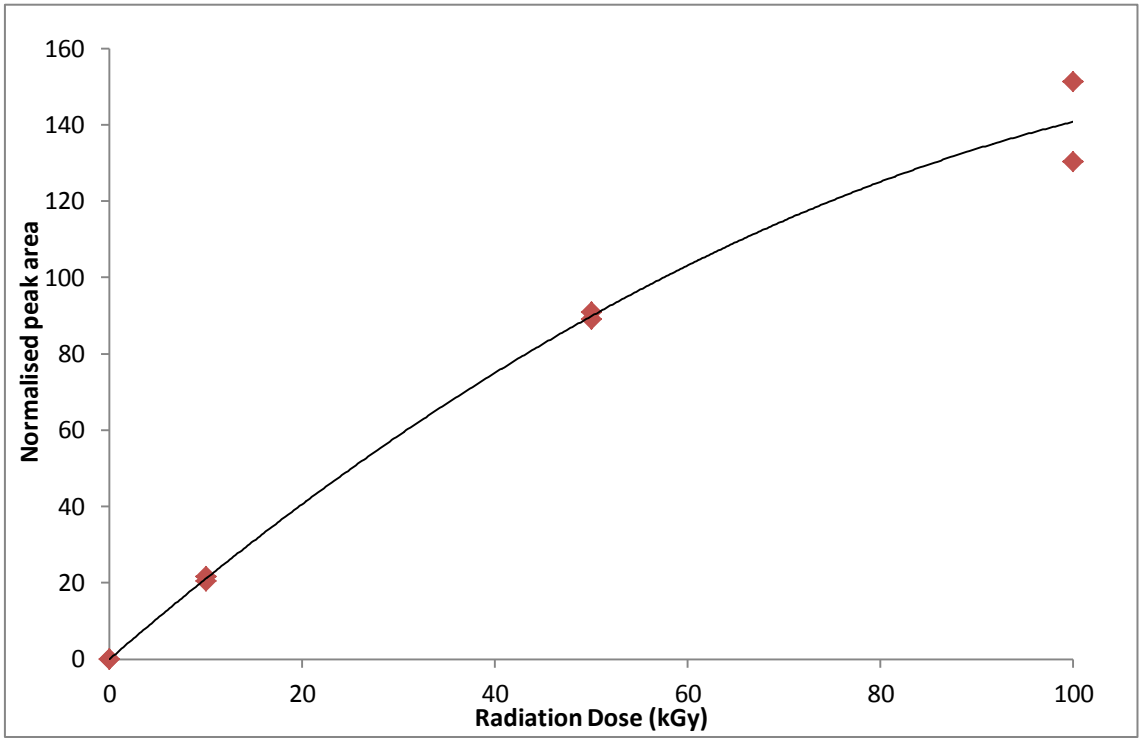

Figure 7.5.4 HPLC 1.074 minute normalised peak area for irradiated TATB against sample radiation dose. A tend line using Equation 7.5.1 has been added for comparison

The equation contains a correction factor to account for sample saturation at higher doses. Saturation would occur as the amount of available TATB decreases as it is radiolitically decomposed. Further irradiation of TATB

samples would be expected to follow this trend until they flatten off at a maximum level due to saturation, but would not be expected to drop off as the trend line would.

In a further attempt to identify the new HPLC peak at 1.07 minutes, samples were sent to AWE plc Aldermaston for analysis by LC-MS.

7.6 LC-MS analysis of irradiated TATB

Samples of both pristine and 100 kGy irradiated TATB were analysed for this project with the kind assistance of Paul O'Nion at AWE plc Aldermaston. The samples were separated using the same column used for the HPLC experiments in Section 7.5 before undergoing mass spectroscopy using negative electrospray ionisation as described in Section 5.9.1.

As with the HPLC results obtained at Cranfield University, a small peak was seen at a retention time of 1.07 minutes which was not seen in the pristine. The mass spectrum was obtained for the 1.07 minutes peak in the 100 kGy irradiated TATB sample and is shown in Figure 7.6.1. The mass spectrum shows a definite peak with a mass of 238.88 m/z. This is equivalent to a neutral mass of 240 g mol^{-1} once the proton knocked off during the electrospray ionisation has been included. Peaks were also identified at 118.89, 336.78 and 540.76 m/z; these peaks were not further investigated during this study because the 238.88 m/z peak was three times the strength of any other peak.

When both the pristine (Figure 7.6.2 a) and 100 kGy (Figure 7.6.2 b) LC-MS chromatograms were extracted at 239 m/z it is possible to see that there is a peak at a retention time of 1.07 - 1.08 in both the pristine and irradiated sample. However, when the peak areas were measured the 100 kGy sample had a peak area of 166508 which was 9 times greater than the 18088 measured for the pristine.

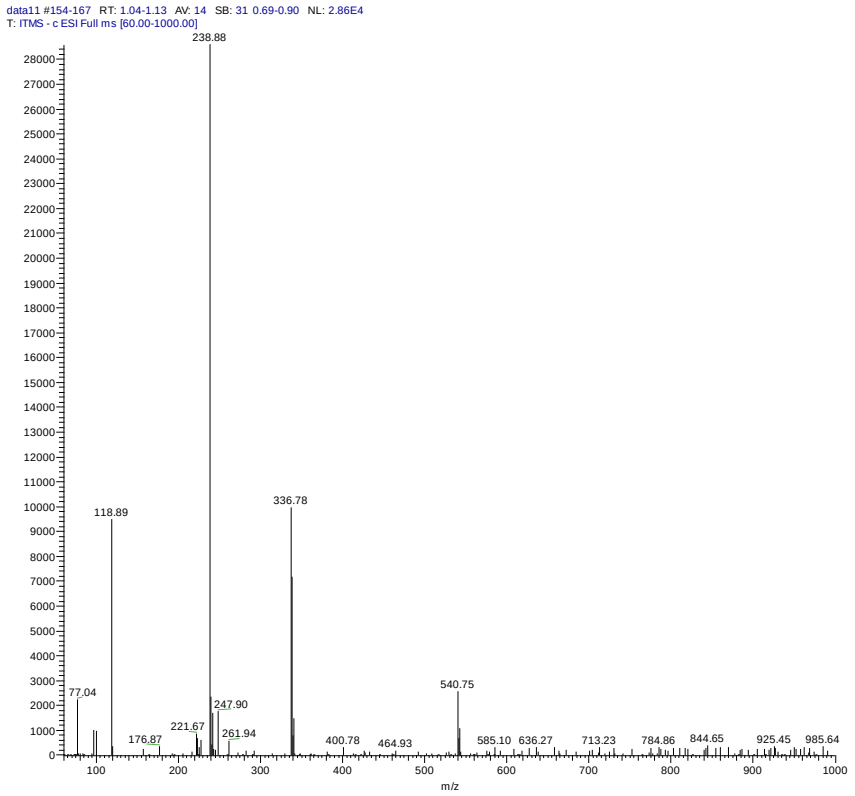

Figure 7.6.1 LC-MS negative electrospray ionisation mass spectrum after background subtraction, for the unidentified 1.07 minute peak in the 100 kGy irradiated TATB sample

This large increase in the amount of the 239 m/z molecule present in the irradiated TATB sample over the pristine is indicative of a radiation-induced decomposition product. There is a trace amount of decomposition product present in the pristine sample which is likely to have come from exposure of the sample to naturally occurring radiation - such as ultraviolet light - during storage and processing.

Negative electrospray ionisation mass spectroscopy is a technique which only removes a single proton during ionisation and does not break up the molecule being analysed. This allows us to confirm the decomposition product forming the radiation-induced HPLC peak at 1.07 minutes has a neutral mass of 240 g mol^{-1}. TATB has a mass of 258 g mol^{-1}; therefore, the radiation-induced decomposition of TATB results in a mass loss of 18 g mol^{-1}, which can indicate a loss of water in a condensation reaction.

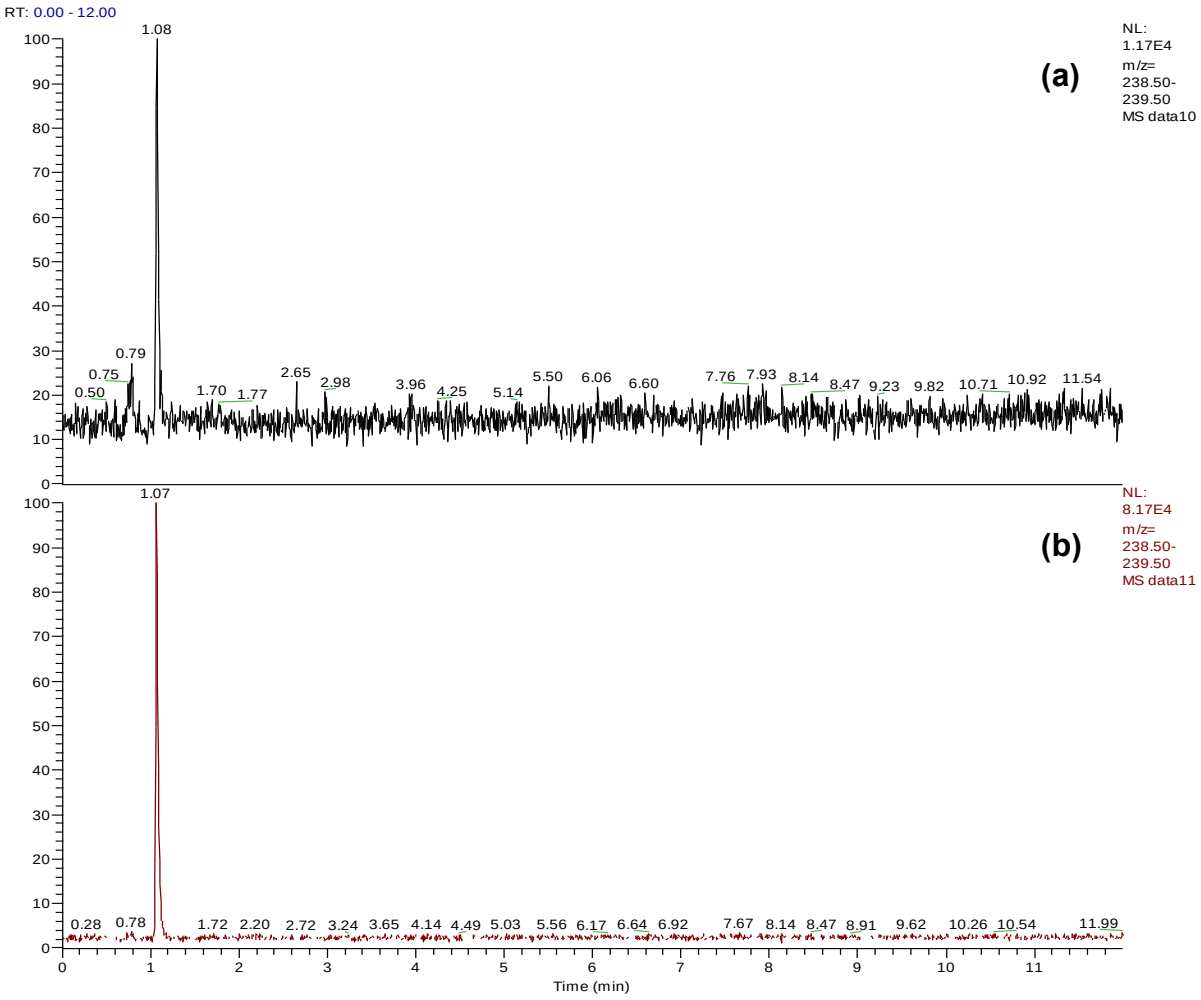

Figure 7.6.2 LC-MS chromatograms extracted at 239 m/z for (a) pristine and (b) 100 kGy irradiated TATB

Gamma radiation of TATB and TCV has shown that the main effects are caused by the radiation effects on the filler TATB. The mechanical properties of TCV show some evidence of radiation-induced changes, however, no conclusive trends can be drawn from the data in this study. It has also been shown that upon radiolysis TATB produces a decomposition product with a mass of 240 g mol^{-1}. Further discussion of these results can be found in Section 8.2.

8 Discussion of results

8.1 FK-800

A summary of the main results from the study of γ-radiation on the fluoropolymer FK-800 is presented in figure 8.1.1.

Table 8.1.1 Summary of the main results for the FK-800 irradiation experiments

Analysis Category	Analysis Technique	Significant Results Upon γ-Irradiation
Mechanical Properties	Tensile load testing	- Increase in Young's modulus - Increase in stress and yield - Decrease in Ultimate tensile strength - Decrease in Extension at σ_s
	DMA	- Initial decrease in storage modulus over rubber plateau at lower radiation doses. - Increase in storage modulus at 100 kGy - Drop off in storage modulus above 70 °C in high dose samples. - Indication of a new transition at ~ -20 °C in 100 and 200 kGy samples. - Initial increase in size of tan δ peak at T_g up to 50 kGy decreasing peak size above 50 kGy.
Glass Transition Temperature	DSC	- Decrease in T_g, max decrease of 2.9 °C at 200 kGy
	DMA	- Increase in T_g, max increase of 2.3 °C at 100 kGy
Molecular Mass	GPC	- Decrease in number average molecular mass - Increase in mass average molecular mass up to 100 kGy, decrease below pristine at 200 kGy. - Increase in molecular mass dispersity - Calculated chain scission rate of up to 1 scission per chain at 200 kGy.
Chemical Analysis	GC-MS	- Detection of fluorine containing compounds. - Large increase in CO_2 from the reaction of CF_4 with the glass sample vial.
	ATR - FT-IR	- Indication of increase in C=C. - Indication of increase in C=O in samples irradiated in air.
Percentage Crystallinity	DSC	- Increase from 0.6 to 7.7 % at 200 kGy.
	X-ray diffraction	- Increase from 0 to 12% - Evidence of atmosphere dependence up to 100 kGy.

The tensile load testing results for E indicate the polymer is becoming stiffer and stronger within its elastic limits. Whilst after the σ_s data indicates the polymer is weakening. The E data is also contradictory to the DMA, which tests the sample within its elastic limits, data. The FK-800 samples are shown to be softer than pristine polymer when irradiated up to 50 kGy, before behaving stiffer than the pristine at 100 kGy and above. When a polymer is γ-irradiated two reactions - chain scission and crosslinking - take place affecting the mechanical properties of the material.

An increase in E can be an indication that crosslinks between polymer chains are forming which stiffen and strengthen the polymer by forming permanent links between polymer chains, and stopping plastic flow. In contrast, the lowering of σ_s and the DMA E' results up to 50 kGy are indicative of main chain scission taking place. Cuts in the polymer backbone will weaken chain entanglements allowing the polymer chains to be pulled apart with less force and increasing molecular motion, softening the polymer during DMA tests. However, chain scission cannot explain the increase in E' in samples irradiated above 50 kGy or the trend for the initial drop and then the samples to recover and stiffen with increasing dose.

GPC of the molecular weight of the irradiated polymer showed that M_n decreased whilst M_w increased with increasing dose. These results suggest that the molecular mass distribution is increasing which is confirmed b and increase in $Đ_m$. The results indicate that a large number of low molecular weight chains are being formed, further supported by the GPC chromatograms. However the data also suggests that along with radiation-induced chain scissions, cross-linking is also taking place resulting in the increase in M_w. These competing reactions lead to the increase in the polymer's $Đ_{M.}$

A calculation previously used by Acevedo et al[81] to calculate the number of scissions per polymer chain based on M_n, was used to calculate the number of scissions per chain for the irradiated FK-800 samples. The equation used is shown in Equation 8.1.1; where S is the number of scissions per molecule, $M_{n,0}$

is the M_n of the pristine material and $M_{n,t}$ is the M_n of the aged (irradiated) sample.

$$S = \left(\frac{M_{n,0}}{M_{n,t}}\right) - 1 \qquad \textbf{(8.1.1)}$$

Table 8.1.2 shows the number of scissions per FK-800 molecule calculated using equation 8.1.1. There is some scatter evident in the data due to the scatter in the GPC M_n results. However, the general trend shows the polymer molecules undergoing more chain scissions than cross-links and that the number of chain scissions increases with increasing radiation dose.

Table 8.1.2 Calculated number of scissions per FK-800 molecule

Radiation Dose (kGy)	1.0 kGy hr^{-1} air (%)	1.0 kGy hr^{-1} vacuum (%)	1.8 kGy hr^{-1} air (%)	1.8 kGy hr^{-1} vacuum (%)
0	0.0	0.0	0.0	0.0
10	0.2	0.1	0.0	0.0
20	0.3	0.7	-0.1	0.3
50	0.2	0.3	0.1	0.0
100	0.2	0.6	0.4	0.7
200	-	-	0.8	1.0

The chain scission of the polymer backbones will reduce the length of the individual polymer chains and in doing so result in less chain entanglements. The resulting increase in chain mobility will lower the polymer's T_g when other factors such as crystallinity are removed. This drop in T_g is seen in the DSC data (Figure 6.2.1) which are taken from the second run of the samples after a thermal cycling to remove the influence of crystallinity. The data show a maximum drop in T_g of 2.9 °C at 200 kGy which is in contrast to the DMA T_g data (Figure 6.2.2). DMA E' results show the formation of a sub T_g transition in the 100 kGy 1.8 kGy hr^{-1} air and 200 kGy 1.8 kGy hr^{-1} vacuum irradiated samples. This additional transition shows some of the characteristics of a glass transition. This new transition may result from the formation of radiation-induced of the low molecular mass chains identified which may have a different monomer ratio to the pristine FK-800 chains and therefore, a different transition temperature.

Headspace gas analysis was used to identify the chemical reactions taking place during irradiation of the Fk-800 samples, and to help identify the mechanisms leading to the chain scissions. The results show the production of CO_2, CO and $SiF_2(CH_3)_2$ but did not show the silicon tetrafluoride (SiF_4) which would be expected based on the previous literature reviewed in Section 2.2. Some evidence of an increase in CO_2 upon irradiation of fluoropolymers has previously been noted in references[35; 82] but no reference has been made to $SiF_2(CH_3)_2$ in previous work.

Charlesby[82] discussed the generation of CO_2 when poly-TFE was irradiated in glass. CF_4 released by the poly-TFE during irradiation could react with the glass to produce SiF_4 and CO_2 under irradiation conditions, via Equation 8.1.2. The lack of SiF_4 seen in the results may be due to the reaction of gaseous SiF_4 with moisture or components in the gas collection kit. The gas collection kit used a silicone septum with the Chromacol vial and a build-up of white residue was seen inside the glass collection kit after testing of the headspace samples. Based on an email from J Stratta on 18th January 2011 confirming the use of trimethylsilane in the GC inlet system; the $SiF_2(CH_3)_2$ detected in the headspace samples is likely due to the reaction of highly reactive fluorine-containing compounds with the trimethylsilane used to deactivate glass parts of the inlet, resulting in the $SiF_2(CH_3)_2$ detected.

$$CF_4 + SiO_2 \rightarrow SiF_4 + CO_2 \qquad \textbf{(8.1.2)}$$

The chemistry of FK-800 when irradiated is controlled by a combination of the individual response of its two constituent monomers. The radiation chemistry of CTFE - 75% of FK-800 - will dominate the chemistry, whilst the interactions of VDF will play a minor role. In previous studies poly-CTFE has been shown to undergo chain scission directly, and to produce radicals when subjected to ionising radiation[32; 36; 83; 84]. However, the exact chemistry for direct chain scission of the polymer backbone is still not fully understood. Hill et al. [84] used ESR to identify radical species (Table 8.1.3) in γ-irradiated poly-CTFE; the study found the radicals formed by radiolysis consisted of both side chain

radicals - from the abstraction of fluorine - and chain end species, resulting from chain scission.

Table 8.1.3 Structure of gamma radiation-induced radicals in poly-CTFE identified by Hill et al. using ESR spectroscopy. Adapted from [84]

Radical number	Radical Structure
I	$-CFCl-CF_2^{\cdot}$
II	$-CF_2-CCl^{\cdot}-CF_2-$
III	$-CF_2-CF^{\cdot}-CFCl-$
IV	$-CF_2-CFCl^{\cdot}$

The results from this study indicate the regions of poly-CTFE in the FK-800 are both undergoing direct chain scission and backbone radical attack upon γ-irradiation. These two reactions leave chain end radicals and unsaturated chain ends in the poly-CTFE regions of the FK-800. The further interactions of fluorine radicals with the polymer's chain ends via the reactions shown in Figure 8.1.1 lead to the formation of the small molecules. Hill et al.[84] did not note the formation of any chlorine radicals in their study; however, in this study the formation of dichlorodifluoromethane indicates chlorine radicals are present and reacting to form small molecules via reaction 3 in Figure 8.1.1. The formation of chlorine radicals is likely to be via side-chain abstraction upon radiolysis as suggested by Florin et al.[32]. However, the abstraction of fluorine predominates over the abstraction of chlorine when poly-CTFE is γ-irradiated.

In contrast to poly-CTFE, poly-VDF has previously been shown to cross-link when irradiated[14; 80]. Poly-VDF undergoes the abstraction of hydrogen and fluorine when irradiated and predominantly undergoes cross-linking reactions. The abstractions lead to the formation of radical sites on the backbone and unsaturation. Figure 8.1.2 shows the reactions which have been proposed by Nasef and Dahlan[80] when poly-VDF was electron beam irradiated.

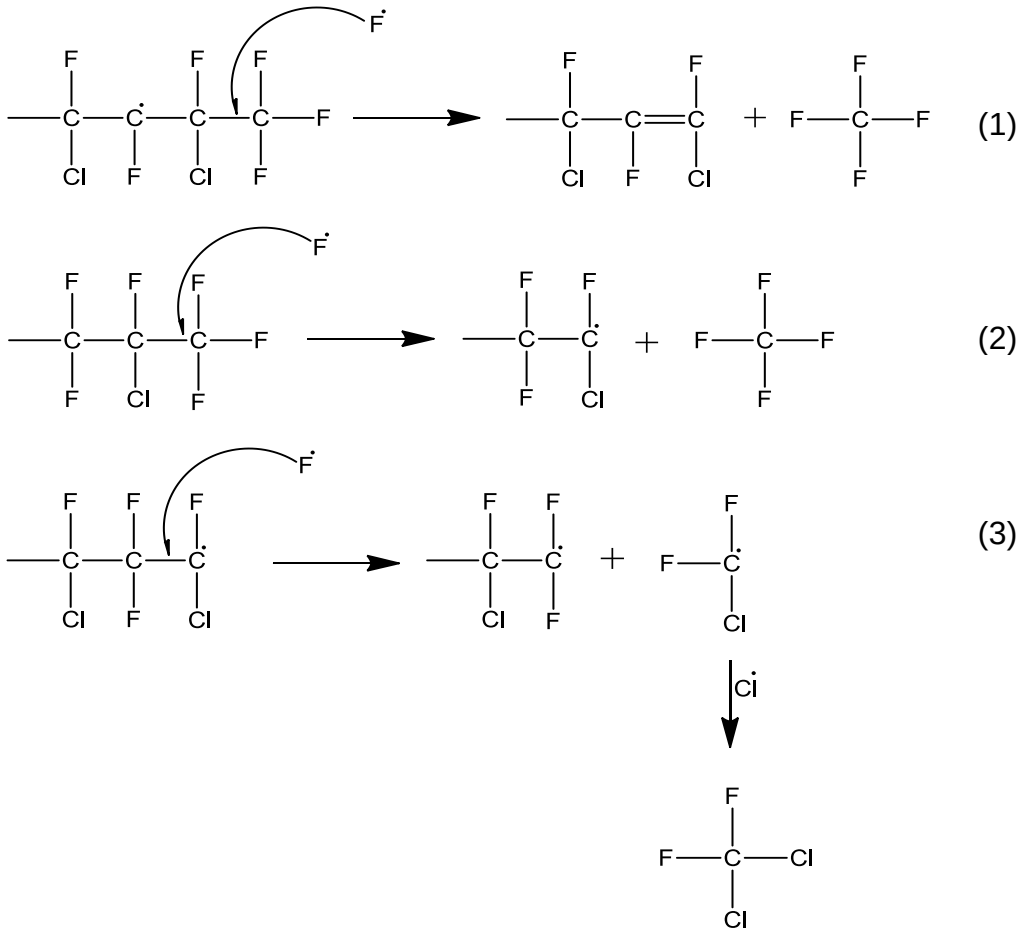

Figure 8.1.1 Suggested CTFE chain end - fluorine radical back-biting reactions to form the small molecules. (1) fluorine radical reaction with a CF_3 end group to form an unsaturated chain end, (2) fluorine radical reaction with a CF_3 end group to form a chain end radical, (3) reaction of fluorine radical with a CTFE chain end radical to form a chain end radical and a small molecule radical which undergoes a further radical reaction

Nasef and Dahlan have included a chain scission reaction in their proposed mechanisms; however, the cross-linking reactions dominate when poly-VDF is gamma irradiated due to the lower energies of the γ-photons. The formation of hydroperoxides in the presence of oxygen has been observed by FT-IR during this study and is shown schematically in Figure 8.1.2 for poly-VDF. Hydroperoxides are also likely to form in poly-CTFE when irradiated in an oxygen containing atmosphere; this is due to the reaction of oxygen with the poly-CTFE's side chain radicals formed by the abstraction of fluorine.

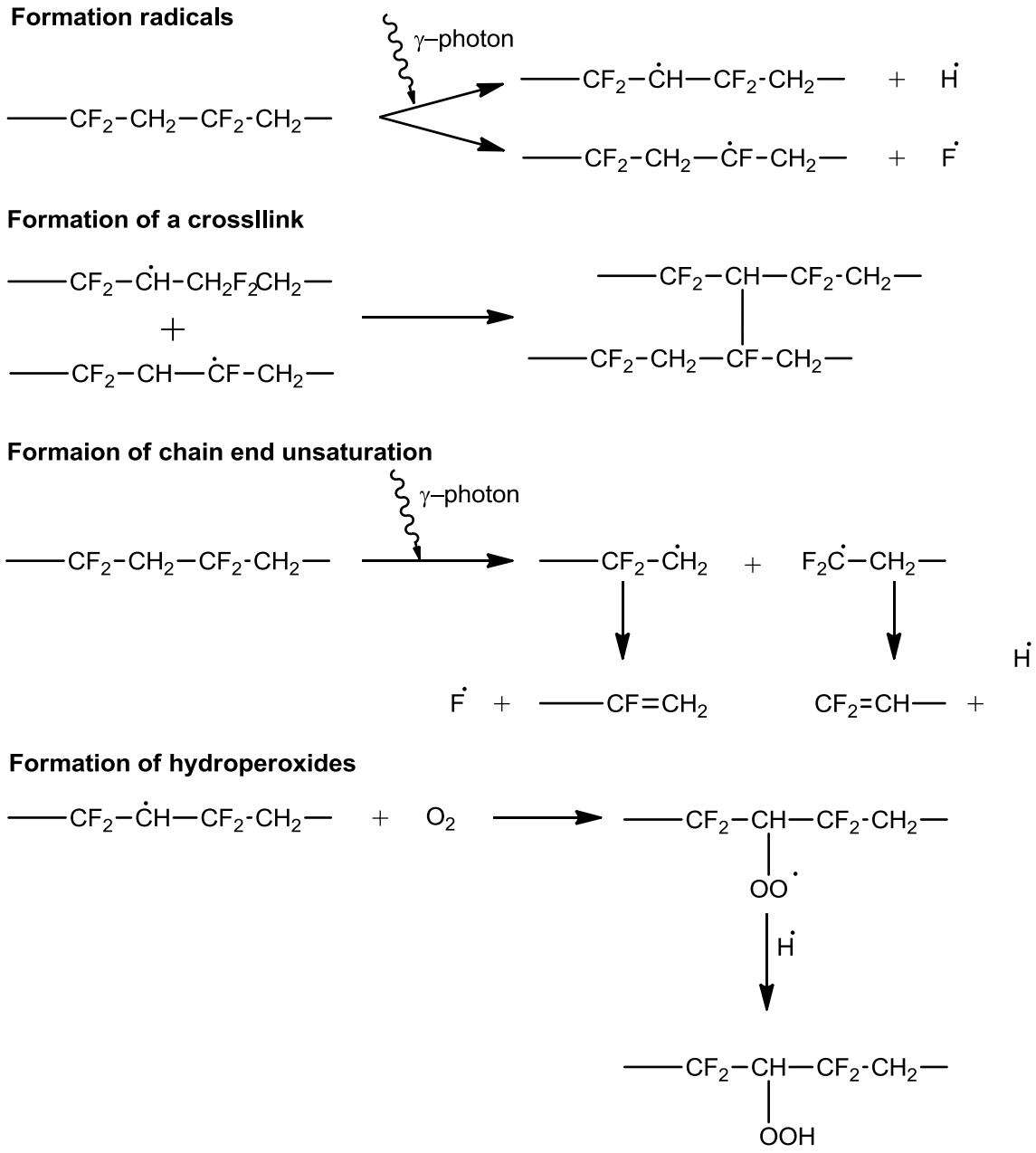

Figure 8.1.2 Nasef and Dahlan's schematic representation of the electron-induced reactions taking place in poly-VDF films, adapted from[80]

The theory that the two monomers in FK-800 are reacting differently to the γ-radiation is supported by the molecular mass results from this study (Section 6.4). The two monomers will continue to cross-link and chain-scission as they would when irradiated as a polymer in their own right. The CTFE regions of the polymer undergo chain-scission resulting in the reduction in M_n.

However, the increase in M_w at lower radiation doses and the increasing $Đ_m$ indicate that the VDF present in FK-800 is forming cross-links to form larger polymer chains and networks.

The production of peroxides indicates that when FK-800 is irradiated in air, atmospheric oxygen is reacting with the main chain radicals formed by the abstraction of fluorine and hydrogen. The reaction of oxygen with the polymer chain radicals explains the atmosphere dependence seen in the crystallinity and M_w results. The oxygen will act to quench the radicals which form on the polymer chain and will in turn reduce the number of possible cross-linking sites, although at higher doses the number of chain scissions is too great for an irradiation atmosphere dependence to still be seen. The samples in this study were 2 mm thick and it may also be the case that oxygen diffusion across the samples was a limiting factor in these experiments.

It has previously been noted that radicals generated when fluoropolymers are irradiated can be very long lived (Section 2.2). The study of Kel F-800 by Mayer et al.[38] also showed evidence by NMR and GPC that cross-linking predominated in legacy samples which had been allowed to age post-irradiation for a period of time. The cross-linking seen may result from slow post-irradiation reactions not seen in the timescale of this study. There was also no mention by Mayer et al. of the atmosphere the samples were irradiated under or how the samples were stored between irradiation and analysis. It may therefore be possible that slow post-irradiation cross-linking may take place over extended periods of time.

The gaseous products detected by GC-MS during this study are either direct products of the irradiation of the polymer, or reaction products from the reaction of irradiation products with the irradiation vial or analysis equipment. The products show that the radiation decomposition products of FK-800 are highly reactive fluorine-containing compounds. These gaseous products and their reactive nature must be considered if FK-800 is to be used in a radiation environment, and further research on directly measuring the volume of gas generated should be considered in any future study.

Chain scission of the FK-800 backbone upon irradiation explains the σ_s, extension at σ_s and some of the lower radiation dose DMA data but, cannot explain the increase in E, or the trend for E' to increase and tan δ peak to decrease with increasing radiation dose. These effects are in themselves indicative of crosslinking; however, it is unlikely that the crosslinking identified in the molecular mass data would be enough to cause the trends in properties seen. Therefore, it is likely that the increase in crystallinity noted in Section 6.3 is acting to crosslink as crosslinks to stiffen the polymer.

The ideal theory of polymer crystallisation is widely described in the literature, including references[85-89] ; however, some aspects of polymer crystallisation will be discussed here with reference to the irradiated FK-800.

A truly amorphous polymer (Figure 8.1.3 A) is a tangled structure of polymer chains with no order, and can be formed by cooling a polymer quickly from a melt to below T_g, freezing the disordered structure. In contrast, when a polymer is allowed to cool slowly from its melt, the polymer's chains can fold back on themselves forming an ordered crystalline structure. Figure 8.1.3 B shows a diagrammatic representation of the growth of two crystal structures and shows how multiple chains can build one structure whilst tying crystals together. The rate of crystallisation is controlled by the temperature of the polymer with the fastest crystallisation rate occurring at temperatures mid-way between the T_g and melt temperature. Below the polymer's T_g the crystallisation process is stopped due to the lack of molecular movement around the polymer's backbone.

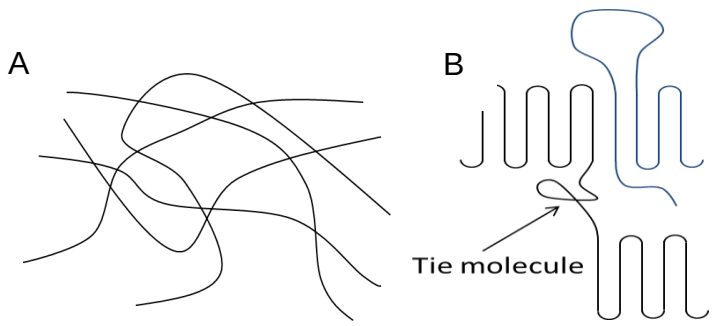

Figure 8.1.3 Diagrammatic representation of an amorphous polymer (A) and the formation of an ordered crystal structure of a crystalline polymer (B)

As the polymer continues to crystallise, the chains continue to fold into a three dimensional structure called a lamella. A diagrammatic representation of a lamella is shown in Figure 8.1.4.

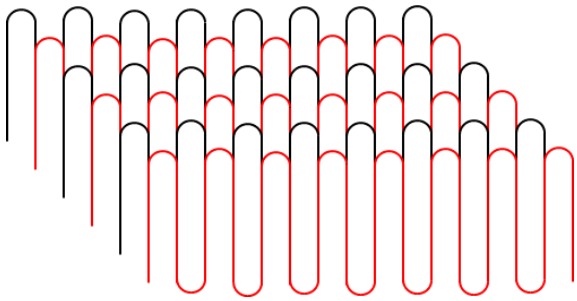

Figure 8.1.4 Diagrammatic representation of a polymer lamella structure

As several lamella structures grow three dimensionally from a central nucleation point, a spherical structure - known as a spherulite - forms with amorphous regions between the lamella (Figure 8.1.5). As well as having truly amorphous regions between the lamella, the structures are connected by tie molecules which interact with multiple lamellae. Large numbers of separate spherulites form as the polymer crystallises and are connected by amorphous regions tying them together.

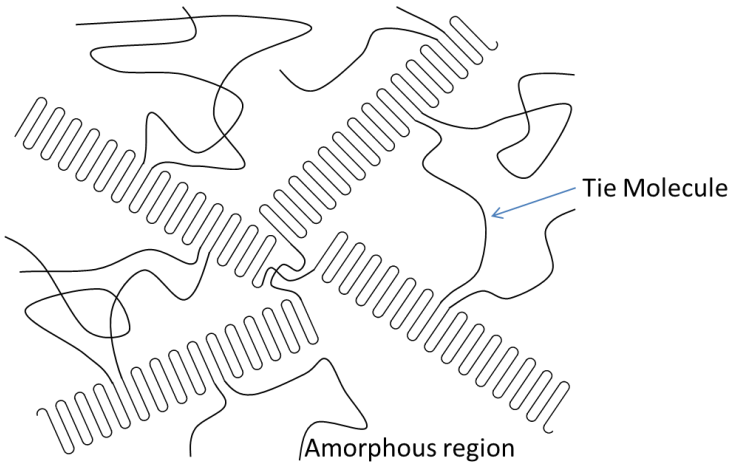

Figure 8.1.5 Diagrammatic representation of a spherulite in a semi crystalline polymer

In the case of the FK-800 used in this study, the polymer was cooled quickly to below T_g within 2 minutes after melt processing into polymer sheets. This rapid

cooling meant that the samples irradiated contained very few crystals at the start of the irradiations. Although the polymer samples were irradiated in the rubbery state (above T_g), the irradiation temperature was controlled at 36.5 °C which is much lower than the ideal crystallisation temperature for FK-800 in the solid phase of ~70 °C, and so the rate of crystallisation would be slow. The slow rate of crystallisation above T_g results from the polymer chain entanglements restricting chain movement and slowing the formation of lamella. In the irradiated FK-800 samples, lamellae formation is unlikely to have occurred over the experimental time scales.

Instead of lamella, it is proposed that the FK-800 is forming small regions of chain aligned fringe micelle crystals, diagrammatically shown in Figure 8.1.6. The fringe micelles form as chain backbones rotate and align opening up space for the next chain to rotate into the free space and further align in the micelle [85; 86].

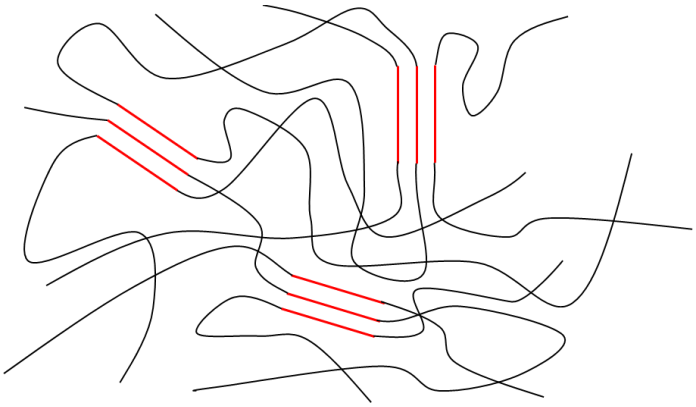

Figure 8.1.6 Diagrammatic representation of proposed fringed micelle crystals in irradiated FK-800. Micelle crystals regions are represented in red

Further evidence indicating the formation of less ordered crystal structures - such as fringe micelles - in the irradiated samples is the temperature at which the crystals melt. Figure 8.1.7 shows the DSC thermograms of two FK-800 samples, one pristine and one irradiated to 200 kGy at 1.8 kGy hr^{-1} under vacuum conditions. Both samples, show a small endothermic melt at ~115 °C whilst the irradiated sample which has 7.7 % calculated crystallinity by DSC, shows an additional large endothermic melt at ~75 °C. The formation of the

lower temperature melt in the irradiated samples indicates the formation of less ordered and / or shorter in length crystals. These lower melt temperature crystals are not as thermally stable as the higher melt temperature crystals, resulting in the ~75 °C melt seen in the 200 kGy sample in figure 8.1.5.

The formation of the micelle crystals in the irradiated samples suggests that the radiation is resulting in chain scissions, as opposed to cross-links, in the backbones of some of the polymer chains. The chain scissions result in the formation of shorter polymer chains which are less influenced by chain entanglements and are free to rotate and align, thus forming crystals. The corresponding increase in density with increase in crystallinity results from the reduction in free volume within the polymer as the crystals form.

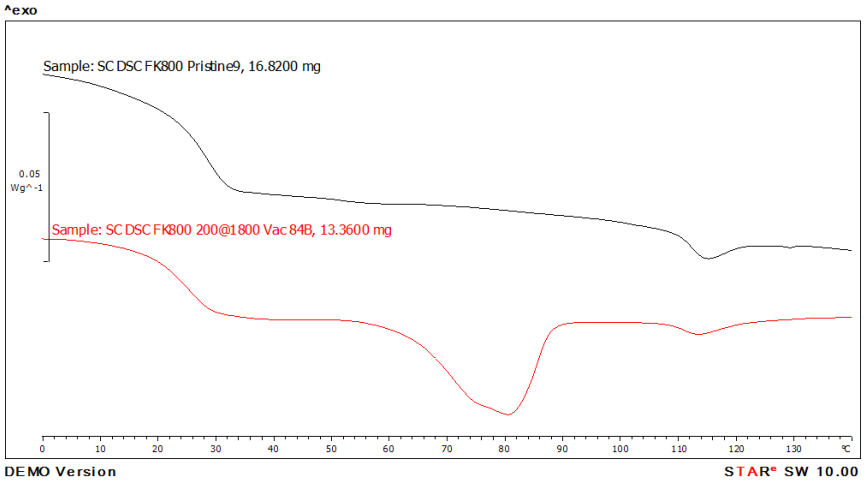

Figure 8.1.7 DSC thermograms for two samples of FK-800 tested at 10 °C min^{-1}. The black line shows a pristine sample whilst the red line shows a sample irradiated to 200 kGy at 1.8 kGy hr^{-1} under vacuum

The formation of chain scissions in the backbone of the FK-800 chains would also explain the drop in σ_s and elongation at σ_s; as the polymer becomes weaker due to fewer chain entanglements from shorter polymer chains. Although the σ_s and elongation at σ_s show the samples softening with increasing radiation dose, the E and σ_y results show the samples stiffening before it yields with increasing radiation dose. This stiffening combined with the increases in crystallinity, indicates that crystals are acting as temporary cross-links between polymer chains in the irradiated samples.

The DMA E' data show an initial drop in stiffness and then an increase to stiffer than the pristine at higher radiation doses, supporting the idea that chain scission is causing the polymer to behave in a softer manner before the crystallinity builds to the point where the crystal links cause the polymer sample to behave in a stiffer manner. An increase in storage modulus between T_g and T_m with increasing crystallinity has previously been seen in Kel F-800 by Hoffman[90], supporting this theory. At 100 kGy the DMA data showed less of a drop in E' over the T_g region and the lowest tan δ peak heights. These results indicate that less of the polymer is undergoing T_g, concurring with the hypothesis that crystals are acting as cross-links restricting the motion of the polymer chains.

To further investigate the hypothesis that the FK-800's increase in crystallinity was resulting in the increase in DMA E' at higher radiation doses, tests were carried out on thermally cycled DMA samples. One sample from each data set was run as before, then allowed to soak at 100 °C for 5 minutes before being cooled at a constant rate of 10 °C min^{-1} to 0 °C before being tested again. The 1 Hz E' values at 50 °C were plotted for both the before and after thermal cycling and are shown in Figure 8.1.8. The data show the rise in E' for the non-cycled samples seen previously but, after cycling, the modulus values are lower for all samples and all lie within a small range of 0.9 - 4.5 MPa. The lower modulus values after thermal cycling show that the crystal cross-links formed during irradiation have a large effect on the E' values of the irradiated polymers, and that removing the crystals by thermally cycling the samples can remove this effect.

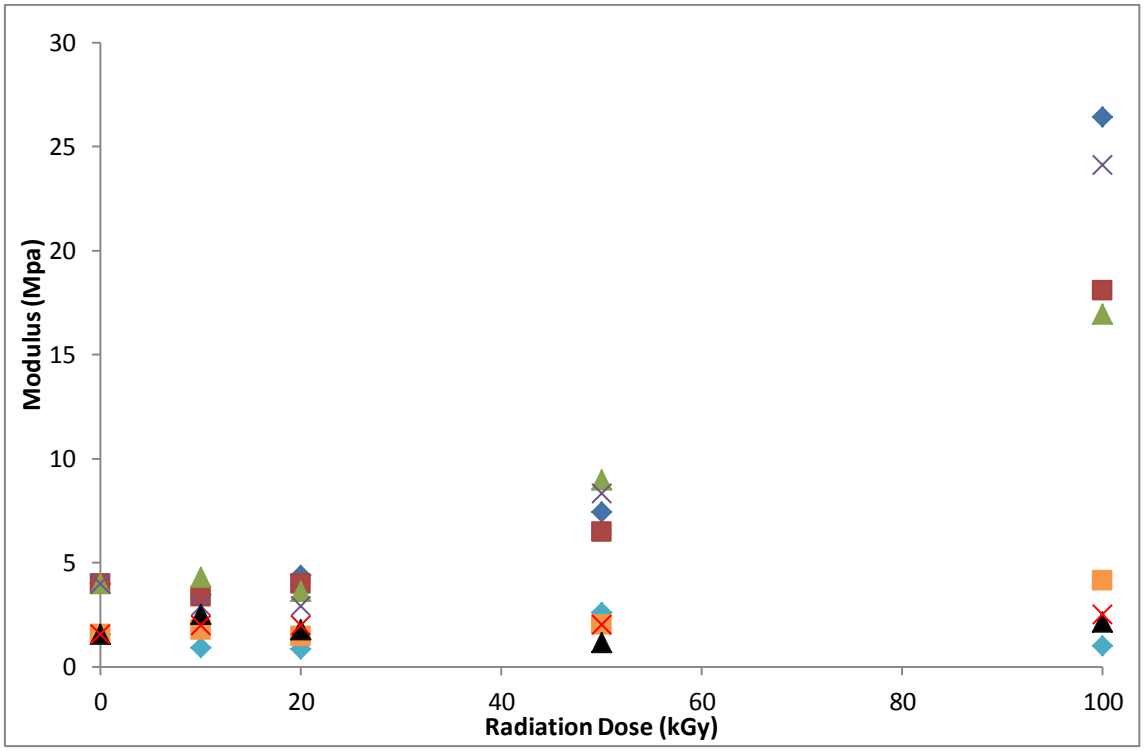

Figure 8.1.8 DMA storage modulus (E') values at 50 °C for irradiated FK-800 samples before and after thermal cycling. Before cycling 1.0 kGy hr^{-1} air (♦) 1.0 kGy hr^{-1} vacuum (■) 1.8 kGy hr^{-1} air (▲) 1.8 kGy hr^{-1} vacuum (X). After thermal cycling 1.0 kGy hr^{-1} Air (♦) 1.0 kGy hr^{-1} Vacuum (■) 1.8 kGy hr^{-1} Air (▲) 1.8 kGy hr^{-1} vacuum (X)

The temperature at which the crystal micelles are seen to melt by DSC of ~ 75 °C (Figure 8.5.1) also corresponds to a drop in E' seen in the irradiated DMA samples (Figures 6.1.8 to 6.1.11), which is further evidence to support the micelle theory. As the DMA samples are heated through the temperature at which the crystal micelles melt - no longer acting as cross-links - in the irradiated samples there is a corresponding drop in E'.

The DMA data show an increase in T_g with increasing radiation dose in samples which have not been thermally cycled. This rise can be explained by the cross-linking effect of the radiation-induced crystals restricting chain motion in these samples, raising the temperature at which molecular rotation along the whole polymer chain can begin.

A combination of the number of chain scissions per molecule and the increase in crystallinity may be causing the dose rate dependence seen in some of the tensile load tests. GPC analysis showed the 20 kGy samples irradiated at 1.0 kGy hr^{-1} show more scissions per molecule than in the higher dose rate samples. This could lead to a higher percentage crystallinity in these samples which could explain the dose rate dependence seen in the E and σ_s data (Figures 6.1.3 and 6.1.4). The increase in crystallinity which would be required to cause this dose rate dependence is not seen on the DSC crystallinity data (Figure 6.3.1), but, as shown in the X-ray diffraction data for the 1.8 kGy hr^{-1} samples, the DSC crystallinity values based on poly-CTFE are not accurate for FK-800.

FK-800 has been shown to undergo chain scission when γ-irradiated. The chain scissions allow the polymer to form crystal micelles, which in turn act to cross link the polymer chains. These two main principals explain the complex and contradictory mechanical behaviour observed. The study of the polymer alone has shown radiation can have a large effect on the mechanical behaviour of FK-800. However, FK-800 only constitutes 5 % of the formulated TCV, and because of this, a further study was conducted on irradiated TCV, to investigate if the observed changes in the polymer affect the formulated PBX.

8.2 TATB and TCV

A summary of the main results from the irradiation study of TATB and TCV are presented in table 8.2.1. Initial testing of the TATB and TCV consisted of small scale hazard testing to show that irradiated TATB and TCV were safe to handle for further experimentation. A very significant change in the TATB and TCV sensitiveness to drop weight impact and electric spark discharge were noted in the results. This coupled with a drop in onset of decomposition and consistent colour change from yellow to green, indicated that a more sensitive decomposition product was produced when TATB and TCV is irradiated. Both TATB and TCV displayed the same trends during the hazard assessment which indicates that a decomposition product of TATB is causing the changes and the FK-800 binder is not playing a part.

Table 8.2.1 Summary of the main results for the TATB and TCV irradiation experiments.

Analysis Category	Analysis Technique	Significant Results Upon γ-Irradiation
TATB		
Hazard Testing	Rotter - Langlie Fof I	- Reduction in Fof I from 165 to 87 at 200 kGy.
	Eclectic spark discharge	- Increase in sensitiveness to electric spark discharge from No ignitions at 4.5 J to Ignitions at 0.45 J but not at 0.045 J.
	Mallet Friction	- No change (0% ignitions with Steel on Steel)
Thermal Analysis	DSC Onset of decomposition	- Maximum 11 °C reduction in onset of decomposition to 371 °C at 200 kGy.
	TGA Onset of decomposition	- Maximum 9 °C reduction in onset of decomposition to 349 °C.
	TGA Mass Loss	- Some evidence of increased non combusted residue after test.
Analysis of Decomposition products	Colour Change	- Change from bright yellow to dark green with increasing dose.
	HPLC	- Detection of new peak with a retention time of 1.07 minutes. - Peak area increased with increasing dose.
	LC-MS	- Molecule responsible for peak at 1.07 minute in HPLC analysis found to have a mass of 240 g mol^{-1}
TCV		
Hazard Testing	Rotter - Langlie Fof I	- Reduction in Fof I from 140 to 117 at 200 kGy.
	Eclectic spark discharge	- Increase in sensitiveness to electric spark discharge from No ignitions at 4.5 J to Ignitions at 0.45 J but not at 0.045 J.
	Mallet Friction	- No change (0% ignitions with Steel on Steel)
Thermal Analysis	DSC Onset of decomposition	- Maximum 12 °C reduction in onset of decomposition to 371 °C at 200 kGy.
	TGA Onset of decomposition	- Maximum 9 °C reduction in onset of decomposition to 349 °C.
Mechanical Properties	Brazilian Disc Test	- No significant change in mechanical properties at 40 °C. - Some evidence of increase central stress at failure with increasing radiation dose.

HPLC was used to separate a decomposition product irradiated TATB, it was found that the area of the unidentified peak of the HPLC chromatogram increased with increasing radiation dose and that the results fitted Equation 7.5.1. The results and equation both suggest that the rate of production of the decomposition product deceases with increasing radiation dose. This is a strong indicating a saturation effect is taking place; however, to confirm this trend is a true trend, further samples would need to be irradiated to higher doses and tested to confirm the data continue to fit the prediction. If the further irradiations at higher total doses were found to fit the trend seen in this study, HPLC could then be used in future as a method of estimating the radiation dose received by unknown samples of TATB.

The concentration of the radiation-induced decomposition product was too low for identification using the HPLC diode array and so LC-MS was carried out on pristine and irradiated TATB. The peak unidentified HPLC was found to have a mass of 240 g mol^{-1} 18 less than pure TATB. A mass loss of 18 g mol^{-1} indicates that a condensation reaction has taken place resulting in the loss of water from the TATB molecule. The loss of water would result from the reaction of one of each of the molecules' amine and nitro groups to give a furazan derivative with a mass of 240 g mol^{-1}. The resulting reaction is shown in Figure 7.6.3 with TATB absorbing a photon and decomposing to give a mono-furazan derivative of TATB and water.

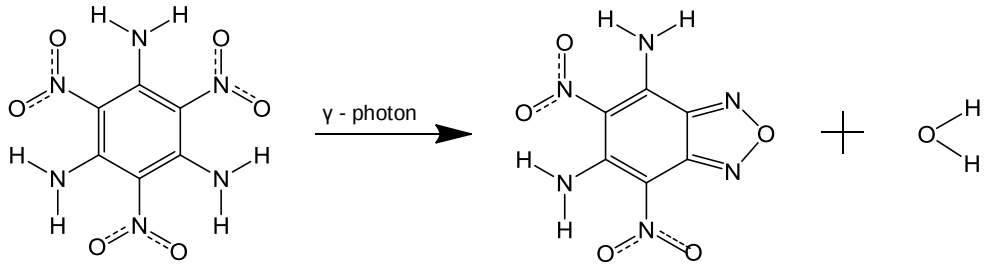

Figure 8.2.1 Reaction of TATB with a γ-photon to form a mono-furazan derivative and water

Furazan derivatives of TATB are known thermal decomposition products of TATB[91-93] and have been detected previously in γ-irradiated TATB by a group at Los Alamos National Laboratory[15] using thin layer chromatography.

The previous Los Alamos study combined with this study indicates that at least one of the radiation-induced decomposition products of TATB is a mono-furazan derivative. No di-furazans, which have previously been reported[15], were detected during this work. However, this is likely to be due to the lower radiation doses used in this study; a maximum of 100 kGy was used in this study compared to a maximum dose of 700 kGy used by Los Alamos. No evidence was found during the LC-MS analysis of the mono-nitroso decomposition product proposed by a Laurence Livermore National Laboratory team[27]. The work conducted during this study in not able to confirm that the mono-furazan decomposition product detected is the cause of the green colour of irradiated TATB. However, it has proven that the mono-furazan is a major radiation decomposition product of TATB and that HPLC can be used as a method for separating and detecting decomposition products of irradiated TATB.

A mono-furazan derivative of TATB is the likely cause of the the drop in F of I (Table 7.1.1), and increased sensitiveness to static discharge (Table 7.1.2) seen in the irradiated TATB. The increased sensitiveness could be a direct result of the sensitiveness of the mono-furazan. No data has been published relating to the sensitiveness of the mono-furazan derivatives of TATB at this time; however, the mono-furoxan derivative of TATB, 5,7-diamino-4,6-dinitrobenzofuroxan (CL-14) (Figure 7.7.1)[94] has been shown to have a higher sensitiveness to impact. In the Los Alamos drop weight impact test[95] CL-14 was found to have a 50 % fire height of 120 cm compared to 490 cm for TATB[95]. The difference between CL-14 and TATB can be explained from an understanding of how TATB forms hydrogen bonds. TATB is a symmetrical molecule able to form an equal number of both inter- and intra- molecular hydrogen bonds around the molecule. The hydrogen bonds both stabilise the individual molecules and TATBs larger crystal structure.. Therefore, because both CL-14 and the mono-furazan suggested in this study are less symmetrical, and unable to form all the stabilising hydrogen bonds that TATB can, they have a higher sensitiveness to external stimuli.

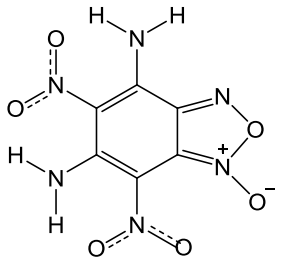

Figure 8.2.2 Diagram of 5,7-diamino-4,6-dinitrobenzofuroxan (CL-14) a mono-furoxan derivative of TATB

Alternatively, it may be that the presence of CL-14 or the mono-furazan disrupts the stable, ordered planer crystal structure[3] TATB forms using hydrogen bonding. However, small amounts of either the mono-furazan or CL-14 in the crystals of TATB could disrupt the ordered crustal. The resulting weaker crystals could also be an explanation for the increases in sensitiveness to external stimuli. However, further work would be required to confirm either of these hypotheses.

Although not reported in the results section; the composition of the headspace gases of the pressed cylinder sample vials was tested along with their mass and density. No significant changes were observed in any of these tests; because the samples were irradiated under vacuum, the collection of headspace gas is inherently more difficult than for samples irradiated in a gaseous atmosphere. This difficulty in collecting the gases, combined with the small sample size (0.6 g) and surface area to volume ratio of the cylinders, resulted in any decomposition gases generated during irradiation either not diffusing out of the sample, or having such a low concentration they could not be detected. The density changes that were seen in the FK-800 binder after irradiation are also not seen in the TCV composition. The lack of a change in density indicates the density of the crystalline explosive filler is not changing with irradiation, and the 5 wt% of binder in the TCV composition - which is undergoing changes - is not enough to influence the density of the whole TCV.

PBXs for use in nuclear weapons require good mechanical properties to both hold the complex shapes required and act as supporting elements throughout their service life. To study the effects of γ-radiation on TCVs mechanical

properties the Brazilian disc biaxial tensile load test was conducted on samples irradiated up to 100 kGy under vacuum. The data showed that radiation had little to no effect on the mechanical properties of the composition. There was some indication that the changes in the binder's mechanical properties (Section 6.1) may be affecting the stiffness of the TCV composition. The binder experiments revealed an increase in E and σ_y which could explain the unconfirmed increase on central stress at failure with increasing radiation dose indicated by the Brazilian disc experiments. However, large changes in the properties of the FK-800 have only translated into a very small change in the mechanical properties of the TCV composition. This study did not investigate the failure mode of the TCV samples and so we do not know if the samples failed due to failure of the binder itself or the binder explosive crystal bond.

The TATB and TCV experiments have shown that the changes in the binder seen in Section 6 have little impact on the properties of a formulated PBX and it is radiolytic decomposition of the TATB filler which has resulted in changes to the hazard characteristics of the PBX.

9 Conclusions

9.1 FK-800

As discussed in Section 2.2, the predominant effect when polymers are γ-irradiated is the breaking of chemical bonds leading to either backbone chain scission or cross-linking. The results of this study show that FK-800 predominantly undergoes chain scission; the scissions are likely to be taking place in regions of poly-CTFE within the polymer whilst some cross-links are forming where VDF is present. The decrease in the sample's M_n measured by GPC gives a calculated chain scission rate of up to 1 scission per FK-800 chain for samples irradiated to a total radiation dose of 200 kGy. There is a contrasting increase in M_w in the FK-800 samples irradiated at doses of up to 100 kGy; this is evidence that, whilst chain scission is the predominant reaction, some cross-linking is also occurring.

Along with the chain scission and cross-linking of the polymer backbone, when FK-800 samples are γ-irradiated the radiation causes the formation of free radicals including those of fluorine and hydrogen; these then react to form highly reactive gases. Evidence from the GC-MS headspace analysis indicates the decomposition gases include HF and F_2 along with CF_4 and other compounds containing fluorine and chlorine. These highly reactive gases can react with the polymers' surroundings - in this study CF_4 reacted with the glass vials to give SiF_4 and CO_2 - which may result in incompatibilities if FK-800 is to be used in an application where it will be exposed to γ-radiation.

Much of this study concentrated on the effects of irradiation on the mechanical properties of FK-800. It was found that chain scission of the FK-800's backbone resulted in a lowering of the polymer's T_g with increasing dose (when tested by DSC). The chain scissions also resulted in a lowering of E' and tan δ peaks for samples irradiated up to total doses of 50 kGy in the DMA experiments. However, crystallinity data show that as the radiation dose increases, the shorter polymer chains are able to rotate and align forming a fringe micelle crystal structure. The micelles act as cross-links between the polymer chains;

this causes the FK-800 samples irradiated to 100 kGy to behave more stiffly between T_g and the crystal micelle melt temperature (~75 °C) in the DMA experiments. The crystal cross-links cause a threefold increase in E' at 50 °C, along with a corresponding drop in strength for the T_g tan δ peak. The drop in tan δ peak indicates that less of the polymer chains are able to undergo the T_g event because their rotational movement is limited by the constraining effect of the crystals. It has been shown that the increase in E' can be reversed by thermally cycling the samples and thus removing the fringe micelle structure.

The tensile properties of FK-800 change significantly upon γ-irradiation. The chain scissions which take place result in a reduction in σ_s and elongation at σ_s. Whilst the chain scissions act to make the irradiated FK-800 samples softer in tensile load tests once taken beyond their yield, the increase in crystallinity causes an increase in E and σ_y. This combined with the DMA data shows that irradiated FK-800 will behave stiffer-stronger within its elastic limits and then will behave softer-weaker once the samples elastic limits have been exceeded. The tensile load tests in this study did not investigate the effects of thermal cycling on the samples due to the destructive nature of the tests.

Some evidence of irradiation dose rate dependence was seen in the E and σ_y results from the tensile load tests, and the density data. The dose rate dependence seen related to a faster rate of change in the samples irradiated to 50 kGy at 1.0 kGy hr^{-1} against the higher dose rate samples. The dose rate dependence may be caused by the extended timescales over which the lower dose rate irradiations took place; however, it is not possible to confirm this without further investigation.

Evidence of irradiation atmosphere dependence was seen in the GPC (M_w and $Đ_m$), FT-IR and X-ray diffraction crystallinity data. However, the X-ray diffraction data only consist of a single sample at each irradiation dose and atmosphere combination. With regards to the FT-IR data, although only the samples irradiated in air show the appearance of a new peak for C=O, it is not reliable enough to confirm an irradiation atmosphere dependence. The GPC M_w data indicate that in the samples irradiated under vacuum, more cross-links and

chain extensions have taken place. This would be consistent with the hypothesis that less oxygen is available to react with and quench the radicals forming on the polymer chains. The limited availability of oxygen would result in a higher number of inter-chain radical reactions forming cross-links and extensions than found in samples where atmospheric oxygen was available to quench the radicals. Based on the evidence from this study it is likely that there is atmosphere dependence when FK-800 is irradiated in air and under vacuum; however, the samples used in this study may have been too thick to allow oxygen in the air-irradiated samples to diffuse through the samples at a fast enough rate during irradiation. Further work would be required to fully understand the effects of irradiation atmosphere on FK-800.

FK-800 has been shown in this study to undergo significant changes in its properties upon γ-irradiation above its T_g. The changes are predominantly related to chain scission of the polymer backbone forming shorter polymer chains and leading to changes in the polymer's crystal structure. The changes noted significantly affect the mechanical properties of the irradiated FK-800 and the way the FK-800 will respond to changes in temperature.

However, when used as a binder in the PBX composition TCV, FK-800 makes up only 5 % by mass of the composition. Nevertheless, the changes in the mechanical properties of the FK-800 are significant, and may have an effect on the properties of a formulated PBX especially if used in higher percentages. The possible effect of the decomposition gases produced when FK-800 is γ-irradiated on any explosive it is formulated with also need to be considered.

9.2 TATB and TCV

No verifiable changes to the mechanical properties of the PBX TCV were noted in this study. However, some evidence of an increase in the central stress at failure and E with γ-irradiation could be seen in the results of the Brazilian test. The sample with the steepest slope and highest central load at failure was a 100 kGy disc. Nevertheless, these changes cannot be confirmed because the sample set was too small.

Although there were no significant changes in the TCV's mechanical properties, significant changes have been seen in the sensitiveness of the TCV when hazard assessments were conducted. An increase in sensitiveness to both impact and electric spark discharge was seen; this was combined with a drop in the onset of decomposition in both DSC and TGA analysis. The TCV samples were also seen to change in colour from a yellow to dark green with increasing radiation dose corresponding to the previously reported studies for TATB based explosives discussed in Section 2.1.1.

During the hazard assessment of the irradiated explosives, the same trends in sensitiveness and onset of decomposition were noted in γ-irradiated samples of both TCV and TATB. The TATB irradiated to 200 kGy in air shows a drop in F of I from 165 to 87 (a value close to that of the conventional high explosive RDX (80)), indicating a substantial change had occurred. This led to the conclusion that it is the radiation-induced changes of TATB and not the FK-800 binder which predominantly affect the properties of irradiated TCV formulation.

An unknown radiation-induced decomposition product of TATB has been separated by HPLC and found to increase in concentration with radiation dose. Analysis of the decomposition product's concentration showed that it fitted to the initial upward trend of Equation 7.5.1 which included a factor for saturation at higher radiation doses. However, the data could also be made to fit a linear trend line; therefore further analysis at higher doses is required to confirm any trend. If the trend can be confirmed it should be possible to use HPLC as a method of calculating the doe received by unidentified samples.

LC-MS analysis of the unknown decomposition species has shown the decomposition product to have a mass of 240 g mol^{-1} strongly supporting the hypothesis that it is the mono-furazan derivative of TATB previously described by Los Alamos National Laboratory[15]. Some evidence of other decomposition products has been seen in the LC-MS mass spectra. This indicates that it is unlikely the mono-furazan is the only decomposition product when TATB is irradiated. Dynamic-TGA mass loss data indicate that one of these species may

be the mono-nitroso derivative suggested by Lawrence Livermore National Laboratory[27], although this species was not detected in the LC-MS analysis.

9.3 General conclusions

In this study the FK-800 fluoropolymer has been shown to predominantly undergo chain scission when γ-irradiated above its T_g in air and under vacuum conditions. The chain scission reactions lead to the release of highly reactive gaseous products and the formation of a fringe micelle crystal structure. The chain scissions act to make the FK-800 softer and weaker; however this is counteracted within the polymer's elastic limits by the fringe micelle crystals acting as cross-links between the chains. This cross-linking effect causes the irradiated samples of FK-800 to behave stiffer and stronger when tested. The fringe micelle crystals can be melted by heating the FK-800 to 80 °C removing the observed cross-linking and strengthening effect.

The changes in the mechanical properties of the FK-800 observed in this study do not cause significant changes in the properties of the TCV PBX. The Brazilian disc data showed that a large change in the mechanical properties of the FK-800 binder has only a small effect on the formulated TCV. The FK-800 binder only constitutes 5 % by mass of the TCV and it may be the case that for PBXs formulated with greater percentages of FK-800, the changes in mechanical properties may be more pronounced. The effect that the reactive decomposition gases will have on the explosive filler should also be considered when developing new formulations containing FK-800 for use where they will be exposed to γ-radiation.

Even though the TCV's mechanical properties show little to no effect from gamma radiation exposure, significant changes were noted in the sensitiveness of both TCV and TATB to external stimulus by impact and electric spark discharge. The changes in sensitiveness of the explosives seen in this study indicate the risk of unintended energetic events increases with exposure to γ-radiation. This change in sensitiveness requires investigation to ensure the safety of any irradiated munition. A mono-furazan derivative of TATB was confirmed as one of the main radiation-induced decomposition products of

TATB and it has also been shown that the concentration of the mono-furazan can be measured by HPLC. However, further work is required to confirm the observed trend.

This study has indicated that whilst γ-radiation has little effect on the mechanical properties of TCV enabling it to be used as a structural element in the complex shapes required in nuclear weapons, further investigation of the changes in the safety characteristics of TCV when exposed to γ-radiation is required for long term use in munitions.

10 Future work

This section describes possible further research recommended the author to answer some of the questions generated during study that were either beyond the scope or impractical during this investigation.

10.1 FK-800

This study has investigated both the mechanical effects and some chemical effects of γ-radiation on FK-800; however, there are some areas which require further study to fully characterise and understand the irradiated material's properties.

Further study is required of the crystalline changes in FK-800, and the effects this has on the tensile properties of the polymer. A full study of irradiated samples using both wide- and small-angle X-ray diffraction to higher radiation doses and at a range of dose rates should be conducted. The aim of this study would be to measure crystallisation rates and the size and type of the crystals formed when FK-800 is irradiated.

The effect of the fringe micelle crystals on the tensile properties of irradiated FK-800 requires further study. Samples that have and have not been thermally cycled after irradiation should be tensile load tested. The thermal cycling would reset the irradiated samples crystallinity, allowing the effect of the fringe micelles on FK-800's tensile properties to be measured.

Some effort was made in this study to explore the effect irradiation dose rate and atmosphere had on irradiated FK-800 samples. Some evidence for dose rate dependence was noted in the tensile load results; however, further investigation at a larger range of radiation doses is required to confirm these findings. Further research on the effects of irradiation atmosphere on the molecular mass of irradiated FK-800 should be carried out using thin films of polymer to fully allow diffusion of gases in and out of the samples. The samples used for this study were 2 mm thick which may have had a diffusion-limiting effect requiring further investigation.

The GPC results for this study were in contrast to those of a study by Mayer et al.[38] in which they studied historic irradiated samples of the analogous polymer Kel-F 800. Post irradiation reactions may have taken place during storage of Mayer's samples that have not yet taken place in the FK-800 samples in this study when tested due to the timescales of this project. Further investigation of the effects of post-irradiation aging should be studied using samples of FK-800 stored at a controlled temperature above T_g over extended periods of time.

10.2 TCV

The mechanical properties of irradiated FK-800 have been shown to change when the samples are thermally cycled due to changes in the polymer's crystallinity. Changes in the crystallinity of the FK-800 binder in formulated samples of TCV were not investigated in this project and further investigation of thermally cycled samples should be conducted to further understand the effects of binder crystallinity on the properties of the formulated TCV.

A bi-axial tensile test at a single temperature was used to analyse samples of irradiated TCV during this study. However, in a real life situation the material may be subjected to vibration stimuli at a range of temperatures. To understand how TCV will perform mechanically in this situation, a DMA study of irradiated TCV should be conducted over a temperature range and at multiple frequencies.

The failure mode of the TCV samples was not investigates in this study due to the complexities of monitoring this in samples of TCV. An investigation into the failure mode could lead to a better understanding of why large changes in the polymer only represented small to no change in the mechanical properties of the TCV.

Some evidence of changes in the energy released during thermal decomposition by DSC was noted during this study. No trend could be confirmed from the DSC analysis in this study. However, further investigation of irradiated TCV using bomb calorimetry would give more accurate values for the

heat of combustion and allow the investigation of changes in energy released from pristine and irradiated TCV.

10.3 TATB

One of the most significant sets of results in this project was the hazard testing of TATB. Substantial changes were seen in both the impact and electric spark discharge sensitiveness tests. The tests carried out in this study were reduced versions of those in the EMTAP manual[76] of tests. Therefore, larger quantities of TATB should be irradiated to fully investigate the sensitiveness and hazard properties of irradiated TATB by performing additional tests from the EMTAP manual.

It was not one of the objectives of this project to test the explosive performance of either irradiated TATB or TCV. However due to the build-up of radiation-induced decomposition products and changes in hazard characteristics noted in this study, tests should be conducted on irradiated TATB to assess the material's explosive performance against pristine TATB.

As part of this study a mono-furazan derivative of TATB was strongly indicated by LC-MS as a radiation-induced decomposition product of TATB. Evidence of further radiation-induced decomposition products was seen in very low quantities in the mass spectra of irradiated TATB, although they were not detected by HPLC. Due to the very low solubility of TATB, detection of low concentrations of decomposition products may not be possible by HPLC by dissolving TATB in DMSO. Further HPLC analysis of irradiated TATB should be conducted using ionic liquids[96] to dissolve the TATB in greater quantities. This will possibly allow the investigation and measurement of other decomposition products of irradiated TATB by HPLC. Additional detection and identification of decomposition products in samples of irradiated TATB may also be possible using tandem mass spectroscopy. The further study of radiation-induced decomposition will aid the understanding of TATB's decomposition pathway when γ-irradiated.

REFERENCES

[1] Dobratz, B. M. (1995), *The Insensitive High Explosive Triamiotrinitrobenzene (TATB): Development and Characterization - 1888 to 1994,* LA-13014-H, Los Alamos National Laboratory.

[2] Kaye, S. M. (1978), "PBX", in *Encyclopaedia of Explosives and Related Items, Volume 8,* US Army Research and Development Command, Picatinny Arsenal, New Jersey, USA, , pp. P60.

[3] Akhavan, J. (2004), *The Chemistry of Explosives,* Second Edition ed, Royal Society of Chemistry.

[4] Meyer, R., Köhler, J. and Homburg, A. (2007), "P", in *Explosives,* 5th ed, Wiley-VCH Verlag GmbH & Co. KGaA, Weinheim, pp. 241-268.

[5] Heller, H. and Bertman, A. L. (1973), *HNS/Teflon, a new Heat-Resistant Explosive,* NOLTR 73-163, Naval Ordnance Laboratory White Oak, Maryland.

[6] Daniel, M. A. (2006), *Polyurethane Binder Systems for Polymer Bonded Explosives,* DSTO-GD-0492, Defence Science Technology Organisation, Edinburgh South, Australia.

[7] Hollands, R., Barnes, P., Moss, R. and Sharp, M. (2006), "Explosive Booster Selection Criteria for Insensitive Munitions Applications", *IMENTS 2006 "Maintaining Performance and Enhanced Survivability Throughout the Lifecycle",* 24-28 April 2006, Bristol UK, IMEMG, http://www.imemg.org/imemg-proceedings.html.

[8] DePiero, S. C. and Hoffman, D. M. (2009), *Formulation and Characterization of LX-17-2 from new FK 800 binder and WA, ATK and BAE TATBs,* LLNL-TR-416360, Lawrence Livermore National Laboratory.

[9] Salisbury, D., Winter, R. and Biddle, L. (2006), "A study of the effect of electrical energy input on detonation failure in wedges of the TATB-Based explosive EDC35", *AIP Conference Proceedings,* Vol. 845 II, pp. 1010.

[10] Thompson, D. G., Brown, G. W., Olinger, B., Mang, J. T., Patterson, B., Deluca, R. and Hagelberg, S. (2010), "The effects of TATB ratchet growth on PBX 9502", *Propellants, Explosives, Pyrotechnics,* vol. 35, no. 6, pp. 507-513.

[11] Rae, P. J., Goldrein, H. T., Palmer, S. J. P., Field, J. E. and Lewis, A. L. (2002), "Quasi-static studies of the deformation and failure of β-HMX based polymer bonded explosives", *Proceedings of the Royal Society A: Mathematical, Physical and Engineering Sciences,* vol. 458, no. 2019, pp. 743-762.

[12] Agrawal, J. P. (2010), "Status of Explosives", in *High Energy Materials,* Wiley-VCH Verlag GmbH & Co. KGaA, , pp. 69-161.

[13] Meyer, R., Köhler, J. and Homburg, A. (2007), "T", in *Explosives,* 5th ed, Wiley-VCH Verlag GmbH & Co. KGaA, Weinheim, pp. 303-357.

[14] Forsythe, J. S. and Hill, D. J. T. (2000), "Radiation chemistry of fluoropolymers", *Progress in Polymer Science (Oxford),* vol. 25, no. 1, pp. 101-136.

[15] Skidmore, C. B., Idar, D. J., Buntain, G. A., Son, S. F. and Sander, R. K. (1998), "Aging and PBX 9502", *Life Cycles of Energetic Materials,* March 29 - April 1 1998, .

[16] *3M Fk-800 Resin Product Information*(2003), available at: http://www.machichemicals.com/pdf/3M_FK-800.pdf (accessed 11/13).

[17] Turner, J.E., (2007;), *The Nucleus and Nuclear Radiation*, Wiley-VCH Verlag GmbH & Co. KGaA.

[18] Avrami, L. (1980), *"Radiation Effects on Explosives, Propellants and Pyrotechnics", Encyclopaedia of Explosives and Related Items, Vol. 9, PATR 2700*.

[19] Avrami, L. and Jackson, H. J. (1976), *Effect of long term low-level gamma radiation on thermal sensitivity of RDX/HMX mixtures.*

[20] Piantanaida, E. and Piazzi, M. (1961), "The Behaviour of Explosives Under the Impact of Gamma-Radiation Part II", *Chimica e I'Industria,* vol. 43, pp. 1389.

[21] Miles, M. H., DeVries, K. L., Britt, A. D. and Moniz, W. B. (1983), "Impact sensitivity of gamma -irradiated HMX.", *Propellants, Explosives, Pyrotechnics,* vol. 8, no. 2, pp. 49-52.

[22] Avrami, L., Jackson, H. J. and Kirshenbaum, M. S. (1973), *Radiation-induced changes in explosive materials.*

[23] Coffey, C. S., De Vost, E. D. and Woody, D. L. (1989), "Towards Developing the Capability to predict the Hazard Response of Energetic Materials Subjected to Impact", *Ninth Symposium (international) On Detonation,* August 1989, Portland, Oregon, USA, pp. 1243.

[24] Padfield, J. and Akhavan, J. (un-published), *Final Report: Feasibility Study on the Effect of Gamma Radiation on Polymer Bonded Explosives,* , Cranfield University, Shrivenham.

[25] Britt, A. D., Moniz, W. B., Chingas, G. C., Moore, D. W., Heller, C. A. and Ko, C. L. (1981), "Free Radicals of TATB", *Propellants, Explosives, Pyrotechnics,* vol. 6, no. 4, pp. 94-95.

[26] Kinloch, S. A. (1991), *Interphase Modification in TATB filled Polymer Bonded Explosives* (PhD thesis), Cranfield University, Shrivenham.

[27] Manaa, M. R., Schmidt, R. D., Overturf, G. E., Watkins, B. E., Fried, L. E. and Kolb, J. R. (2002), "Towards unravelling the photochemistry of TATB", *Thermochimica Acta,* vol. 384, no. 1-2, pp. 85-90.

[28] Sharma, J. and Owens, F. J. (1979), "XPS study of UV and shock decomposed triamino-trinitrobenzene", *Chemical Physics Letters,* vol. 61, no. 2, pp. 280-282.

[29] Oshima, A., Tabata, Y., Kudoh, H. and Seguchi, T. (1995), "Radiation induced crosslinking of polytetrafluoroethylene", *Radiation Physics and Chemistry,* vol. 45, no. 2, pp. 269-273.

[30] *Nuclear and Space Radiation Effects on Materials,* (1970), NASA SP-8053.

[31] Clough, R. L. and Gillen, K. T. (1991), "Radiation Resistance of Polymers and Composites", in Clegg, D. W. and Collyer, A. A. (eds.) Elsevier Science Publications Ltd, England, pp. 79.

[32] Florin, R. E. and Wall, L. A. (1961), "Gamma irradiation of fluorocarbon polymers.", *Journal of Research of the National Bureau of Standards, Section A: Physics and Chemistry,* vol. 65A, pp. 375-387.

[33] "Section F: Miscellaneous", (1984), in Weast, R. C. (ed.) *CRC Handbook of Chemistry and Physics,* 64th ed, CRC Press, INC., USA.

[34] Burgess, C. E., Woodward, J. D., Rainwater, K. A., Lightfoot, M. J. and Richardson, B. R. (1998), *Literature Review of Lifetime of DoE Materials: Aging of Plastic Bonded Explosives and the Explosives and Polymers Contained Therin,* ANRCP-1998-12, Amarillo National Resource Centre for Plutonium.

[35] Iskakov, L. I. (1989), "Gaseous products in the radiolysis of polymers", in Milinchuk, V. K. and Tupikov, V. I. (eds.) *Organic Radiation Chemistry Handbook,* English Edition ed, Ellis Harwook Ltd, England, pp. 126.

[36] Hill, D. J. T., Thurecht, K. J. and Whittaker, A. K. (2003), "New Structure Formation on γ-irradiation of Poly(chlorotrifluoroethylene)", *Radiation Physics and Chemistry,* vol. 67, no. 6, pp. 729-736.

[37] Nigrey, P. J. and Dickens, T. G. (1996), *Effects of Simulant Hanford Tank Waste on Plastic Packing Components,* CONF-960804--34, Sandia National Laboratories.

[38] Mayer, B. P., Lewicki, J. P., Chinn, S. C., Overturf, G. E. and Maxwell, R. S. (2012), "Nuclear magnetic resonance and principal component analysis for investigating the degradation of poly[chlorotrifluoroethylene-co-(vinylidene fluoride)] by ionizing radiation", *Polymer Degradation and Stability,* vol. 97, no. 7, pp. 1151-1157.

[39] Waring, S. C. (2002), *Effect of Gamma Irradiation on the Prepolymer polyNIMMO* (PhD thesis), Cranfield University, Shrivenham.

[40] *Caburn-MDC Europe catalogue section 2.5*(2011), available at: http://caburn.co.uk/resources/downloads/pdfs/sec2.5.2.pdf (accessed June/18/2012).

[41] *Caburn-MDC Europe catalogue section 5.2.3*(2007), available at: http://caburn.co.uk/resources/downloads/pdfs/sec5.2.3.pdf (accessed June/18/2012).

[42] Morris, J. and Penhale, L. G. (1965), "Multicurie Gamma Irradiation Facility - Design and Realization", *Nuclear Engineering,* vol. 10, December, pp. 469.

[43] Walton, D. L.,P. (2000), *Polymers,* Oxford University Press, Oxford.

[44] Billmeyer, F. W. (1984), "Analysis and testing of polymers", in *Textbook of Polymer Science,* 3rd ed, John Wiley & Sons, New York, pp. 229.

[45] Callister, W. D. (2007), "Characteristics, Applications and Processing of Polymers", in *Materials Science and Engineering an Introduction,* 7th ed, John Wiley & Sons, Inc., USA, pp. 523.

[46] Mark, J. E., Eisenberg, A., Graessley, W. W., Mandelkern, L., Samulski, E. T., Koenig.J.L. and Wignall, G. D. (1993), *Physical Properties of Polymers,* 2nd ed, American Chemical Society, Washington, DC.

[47] Menard, K. P. (2008), *Dynamic Mechanical Analysis, A Practical Introduction,* 2nd ed, CRC Press, Boca Raton.

[48] Duncan, J. (2008), "Principals and Applications of Mechanical Thermal Analysis", in Gabbott, P. (ed.) *Principals and Applications of Thermal Analysis,* 1st ed, Blackwell Publishing Ltd, Oxford, pp. 119.

[49] Schultz, J. (1974), "Time-Dependent Mechanical Behaviour", in *Polymers Material Science,* Prentice-Hall inc, Englewood Cliffs, pp. 359-379.

[50] Gedde, U. W. (1995), "The Glassy Amorphous State", in *Polymer Physics,* 1st ed, Chapman & Hal, London, pp. 77-98.

[51] Roylance, D. (1996), "Viscoelastic Response of Polymers", in *Mechanics of Materials,* John Wiley & Sons, inc, New York, pp. 21-27.

[52] *Mechanical Properties: Viscoelasticity* (2008), available at: http://gertrude-old.case.edu/276/materials/05.htm (accessed 10/09/13).

[53] *Introduction to Dynamic Mechanical Analysis (1)*(2012), available at: http://www.anasys.co.uk/library/dma1.htm (accessed 3/27/13).

[54] Li, D. and Wong, L. N. Y. (2012), "The Brazilian Disc Test for Rock Mechanics Applications: Review and New Insights", *Rock Mechanics and Rock Engineering,* pp. 1-19.

[55] Williamson, D. M., Palmer, S. J. P., Proud, W. G. and Govier, R. (2007), "Brazilian disc testing of a UK PBX above and below the glass transition temperature", *AIP Conference Proceedings,* Vol. 955, pp. 803.

[56] Palmer, S. J. P., Field, J. E. and Huntley, J. M. (1993), "Deformation, Strengths and Strains to Failure of Polymer Bonded Explosives", *Proceedings of the Royal Society of London. Series A: Mathematical and Physical Sciences,* vol. 440, no. 1909, pp. 399-419.

[57] Gent, A. N. and Lindley, P. B. (1959), "Internal Rupture of Bonded Rubber Cylinders in Tension", *Proceedings of the Royal Society A: Mathematical, Physical and Engineering Sciences,* vol. 249, no. 1257, pp. 195-205.

[58] Awaji, H. and Sato, S. (1978), "Combines mode fracture toughness measurement by the disk test", *Journal of Engineering Materials and Technology, Transactions of the ASME,* vol. 100, no. 2, pp. 175-182.

[59] Gabbott, P. (2008), "A Practical Introduction to Differential Scanning Calorimetry", in Gabbott, P. (ed.) *Principles and Applications of Thermal Analysis,* Blackwell Publishing, Oxford, pp. 2.

[60] Blaine, R. L. and Waguespack, L. E. (2001)*, Determination of Polymer Crystal Molecular Weight Distribution by DSC*, available at: www.tainstruments.com/library_download.aspx?file=TA276.pdf (accessed 7/10/2013).

[61] Hoffman, D. M., Matthews, F. M. and Pruneda, C. O. (1989), "Dynamic mechanical and thermal analysis of crystallinity development in Kel-F 800 and TATB/Kel-F 800 plastic bonded explosives. Part I. Kel-F 800", *Thermochimica Acta,* vol. 156, no. 2, pp. 365-372.

[62] Bottom, R. (2008), "Thermogravimetric Analysis", in Gabbott, P. (ed.) *Principals and Applications of Thermal Analysis,* Blackwell Publishing, Oxford, pp. 87.

[63] *User's Manual Sartorius YDK 01, YDK 01-0D, YDK 01 LP,Density Determination Kit*(2004), available at: https://scaleman.com/index.php/aitdownloadablefiles/download/aitfile/aitfile_id/514/ (accessed 7/16/13).

[64] Currell, G. (2000), "Gas Chromatography", in *Analytical Instrumentation, Performance, Characteristics and Quality,* John Wiley &sons Ltd., Chichester, pp. 159.

[65] Claydon, J., Greeves, N., Warren, S. and Wothers, P. (2009), "Determining organic structures", in *Organic Chemistry,* Oxford University press, Oxford, United Kingdom, pp. 47-80.

[66] Rouessac, F. R.,A. (2007), "Mass Spectrometry", in *Chemical Analysis Modern Instrumentation Methods and Techniques,* 2nd ed, John Wiley & Sons Ltd, Chichester, pp. 369.

[67] de Hoffmann, E. T.,V. (2007), "Mass Analysers", in *Mass Spectrometry Principals and Applications,* 3rd ed, John Wiley & Sons Ltd, Chichester, pp. 85.

[68] Currell, G. (2000), "High Performance Liquid Chromatography", in *Analytical Instrumentation Performance Characteristics and Quality,* John Wiley & Sons Ltd., Chichester, pp. 141.

[69] Rouessac, F. R.,A. (2007), "High Performance Liquid Chromatography", in *Chemical Analysis Modern Instrumentation Methods and Techniques,* 2nd ed, John Wiley & Sons Ltd, Chichester, pp. 63.

[70] Currell, G. (2000), "Mass Spectrometry Systems", in *Analytical Instrumentation Performance Characteristics and Quality,* John Wiley & Sons Ltd., Chichester, pp. 183.

[71] Rouessac, F. R.,A. (2007), "Size exclusion chromatography", in *Chemical Analysis Modern Instrumentation Methods and Techniques,* 2nd ed, John Wiley & Sons Ltd, Chichester, pp. 135.

[72] Billmeyer, F. W. (1984), "The Science of Lage Molecules", in *Textbook of Polymer Science,* 3rd ed, John Wiley & Sons, New York, pp. 3.

[73] Rouessac, F. R.,A. (2007), "Infrared Spectroscopy", in *Chemical Analysis Modern Instrumentation Methods and Techniques,* 2nd ed, John Wiley & Sons Ltd, Chichester, pp. 207.

[74] Alexander, L. E. (1969), *X-ray Diffraction Methods in Polymer Science,* Wiley-interscience, New York.

[75] Renouf, A. C. (2004), *A degradation study of PLLA containing lauric acid: the effect of composition and microstructure* (PhD thesis), Corpus Christi College, University of Cambridge, Cambridge.

[76] Moss, R. (2004), *Energetic Materials Testing and Assessment Policy Committee (EMTAP) Manual of Tests,* Issue 2, DOSG, UK MOD, UK.

[77] *RSC Analytical Methods Committee technical brief, Robust statistics: a method of coping with outliers.*(2012), available at: http://www.rsc.org/images/robust-statistics-technical-brief-6_tcm18-214850.pdf (accessed 09/07/11).

[78] Sichina, W.J., (2000), *Thermal analysis application note, Measurment of T_g by DSC*, Perkin Elmer instruments, USA.

[79] Mark, J. E., Eisenberg, A., Graessley, W. W., Mandelkern, L., Samulski, E. T., Koenig, J. L. and Wignall, G. D. (1993), "The Crystalline State", in *Physical Properties of Polymers,* 2nd ed, American Chemical Society, Washington, DC, pp. 145.

[80] Nasef, M. M. and Dahlan, K. Z. M. (2003), "Electron irradiation effects on partially fluorinated polymer films: Structure-property relationships", *Nuclear Instruments and Methods in Physics Research, Section B: Beam Interactions with Materials and Atoms,* vol. 201, no. 4, pp. 604-614.

[81] Acevedo, M. E., Quijada, R. and Vallette, M. C. (2008), "Study of the effect of branching in degradation of polyethylenes obtained via metallocene catalyst", *Journal of the Chilean Chemical Society,* vol. 53, no. 2, pp. 1490-1493.

[82] Charlesby, A. (1960), "Polytetrafluorethylene (PTFE)", in Charlesby, A. (ed.) *Atomic radiation and polymers,* Pergamon Press ltd., Oxford, pp. 348.

[83] Charlesby, A. (1960), *Atomic radiation and Polymers,* Pergamon Press ltd., Oxford.

[84] Hill, D. J. T., Thurecht, K. J. and Whittaker, A. K. (2003), "A study of the radiation chemistry of (chlorotrifluoroethylene) by ESR spectroscopy", *Radiation Physics and Chemistry,* vol. 68, pp. 857-864.

[85] Billmeyer, F. W. (1984), "Morphology of crystalline polymers", in 3rd ed, John Wiley & Sons, New York, pp. 273.

[86] Bower, D. I. (2002), "Morphology and motion", in *An introduction to polymer physics,* Cambridge University Press, Cambridge, UK, pp. 117.

[87] Callister, W. D. (2007), "Polymer structures", in 7th ed, John Wiley & Sons, Inc., USA, pp. 489.

[88] *Polymer Crystallinity* (2005), available at: http://www.pslc.ws/macrog/crystal.htm (accessed 4/7/13).

[89] *Polymer Chemistry, Polymer Crystallinity* (2000), available at: http://faculty.uscupstate.edu/llever/Polymer%20Resources/Crystalline.htm (accessed 4/7/13).

[90] Hoffman, D. M., Matthews, F. M. and Pruneda, C. O. (1989), "Dynamic mechanical and thermal analysis of crystallinity development in Kel-F 800 and TATB/Kel-F 800 plastic bonded explosives. Part I. Kel-F 800", *Thermochimica Acta,* vol. 156, no. 2, pp. 365-372.

[91] Gautier, L., Poullain, D., Thevenot, G. and Belmas, R. (2002), "Thermal decomposition of TATB.", *Proceedings of the International Pyrotechnics Seminar,* vol. 29th, pp. 289-291.

[92] Wu, C. J. and Fried, L. E. (2000), "Ring closure mediated by intramolecular hydrogen transfer in the decomposition of a push-pull nitroaromatic: TATB", *Journal of Physical Chemistry A,* vol. 104, no. 27, pp. 6447-6452.

[93] Sharma, J., Forbes, J. W., Coffey, C. S. and Liddiard, T. P. (1987), "The physical and chemical nature of sensitization centres left from hot spots caused in triaminotrinitrobenzene by shock or impact", *Journal of Physical Chemistry,* vol. 91, no. 19, pp. 5139-5144.

[94] Mehilal, Sikder, A. K., Sinha, R. K. and Gandhe, B. R. (2003), "Cost-effective synthesis of 5,7-diamino-4,6-dinitrobenzofuroxan (CL-14) and its evaluation in plastic bonded explosives", *Journal of hazardous materials,* vol. 102, no. 2-3, pp. 137-145.

[95] Rice, B. M. and Hare, J. J. (2002), "A quantum mechanical investigation of the relation between impact sensitivity and the charge distribution in energetic molecules", *Journal of Physical Chemistry A,* vol. 106, no. 9, pp. 1770-1783.

[96] Hoffman, D. M. and Fontes, A. T. (2010), "Density distributions in TATB prepared by various methods", *Propellants, Explosives, Pyrotechnics,* vol. 35, no. 1, pp. 15-23.

BIBLIOGRAPHY

Callister, W. D. (2007), *Materials Science and Engineering an Introduction,* 7th ed, John Wiley & Sons, Inc., USA.

Leroy, C., Rancoita, P. and Editors (2004), *Principles of Radiation Interaction in Matter and Detection.* World Scientific Publishing Co. Pte. Ltd., Singapore.

Mark, J. E., Eisenberg, A., Graessley, W. W., Mandelkern, L., Samulski, E. T., Koenig.J.L. and Wignall, G. D. (1993), *Physical Properties of Polymers,* 2nd ed, American Chemical Society, Washington, DC, USA.

Menard, K. P. (2008), *Dynamic Mechanical Analysis, A Practical Introduction,* 2nd ed, CRC Press, Boca Raton, USA.

Milinchuk, V. K. and Tupikov, V. I. (1989), *Organic Radiation Chemistry Handbook,* Ellis Horwood Limited., Chichester, UK.